NUREG/CR-6914, Vol. 2
LA-UR-05-0124

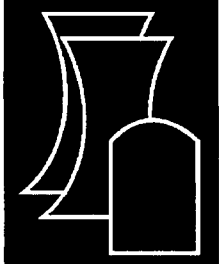

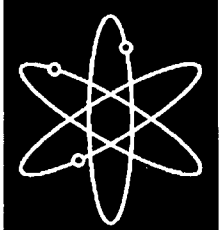

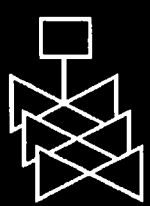

Integrated Chemical Effects Test Project: Test #1 Data Report

Los Alamos National Laboratory

U.S. Nuclear Regulatory Commission
Office of Nuclear Regulatory Research
Washington, DC 20555-0001

AVAILABILITY OF REFERENCE MATERIALS IN NRC PUBLICATIONS

NRC Reference Material

As of November 1999, you may electronically access NUREG-series publications and other NRC records at NRC's Public Electronic Reading Room at http://www.nrc.gov/reading-rm.html. Publicly released records include, to name a few, NUREG-series publications; *Federal Register* notices; applicant, licensee, and vendor documents and correspondence; NRC correspondence and internal memoranda; bulletins and information notices; inspection and investigative reports; licensee event reports; and Commission papers and their attachments.

NRC publications in the NUREG series, NRC regulations, and *Title 10, Energy*, in the Code of *Federal Regulations* may also be purchased from one of these two sources.

1. The Superintendent of Documents
   U.S. Government Printing Office
   Mail Stop SSOP
   Washington, DC 20402–0001
   Internet: bookstore.gpo.gov
   Telephone: 202-512-1800
   Fax: 202-512-2250
2. The National Technical Information Service
   Springfield, VA 22161–0002
   www.ntis.gov
   1–800–553–6847 or, locally, 703–605–6000

A single copy of each NRC draft report for comment is available free, to the extent of supply, upon written request as follows:

Address: U.S. Nuclear Regulatory Commission
Office of Administration
Mail, Distribution and Messenger Team
Washington, DC 20555-0001
E-mail: DISTRIBUTION@nrc.gov
Facsimile: 301–415–2289

Some publications in the NUREG series that are posted at NRC's Web site address http://www.nrc.gov/reading-rm/doc-collections/nuregs are updated periodically and may differ from the last printed version. Although references to material found on a Web site bear the date the material was accessed, the material available on the date cited may subsequently be removed from the site.

Non-NRC Reference Material

Documents available from public and special technical libraries include all open literature items, such as books, journal articles, and transactions, *Federal Register* notices, Federal and State legislation, and congressional reports. Such documents as theses, dissertations, foreign reports and translations, and non-NRC conference proceedings may be purchased from their sponsoring organization.

Copies of industry codes and standards used in a substantive manner in the NRC regulatory process are maintained at—

The NRC Technical Library
Two White Flint North
11545 Rockville Pike
Rockville, MD 20852–2738

These standards are available in the library for reference use by the public. Codes and standards are usually copyrighted and may be purchased from the originating organization or, if they are American National Standards, from—

American National Standards Institute
11 West 42nd Street
New York, NY 10036–8002
www.ansi.org
212–642–4900

Legally binding regulatory requirements are stated only in laws; NRC regulations; licenses, including technical specifications; or orders, not in NUREG-series publications. The views expressed in contractor-prepared publications in this series are not necessarily those of the NRC.

The NUREG series comprises (1) technical and administrative reports and books prepared by the staff (NUREG–XXXX) or agency contractors (NUREG/CR–XXXX), (2) proceedings of conferences (NUREG/CP–XXXX), (3) reports resulting from international agreements (NUREG/IA–XXXX), (4) brochures (NUREG/BR–XXXX), and (5) compilations of legal decisions and orders of the Commission and Atomic and Safety Licensing Boards and of Directors' decisions under Section 2.206 of NRC's regulations (NUREG–0750).

NUREG/CR-6914, Vol. 2
LA-UR-05-0124

Integrated Chemical Effects Test Project: Test #1 Data Report

Manuscript Completed: August 2006
Date Published: December 2006

Principal Investigator: J. Dallman

Prepared by
J. Dallman, J. Garcia, M. Klasky, B. Letellier
Los Alamos National Laboratory
Los Alamos, NM 87545

K. Howe
University of New Mexico
Department of Civil Engineering
Albuquerque, NM 87110

B.P. Jain, NRC Project Manager

Prepared for
Division of Fuel, Engineering and Radiological Research
Office of Nuclear Regulatory Research
U.S. Nuclear Regulatory Commission
Washington, DC 20555-0001
NRC Job Code Y6999

NUREG/CR-6914, Volume 2, has been reproduced from the best available copy.

INTEGRATED CHEMICAL EFFECTS TEST PROJECT: TEST #1 DATA REPORT

ABSTRACT

A 30-day test was conducted in the Integrated Chemical Effects Test (ICET) project test apparatus. This was the first of a series of five tests. The test simulated the chemical environment present inside a pressurized water reactor containment water pool after a loss-of-coolant-accident. The initial chemical environment contained 15.14 kg of boric acid, 1.197 g of lithium hydroxide, and 5.87 kg of sodium hydroxide. An additional 2.27 kg of sodium hydroxide was added beginning at 30 minutes and lasting until 4 hours into the test. The test was conducted for 30 days at a constant temperature of 60°C. The materials tested within this environment included representative amounts of submerged and unsubmerged aluminum, copper, concrete, zinc, carbon steel, and fiberglass insulation samples. Representative amounts of concrete dust and latent debris were also added to the test solution. Water was circulated through the bottom portion of the test chamber during the entire test to achieve representative flow rates over the submerged specimens. The test solution reached a pH of 9.5 by the end of the NaOH injection and remained at approximately that level for the 30-day duration of the test. The test solution turbidity was initially about 12 NTU but decreased to less than 1 NTU within 72 hours. However, samples of the test solution cooled to 23°C showed an increase in turbidity from less than 20 NTU at Day 4 to about 130 NTU at Day 30. Total suspended solids (TSS) in the test solution varied somewhat during the test and were roughly in the range of 10 mg/L to about 30 mg/L for the solution at 60°C. End-of-test evaluations indicated TSS levels in the test solution of about 1800 mg/L at 22°C and 100 mg/L at 55°C. Precipitants were formed as the solution was cooled to room temperature. The precipitants were not apparent at the test temperature of 60°C. Analyses of the test solution indicated that high levels of aluminum were present, with levels rising from near zero at the beginning of the test to approximately 350 mg/L after 20 days of testing. Post-test evaluations indicated that the submerged aluminum coupons had lost about 25% of their weight during the test. Examinations of fiberglass taken from the test apparatus after 15 days of testing indicated evidence of chemical products and a web-like material that spanned individual fibers. After 30 days of testing, the web-like material was more prevalent and contiguous webbing appeared to span multiple fibers. Shear-dependent viscosity measurements indicated that the test solution was representative of Newtonian fluid. Samples from the second half of the test exhibited non-Newtonian behavior upon cooling to room temperature.

CONTENTS

ABSTRACT iii

EXECUTIVE SUMMARY xi

ACKNOWLEDGMENTS xiii

ABBREVIATIONS xv

FIGURES viii

TABLES x

1.0 INTRODUCTION 1

2.0 BACKGROUND AND OBJECTIVE 3

3.0 EXPERIMENTAL MATERIALS AND METHODS 5

3.1 Chemical Test Apparatus Functional Description 5

3.2 Chemical Tank Assembly and Circulation Details 8

3.2.1 Materials 8

3.2.2 Tank Sizing 8

3.2.3 Coupon Racks 13

3.2.4 Tank Insulation 14

3.2.5 Tank Heaters 14

3.2.6 Pump Selection 14

3.3 Experimental Plan and Test Matrix 15

3.4 Analytical Methods 17

3.4.1 Scanning Electron Microscopy (SEM) 18

3.4.2 Energy Dispersive Spectroscopy (EDS) 19

3.4.3 Transmission Electron Microscopy (TEM) 20

3.4.4 Inductively Coupled Plasma by Atomic Emission Spectroscopy (ICP-AES) 20

3.4.5 X-Ray Fluorescence (XRF) 21

3.4.6 X-Ray Diffraction (XRD) 22

3.4.7 Wet Chemistry Analyses 22

3.5 QA Program 24

4.0 EXPERIMENTAL RESULTS 27
4.1 Test Operation and Sequence 27
4.1.1 Description 27
4.1.2 Process Control 27
4.1.3 Hydrogen Generation 28
4.2 Coupon Racks 28
4.2.1 Physical Observations 29
4.2.2 Weight Measurements 31
4.3 NUKON™ Fiberglass Samples 32
4.3.1 SEM/EDS 33
4.4 Concrete Samples 36
4.5 Solution Chemistry 36
4.5.1 Water Color 37
4.5.2 Turbidity 39
4.5.3 Total Suspended Solids 41
4.5.4 pH 44
4.5.5 Constant-Shear Kinematic Viscosity 45
4.5.6 Shear-Dependent Viscosity 46
4.5.7 Metal Ion Concentrations 51
4.6 Precipitated Solids 54
4.6.1 TEM 55
4.6.2 Additional Analytical Results 59
5.0 RECOMMENDATIONS 65
6.0 REFERENCES 67

APPENDICES

Appendix A: SEM Data for 24-Hour High-Volume Filtrate ..... A-i

Appendix B: SEM/EDS Data for Test-1 Day-15 Fiberglass and Filtrate ..... B-i

Appendix C: SEM/EDS Data for Test-1 Day-30 Fiberglass and Filtrate ..... C-i

Appendix D: SEM/EDS Data for White Precipitate, Day-30 Fiberglass, Drain Screen Debris, Pipe Residue, Tank Sediment, Concrete Sample, Latent Debris Baselines, Test-1 Day-30 High-Volume Filtrate ..... D-i

Appendix E: TEM Analyses of Test-1 Day-15 Water Samples ..... E-i

Appendix F: TEM Analyses of Test-1 Day-30 Water Samples ..... F-i

Appendix G: TEM Analyses of Pre-Test 1 Laboratory Solution ..... G-i

Appendix H: Sediment Analysis for Test #1 ..... H-i

Appendix I: Test #1 Coupons ..... I-i

FIGURES

Figure 1. Test loop process flow diagram. 6
Figure 2. Photograph of the test loop. 7
Figure 3. Photograph of the data acquisition system. 7
Figure 4. External view of the ICET tank. 9
Figure 5. The distribution header, heaters, and thermocouples inside the lower tapered reservoir of the ICET tank. 9
Figure 6. The top and bottom angle irons for supporting coupon racks in the upper section of the ICET tank. 10
Figure 7. One of four spray nozzles located in each upper corner of the ICET tank. This photo was taken through the upper access hatch while the lid was in place. 10
Figure 8. The cover lid of the ICET tank showing the top observation window (lower) and top access hatch with handle (upper). 11
Figure 9. Front-view as-built dimensions of tank and piping system. Dimensions are in inches; shaded regions represent CPVC piping. 12
Figure 10. Side-view, as-built dimensions of tank and piping system. Dimensions are in inches; shaded regions represent CPVC piping. 13
Figure 11. Photograph of a loaded coupon rack. 14
Figure 12. Circulation pump for the ICET system. 15
Figure 13. Production of secondary electrons from an electron beam. 18
Figure 14. Production of backscattered electrons from an electron beam. 19
Figure 15. Illustration of the operation principle of XRF. 21
Figure 16. Coupon rack configuration in the ICET tank. 29
Figure 17. Coupon racks inside ICET tank before start of test. 30
Figure 18. Coupon rack being loaded into the ICET tank. 30
Figure 19. Coupon rack following removal from the ICET tank. 31
Figure 20. SEM image for a pretest sample of clean fiberglass. 34
Figure 21. SEM image for a Day-15 test sample illustrating crusty deposits or growth on fiberglass. 34
Figure 22. SEM image for a Day-30 test sample illustrating membrane films deposited between fibers. 35
Figure 23. SEM image for a Day-15 test sample (sample #4023) magnified 230 times, illustrating deposits between fibers. 35

Figure 24. Day-15, sample #4 counting spectrum (EDS 4-16) taken for the cracked deposits at the right-hand side of Figure 23. 36
Figure 25. Daily water grab sample extraction. 37
Figure 26. Wet chemistry analyses. 38
Figure 27. Bench-top water sample characterization. 39
Figure 28. Turbidity trend at the test temperature observed during ICET Test #1. 40
Figure 29. Turbidity measured at 23°C and 60°C during ICET Test #1. 41
Figure 30. Total suspended solids during ICET Test #1. 42
Figure 31. TSS results for the end-of-test precipitation experiment. 42
Figure 32. Temperature-precipitate relationship upon heating the end-of-test solution after precipitate has formed. 43
Figure 33. Temperature-precipitate relationship upon cooling and heating of end-of-test solution. 44
Figure 34. pH trend observed during ICET Test #1. 44
Figure 35. Kinematic viscosity of solution in ICET Test #1 at 60.0°C. 45
Figure 36. Kinematic viscosity of solution in ICET Test #1 at 23.0°C. 46
Figure 37. Sample 1220-U at 25°C rheology. Blue data lines (boxes) indicate viscosity. Red data lines (circles) indicate shear stress. 48
Figure 38. 1220-F at 25°C rheology. Blue data lines (boxes) indicate viscosity. Red data lines (circles) indicate shear stress. 48
Figure 39. 1220 U and 1220 F viscosity series comparison at 25°C. 49
Figure 40. 1220 U and F series viscosity comparison at 60°C. 49
Figure 41. 60°C viscosity aging study plot. 50
Figure 42. 25°C viscosity aging study plot. 50
Figure 43. Aluminum concentration trend in ICET Test #1 daily water samples. 51
Figure 44. Calcium concentration trend in ICET Test #1 daily water samples. 51
Figure 45. Copper concentration trend in ICET Test #1 daily water samples. 52
Figure 46. Silicon concentration trend in ICET Test #1 daily water samples. 52
Figure 47. Zinc concentration trend in ICET Test #1 daily water samples. 53
Figure 48. Sodium concentration trend in ICET Test #1 daily water samples. 53
Figure 49. Electron micrograph magnified 50,000 times for the Day-15 filtered test sample. 55
Figure 50. Electron micrograph magnified 4000 times for the Day-30 unfiltered test sample. 56
Figure 51. Electron micrograph magnified 10,000 times for the Day-30 unfiltered test sample. 57
Figure 52. Electron micrograph magnified 50,000 times for the Day-30 unfiltered test sample. 57
Figure 53. TEM image magnified 20 times for Day-15 filtered water sample. 58

Figure 54. TEM micrograph magnified 20 times from the Day-30 unfiltered sample. (TEM-U-20cm-bin-03) 59
Figure 55. Intensity vs scattering angle for post-T1 dry sludge (sample 1), bottom–moist paste, top–dry powder. 60
Figure 56. Intensity vs scattering angle for post-T1 dried sludge (sample 2). 60

TABLES

Table 1. Material Quantity/Sump Water Volume Ratios for the ICET Tests 16
Table 2. Test Series Parameters 17
Table 3. Methods for Chemical Analysis 23
Table 4. Range of Weight Gains for Each Unsubmerged Coupon Material Type 32
Table 5. NUKON™ Glass Composition 32
Table 6. Metal Concentrations for ICET Test #1 54
Table 7. Composition of Precipitates 61
Table 8. Main Elemental Components of Precipitate 62
Table 9. Filtered Precipitate ICP Results 62
Table 10. Solid Sample and Reference ICP Results 63
Table 11. Elemental Composition (wt %) of 30-Day High-Volume Filtrate 63

EXECUTIVE SUMMARY

The U.S. Nuclear Regulatory Commission (NRC) Office of Nuclear Regulatory Research has developed a comprehensive research program to support resolution of Generic Safety Issue (GSI)-191. GSI-191 addresses the potential for debris accumulation on pressurized-water-reactor (PWR) sump screens with the consequent loss of emergency-core-cooling-system (ECCS) pump net-positive-suction-head margin. Among the GSI-191 research program tasks is the experimental investigation of chemical effects that may exacerbate sump-screen clogging.

The Integrated Chemical Effects Test (ICET) Project represents a joint effort by the U.S. NRC and the nuclear utility industry, undertaken through the Memorandum of Understanding on Cooperative Nuclear Safety between NRC and EPRI, Addendum on Integral Chemical Effects Testing for PWR ECCS Recirculation. The ICET Project simulates the chemical environment present inside a containment water pool after a loss-of-coolant-accident and monitors the chemical system for an extended period of time to identify the presence, composition, and physical characteristics of chemical products that form during the test. The ICET test series is being conducted by Los Alamos National Laboratory at the University of New Mexico, with the assistance of professors and students in the civil engineering department.

This report describes the ICET experimental apparatus and surveys the principal findings of Test #1. As an interim data report compiled during preparation for subsequent ICET tests, this description summarizes both primary and representative findings that were available at the time the report was prepared. It is anticipated that additional analyses will be conducted by the NRC and the nuclear power industry to enhance the understandings obtained from this test.

All of the ICET tests are being conducted in an environment that simulates expected containment pool conditions during recirculation. The initial chemical environment contains 2800 mg/L of boron, 100 mg/L of hydrochloric acid (HCl), and 0.7 mg/L of lithium hydroxide (LiOH). Tests are conducted for 30 days at a constant temperature of 60°C (140°F). The materials tested within this environment include representative amounts of submerged and unsubmerged aluminum, copper, concrete, zinc, carbon steel and insulation samples. Representative amounts of concrete dust and latent debris are also added to the test solution. Tests consist of an initial 4-hour spray phase to simulate containment spray interaction with the unsubmerged samples. Water is circulated through the bottom portion of the test chamber during the entire test to achieve representative flow rates over the submerged specimens.

ICET Test #1 was conducted using NaOH to control pH, with a target pH of 10. Insulation samples consisted of scaled amounts of NUKON™ fiberglass material. In addition, 373 metal coupon samples and 1 concrete sample were contained within the test apparatus. Process control consisted of monitoring online measurements of recirculation flow rate, test solution temperature, and pH. Flow rate and temperature were controlled to maintain the desired values of 25 gpm and 140°F. Daily water samples were obtained to conduct pH, turbidity, total suspended solids, kinematic viscosity, and shear-dependent viscosity measurements, and for analytical laboratory evaluations of the chemical elements present. In addition, microscopic evaluations were conducted on water sample filtrates, fiberglass, coupons, sediment, and precipitated solids.

An initial amount of NaOH was included with the test solution and the other test chemicals before the test. The remaining NaOH was injected during the first 30 minutes of the 4-hour spray phase, and the amount of injected NaOH was determined so that the spray fluid pH did not exceed a value of 12 during the injection phase. At the end of NaOH injection, the test solution pH was approximately 9.5. The test solution pH decreased slightly during the test and was approximately 9.4 at the end of the test. The test

ran uninterrupted for 30 days, and the conditions were maintained within the accepted flow and temperature ranges.

Observations of the test solution indicated different behavior of the solution at room temperature vs test temperature. At 140°F, no chemical byproducts were visible in the water. However, at room temperature, precipitates were observed after 8 hours into the test and throughout the 30-day run. Turbidity and total suspended solids also increased from test temperature as the solution was cooled to room temperature.

Analyses of the test solution indicated that high levels of aluminum were present, with levels rising from near zero at the beginning of the test to approximately 350 mg/L after 20 days of testing. This effect was further indicated in posttest examinations of the submerged aluminum sample coupons, each of which lost approximately 25% of its pretest mass.

Examinations of fiberglass taken from the test apparatus after 15 days of testing indicated evidence of chemical products and a web-like material that spanned individual fibers. After 30 days of testing, the web-like material was more prevalent, and contiguous webbing appeared to span multiple fibers.

Daily measurements of the constant-shear kinematic viscosity revealed an approximately constant value at test temperature for both filtered and unfiltered samples. However, upon cooling to room temperature, the filtered and unfiltered sample viscosity started increasing after approximately 4 days of testing through approximately 23 days. Shear-dependent viscosity measurements indicated that the test solution was representative of Newtonian fluid. Samples from the second half of the test exhibited non-Newtonian behavior upon cooling to room temperature.

The ICET test series is being conducted under an approved quality assurance (QA) program, and QA procedures and project instructions were reviewed and approved by the project sponsors. Analytical laboratory results are generated under an EPA-approved quality control (QC) program, and other laboratory analyses are performed using standard practices as referenced in the body of this report.

ACKNOWLEDGMENTS

The principal authors of this report gratefully acknowledge the assistance of the following persons, without whom successful completion of the first Integrated Chemical Effects Test (ICET) could not have been accomplished. Graduate students Will Roesch and James Madrid of Los Alamos National Laboratory's (LANL's) Nuclear Design and Risk Analysis Group worked tirelessly to help design and construct the apparatus, manage all aspects of sample coupon preparation, and assist with daily water sampling. Mr. John Gisclon, the Electric Power Research Institute ICET Test Program Lead, contributed much practical, timely advice on preparation of the quality assurance (QA) program and experimental procedures and spent several weekends of personal time observing and helping to guide preparation of the test apparatus. Mr. Tim Andreychek of Westinghouse Electric Company, LLC, coordinated preparation of the ICET test plan and provided practical advice on the instrumentation and experimental procedures implemented for the test series. Dr. Al Csontos from the United States Nuclear Regulatory Commission (NRC) was instrumental in identifying the diagnostic methods and University of New Mexico resources needed for sample inspection and identification of gelatinous chemical reaction products. Mr. Michael Niehaus from Sandia National Laboratories provided a characterization of time-dependent strain-rate viscosity measurements for the circulating solution. Dr. William Kubic of LANL's Nuclear Design and Risk Analysis Group (D-5) performed initial literature reviews explaining the various precursor indications of gel formation and reviewed chemical engineering calculations critical to test performance quality. Mr. Luke Bartlein, also of Group D-5, contributed to the design and fabrication of the test tank and specification of equipment. Mr. James Young, of Group PS-1, provided valuable reviews and inputs to QA documentation and practices. The authors also express their gratitude for the contributions and continued participation of numerous NRC staff members who reviewed the QA program, test procedures, project instructions, and preliminary data to ensure relevance to plant safety, high-quality defensible results, and timely execution of this test.

Ms. Nancy Butner provided invaluable assistance with project management, budget analysis and reporting, contract administration, and final report preparation.

ABBREVIATIONS

BSE	Back-Scattered Electron
CPVC	Chlorinated Polyvinyl Chloride
DAS	Data Acquisition System
DHR	Decay Heat Removal
ECCS	Emergency Core-Cooling System
EDS	Energy-Dispersive Spectroscopy
EPRI	Electric Power Research Institute
ICET	Integrated Chemical Effects Tests
ICP-AES	Inductively Coupled Plasma-Atomic Emission Spectroscopy
IOZ	Inorganic Zinc
LANL	Los Alamos National Laboratory
LCS	Lab Control Spike
LOCA	Loss-of-Coolant Accident
MB	Method Blank
MD	Matrix Duplicate
MS	Matrix Spike
MSDA	Matrix Spike Duplicate Accuracy
NRC	Nuclear Regulatory Commission
NTU	Nephelometric Turbidity Unit
ppt	Precipitate
PVC	Polyvinyl Chloride
PWR	Pressurized-Water Reactor
QA	Quality Assurance
QC	Quality Control
RO	Reverse Osmosis
SEI	Secondary Electron Image
SEM	Scanning Electron Microscopy
SS	Stainless Steel
T1	ICET Test #1
TEM	Transmissive Electron Microscopy
TSP	Trisodium Phosphate
TSS	Total Suspended Solid
UNM	University of New Mexico
U.S.	United States
XRD	X-Ray Diffraction
XRF	X-Ray Fluorescence

1.0 INTRODUCTION

The Integrated Chemical Effects Test (ICET) Project represents a joint effort by the United States (U.S.) Nuclear Regulatory Commission (NRC) and the nuclear utility industry[1] to simulate the post-loss-of-coolant-accident (LOCA) chemical environment present inside a containment structure and to monitor the chemical system for an extended period of time to identify the presence, composition, and physical characteristics of chemical products that may form. Among the many secondary objectives (not addressed by the ICET Project), should products of this nature be found during the ICET series, are interests in determining the cause and potential quantity of the products and to characterize their head-loss properties in combination with fibrous debris. The ICET test series is being conducted by Los Alamos National Laboratory (LANL) at the University of New Mexico (UNM), with the assistance of professors and students in the civil engineering department.

This report describes the ICET experimental apparatus and procedures and surveys the principal data and observations from Test #1. As an interim data report compiled during preparation for subsequent ICET tests, this exposition summarizes both primary and representative findings, but it cannot be considered comprehensive. For example, only a small selection out of several hundred photographs is presented here. In addition, this report focuses on the presentation of observations and data without in-depth analyses or interpretations. Observed trends and typical behaviors are noted. Section 2 of this report presents more thoroughly the objectives and background of the ICET test series. Section 3 describes the experimental apparatus, the analytic methods used to characterize samples, and the quality assurance (QA) process that governs the performance of these tests. Section 4 presents key results in both graphical and narrative form. Section 5 addresses some of the practical lessons learned during Test #1 and makes recommendations for minor changes to the experimental procedure to improve subsequent tests.

2.0 BACKGROUND AND OBJECTIVE

Containment buildings of pressurized-water reactors (PWRs) are designed to accommodate the energy release following a postulated accident. They also permit recirculation of reactor coolant and emergency-core-cooling-system (ECCS) water to the decay heat removal (DHR) heat exchangers. The water collected in the sump from the reactor coolant system, the safety injection system, and the containment spray system is recirculated to the reactor core to remove residual heat. The sump contains a screen that protects system structures and components in the containment spray and emergency-core-cooling-system (ECCS) flow paths from the effects of debris that could be transported to the sump. Concerns have been raised that fibrous insulation material could form a mat on the screen, which would obstruct flow, and that chemical reaction products such as gelatinous or crystalline precipitates could migrate to the screen, causing further blockage and increased pressure-head losses across the debris bed. Other adverse chemical effects include the possibility of increased bulk fluid viscosity that also would increase flow losses through a debris bed.

The ICET test series was conceived as a limited-scope suite of five different tests containing different constituents, with each test lasting between 15 and 30 days. A complete rationale for the selection of these test conditions is provided in Ref. 2, but in brief, the ICET apparatus consists of a large stainless-steel (SS) tank with heating elements, spray nozzles, and associated recirculation pump and piping to simulate the post-LOCA chemical environment. Samples of structural metals, concrete, and insulation debris are scaled in proportion to their relative surface areas found in containment and in proportion to a maximum test dilution volume of 250 gal. of circulating fluid. Representative chemical additives, temperature, and material combinations are established in each test; the system then is monitored while corrosion and mixing occur for a duration comparable to the ECCS recirculation mission time.

The primary objectives for the ICET test series are to (1) determine, characterize, and quantify chemical reaction products that may develop in the containment sump under a representative post-LOCA environment; and (2) determine and quantify any gelatinous material that could be produced during the post-LOCA recirculation phase. For the purpose of this report, the term "gelatinous material" generically refers to any observed sample constituent with amorphous, hydrated, or noncrystalline physical characteristics. This adjective is sufficient to distinguish from chemical products that are crystalline in nature, but it is not intended to imply any specific head-loss behavior. The ICET series is not presently designed to test the head-loss characteristics of chemical products that might be observed.

3.0 EXPERIMENTAL MATERIALS AND METHODS

In this section are summarized the functional description and physical attributes of the ICET test apparatus, the ICET experimental plan and test matrix to provide context for the results of Test #1, several of the analytic methods that were applied for daily monitoring and sample analysis, and the QA program that is being followed during execution of the ICET series.

3.1 Chemical Test Apparatus Functional Description

The test apparatus was designed to meet the functional requirements of Ref. 2. Functional aspects of the test apparatus that meet those requirements are discussed as follows.

1. The central component of the system is a test tank. The test apparatus was designed to preclude the settling of solids in the test piping.

2. The test tank is capable of maintaining both a liquid and vapor environment, as would be expected in containment post-LOCA.

3. The test loop is capable of controlling the liquid temperature at 140°F within a range of ±5°F.

4. The system is capable of circulating water at flow rates that simulate spray flow rates per unit area of containment cross section.

5. The test tank provides for water flow over submerged test coupons, which is representative of containment pool fluid velocities expected at plants.

6. Piping and related isolation valves were provided such that a section of piping can be isolated without interrupting performance of the test.

7. The pump discharge line was split in two, with one branch directed to the spray header located in the vapor space inside the tank and the other branch returning to the liquid side of the tank. Each branch was provided with an isolation valve and flow meter.

8. A flow meter was provided in the recirculation piping.

9. The pump circulation flow rate is controlled at the pump discharge to be within ±5% of the flow required to simulate fluid velocities in the tank. Flow is controlled manually.

10. The tank accommodates a rack of immersed sample coupons, including the potential reaction constituents identified in the test plan.

11. The tank also accommodates six racks of sample coupons that are exposed to a spray of liquid that simulates the chemistry of a containment spray system. Provision was made for visual inspection of the spray rack.

12. The tank provides for sufficient space between the test coupons so as to preclude galvanic interactions among the coupons. The different metallic test coupons are electrically isolated from each other and the test stand to prevent galvanic effects resulting from metal-to-metal contact between specimens or between the test tank and the specimens.

13. The fluid volumes and sample surface areas were based on scaling considerations that relate the test conditions to actual plant conditions.

14. All components of the test loop were made of corrosion-resistant material (for example, SS for metallic components).

The as-built test loop consists of a test tank, a recirculation pump, 2 flow meters, 10 isolation valves, and pipes for connecting the major components, as shown schematically in Figure 1. Figure 2 and Figure 3 provide photographs of the test loop and the data acquisition system, respectively.

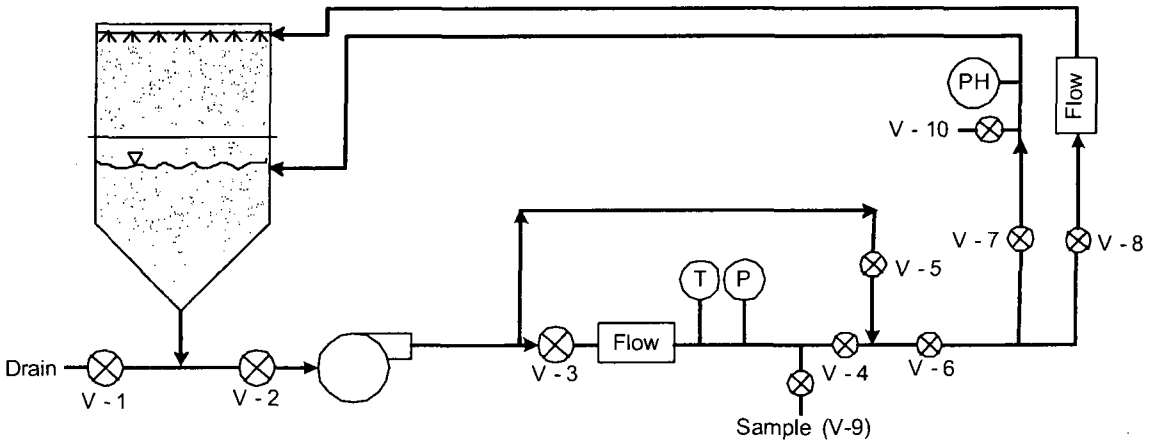

Figure 1. Test loop process flow diagram.

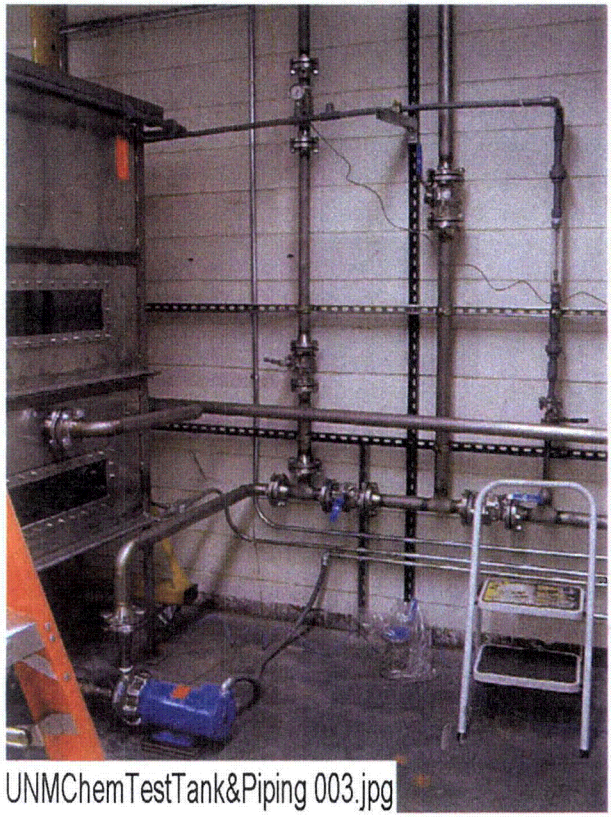

Figure 2. Photograph of the test loop.

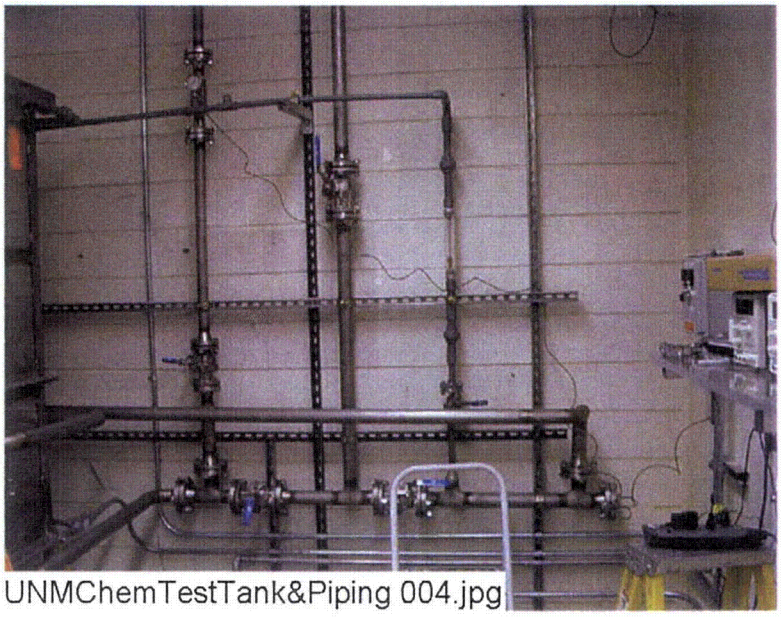

Figure 3. Photograph of the data acquisition system.

3.2 Chemical Tank Assembly and Circulation Details

3.2.1 Materials

The tank, piping, and components were designed of materials that are chemically resistant to a mixture of reverse-osmosis (RO)-treated water, sodium hydroxide (NaOH), trisodium phosphate (TSP), lithium hydroxide (LiOH), hydrochloric acid (HCl), and boric acid in a pH range of 7.0 to 12.0 and a temperature of 140°F. Only one pH control chemical, either NaOH (resulting in a pH of approximately 10) or TSP (resulting in a pH of approximately 7), is used in a given test. The tank is constructed of type 304 SS, with polycarbonate view windows and Goretex® gaskets. The bottom portion of the tank is constructed of 1/8-in.-thick sheet steel reinforced with 1/4-in.-thick by 2-in.-wide angle iron. The upper portion of the tank is constructed of 1/16-in.-thick sheet steel with 1/4-in.-thick by 2-in.-wide angle iron supports. The lid is 1/16-in.-thick sheet steel with 1/4-in.-thick by 2-in.-wide angle iron. One polycarbonate window with Goretex® gaskets is located in the bottom tank section, the top tank section, and the tank lid, for a total of three observation ports.

SS was used for the circulation piping to eliminate the possibility of chemical leaching from the material into the solution. SS also was chosen for the recirculation pump, tank internals, and instruments to ensure that no leaching occurred. To facilitate the construction and assembly of the flow path from the recirculation piping to the spray nozzles, a different material, chlorinated polyvinyl chloride (CPVC) piping, was chosen.

Although leaching from the SS was not an issue, some of the other materials could not be guaranteed against leaching based only on their material descriptions. Thus, separate leaching tests were conducted with bench-scale experiments. CPVC pipe and the solvent used to connect fittings were soaked in a solution of the test chemicals for five days at 70°C. The solution was then tested; results indicated that the level of chloride (the element that might be expected to leach) was not detectable. A secondary concern was whether the CPVC would absorb chemicals, notably boron or sodium. The samples were tested, and results indicated only trace amounts of boron and sodium.

Similarly, the Goretex® gasket material was tested for possible leaching in the test solution chemistry. Chloride and silica are the two elements that could possibly leach from the gasket material. It was found that the scaled amount that did leach was two orders of magnitude less than what was expected from the test additives and fiberglass insulation.

Thus, it was concluded that the test apparatus materials would not contribute chemically to the test solution in concentrations that would impact the test results.

3.2.2 Tank Sizing

The tank is designed to hold 250 gal. of chemical solution, with 2 to 3 inches between the top of the water level and the top half of the tank. The bottom half of the tank is designed to accommodate 250 gal. of solution, a single 60-coupon rack, and mesh cassettes containing 4 ft^3 of fiberglass insulation. The upper portion of the tank is designed to accommodate 6 coupon racks, each containing up to 60 coupons. The tank is nominally 4 ft × 4 ft × 6.6 ft in height, as shown in Figure 4.

Figure 4 through Figure 8 present photographs of the ICET tank, the cover lid, and the internal components, which include the top and bottom angle irons for supporting the racks, the distribution headers, the heaters, the thermocouples, and the spray nozzles.

Figure 4. External view of the ICET tank.

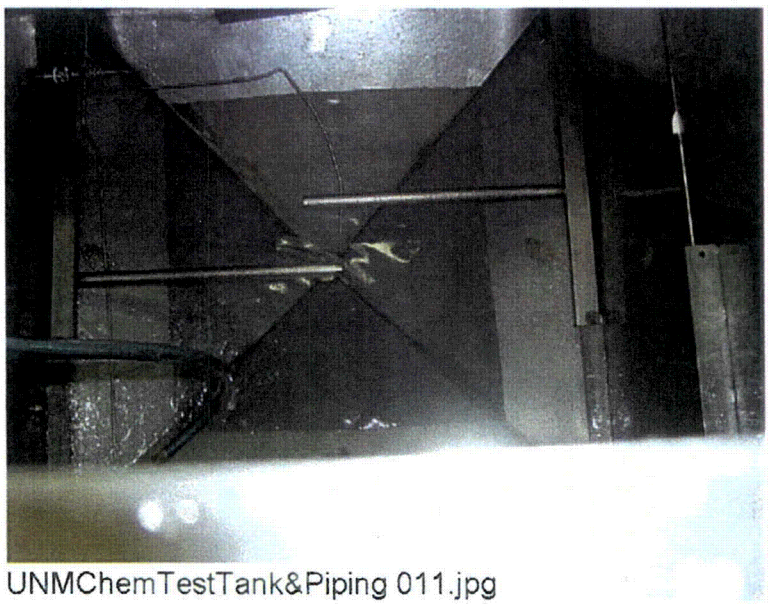

Figure 5. The distribution header, heaters, and thermocouples inside the lower tapered reservoir of the ICET tank.

Figure 6. **The top and bottom angle irons for supporting coupon racks in the upper section of the ICET tank.**

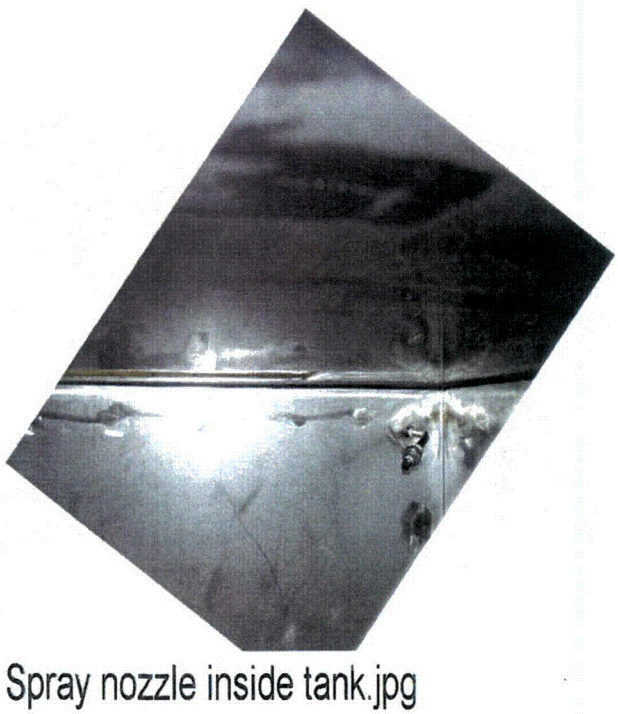

Figure 7. **One of four spray nozzles located in each upper corner of the ICET tank. This photo was taken through the upper access hatch while the lid was in place.**

Figure 8. The cover lid of the ICET tank showing the top observation window (lower) and top access hatch with handle (upper).

Figure 9 and Figure 10 present as-built dimensioned drawings of the tank and piping system from both the front and side views, respectively. Given that the tank system is oriented approximately along the standard geographic compass directions, the front view depicts the east face of the tank and the side view depicts the north face of the tank.

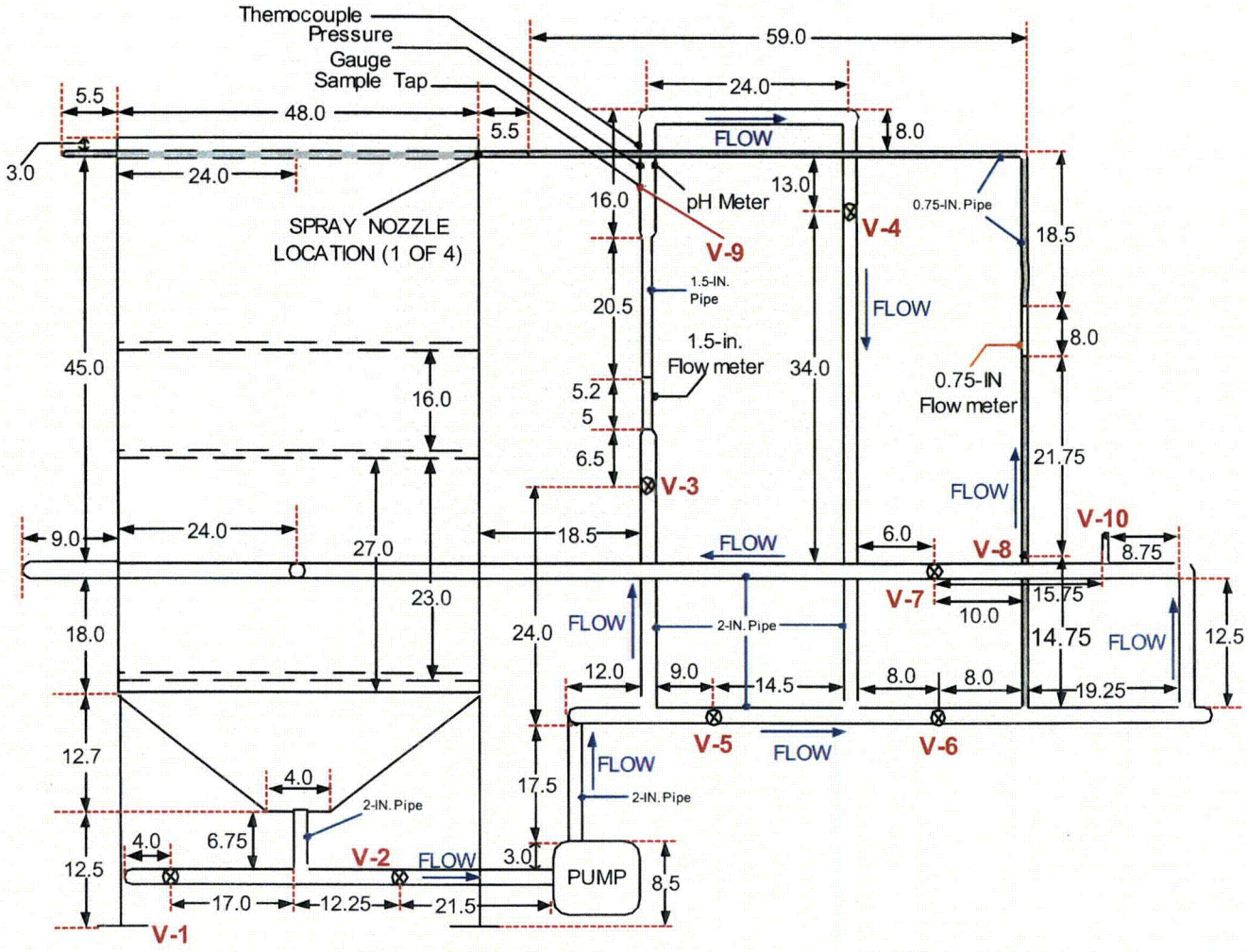

Figure 9. Front-view as-built dimensions of tank and piping system. Dimensions are in inches; shaded regions represent CPVC piping.

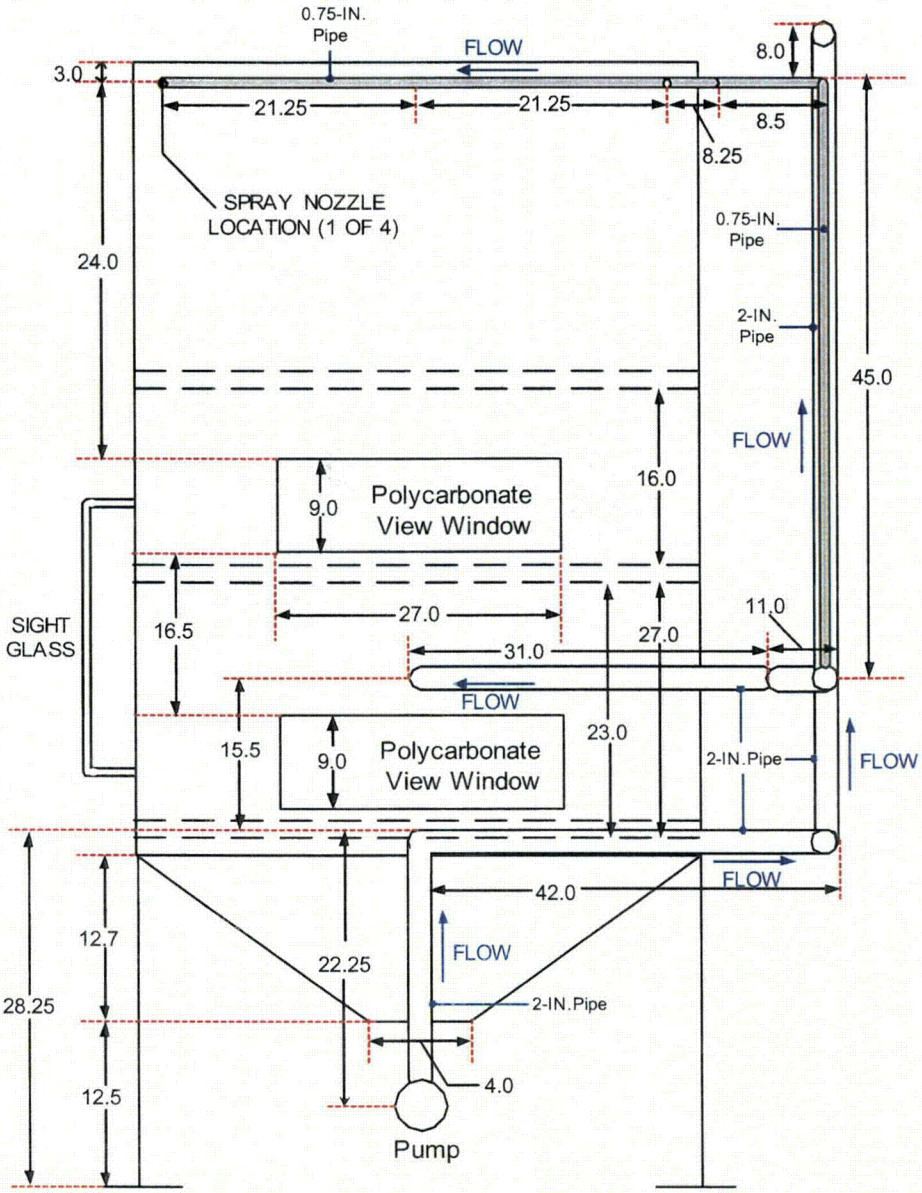

Figure 10. Side-view, as-built dimensions of tank and piping system. Dimensions are in inches; shaded regions represent CPVC piping.

3.2.3 Coupon Racks

The coupon racks are constructed of 1.5-in.-diam CPVC plastic piping. (see Figure 11). The racks prevent metal-to-metal contact between adjacent coupons and between the coupons and the rest of the tank assembly. This feature limits galvanic corrosion potential. Leaching tests were performed on the CPVC material and welding solvent to ensure that no detectable contributions to the chemical system would occur. Two complete sets of racks were built to facilitate staging of coupons for subsequent tests. The coupons can add up to 180 lb of weight to each CPVC-rack assembly. At elevated temperatures, the racks require support from 2-in.-wide SS angle irons strapped to the bottoms of the racks. These supports bridge the gap between the two sides of the tank and rest on the internal 2-in.-wide SS angle irons. A 16-

in. gap exists on each of the internal support angle irons to accommodate the lowering and emplacement of the nominal 14-in.-wide racks. The gap is then bridged with a length of angle iron that is pinned in place before the next tiers of racks are placed on top. See Figure 6 for the locations of the gaps and Figure 5 for an illustration of the short bridge angles.

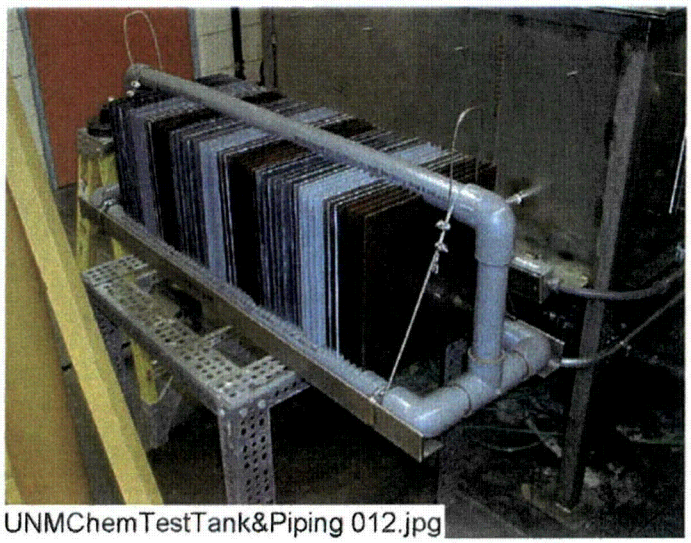

Figure 11. Photograph of a loaded coupon rack.

3.2.4 Tank Insulation

The tank is insulated with fiberglass boards. The surface area of the tank and top is approximately 130 ft^2. Approximately 50 linear feet of 2-in. diameter pipe remain uninsulated. The temperature of the fluid is nominally 140°F, and the outside surrounding air is approximately 70°F. The resulting heat loss from the tank and piping is approximately 1.2 kW.

3.2.5 Tank Heaters

The tank heaters are titanium jacketed to prevent corrosion and interaction of solution chemistry during the test series. Each heater is rated to supply 3.5 kW, thus providing excess (greater than the 1.2 kW required) redundant heating capacity and the ability to operate the tank assembly at higher temperatures if desired in the future. This additional capacity permits the convenience of having uninsulated piping runs. Under the existing electrical wiring configuration, only one heating element can be operated at a time. The locations of the two heaters inside the ICET tank are shown in Figure 5.

3.2.6 Pump Selection

The pump wetted parts are SS, and the seals are compatible with boric acid and sodium hydroxide solutions. The pump is sized to provide a flow rate of up to 100 gpm. The pump has a variable speed controller so that the desired flow can be achieved, regardless of the system head loss. Calculations of the desired velocities in the tank result in a nominal flow rate of approximately 25 gpm during test operation. A photograph of the pump selected for the ICET system is presented in Figure 12.

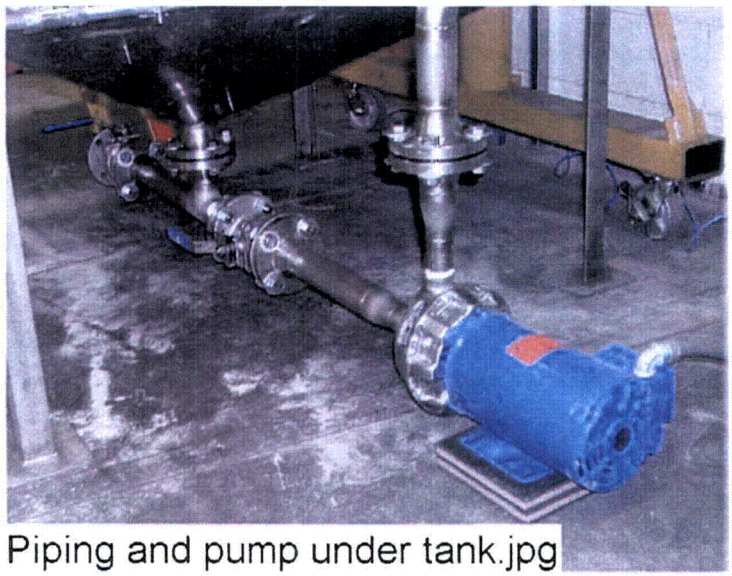

Figure 12. Circulation pump for the ICET system.

Each of the two injection flow headers, placed below the water line along the top of the submerged coupon rack, consists of a 1-in.-diam pipe with a symmetric pattern of holes to distribute the solution discharge. The desired flow velocity across the submerged coupons was accounted for, along with the desired loop flow rate and pump characteristics. The number and size of holes in the flow headers were calculated, and the holes were drilled symmetrically in each header. The primary goal of header design was to achieve a uniform flow pattern across the submerged coupons with velocities in the 0–3 cm/s range. During loop shakedown activities, plastic streamers were placed at various places in the tank to provide a visualization of the flow pattern. Then, the hole sizes were adjusted to achieve the desired pattern. Finally, food dye was introduced to determine the actual velocities. Tank velocities within the desired range were obtained.

The as-built configuration provides excess pressure head and flow capacity, even permitting for a doubling of the flow rate, if desired. A photograph showing one of the two parallel distribution headers is presented in Figure 5. One of the recirculation supply lines is shown in Figure 4 between the upper and lower observation windows.

3.3 Experimental Plan and Test Matrix

ICET test parameters were selected based on the results of surveys of U.S. nuclear power plants. Quantities of test materials were selected to preserve the scaling of representative ratios between material surface areas and total cooling-water volumes. Chemical additives also simulate the post-LOCA sump environment.

The materials included in the tests are zinc, aluminum, copper, carbon steel, concrete, and insulation materials, such as fiberglass and calcium silicate. The amounts of each material are given in Table 1 in the form of material-surface-areas to water-volume ratios, with the exceptions of concrete dust, which is presented as a mass to water-volume ratio, and fiberglass and calcium silicate, which are presented as insulation-volume to water-volume ratios. Also shown in the table are the percentages of the materials that are submerged and unsubmerged in the test chamber.

Table 1. Material Quantity/Sump Water Volume Ratios for the ICET Tests

Material	Value of Ratio for the Test (Ratio Units)	Percentage of Material Submerged (%)	Percentage of Material Unsubmerged (%)
Zinc in Galvanized Steel	8.0 (ft^2/ft^3)	5	95
Inorganic Zinc Primer Coating (Non-Top Coated)	4.6 (ft^2/ft^3)	4	96
Inorganic Zinc Primer Coating (Top Coated)	0.0 (ft^2/ft^3)	–	–
Aluminum	3.5 (ft^2/ft^3)	5	95
Copper (Including Cu-Ni alloys)	6.0 (ft^2/ft^3)	25	75
Carbon Steel	0.15 (ft^2/ft^3)	34	64
Concrete (Surface)	0.045 (ft^2/ft^3)	34	64
Concrete (Particulate)	0.0014 (lbm/ft^3)	100	0
Insulation Material (Fiberglass or Calcium Silicate)	0.137 (ft^3/ft^3)	75	25

The physical and chemical parameters, which are critical for defining the tank environment and have a significant effect on sump-flow blockage potential and gel formation, have been identified in Ref. 2. These physical and chemical parameters are summarized as follows.

Physical parameters:

Water volume in the test tank:	949 L	(250 gal.)
Circulation flow:	0-200 L/min	(0–50 gpm)
Spray flow:	0-100 L/min	(0–25 gpm)
Sump temperature:	60°C	(140°F)

Chemistry parameters:

H_3BO_3 concentration:	2800 mg/L as boron
$Na_3PO_4 \cdot 12H_2O$ concentration:	as required to reach pH 7 in the simulated sump fluid
NaOH concentration:	as required to reach pH 10 in the simulated sump fluid
HCl concentration:	100 mg/L
LiOH concentration:	0.7 mg/L as Li

The parameters planned for each ICET test run are described in Table 2.

Table 2. Test Series Parameters

Run	Temp (°C)	TSP $Na_3PO_4 \cdot 12H_2O$	NaOH	pH Target	Boron (ppm)	Note
1	60	N/A	Yes	10	2800	100% fiberglass insulation test. High pH, NaOH concentration, as required by pH (see Notes 2 and 3).
2	60	Yes	N/A	7	2800	100% fiberglass insulation test. Low pH, TSP concentration, as required by pH.
3	60	N/A	Yes	10	2800	80% calcium silicate/20% fiberglass insulation test. High pH, NaOH concentration, as required by pH (see Note 3).
4	60	Yes	N/A	7	2800	80% calcium silicate/20% fiberglass insulation test. Low pH, TSP concentration, as required by pH.
5	60	TBD	TBD	TBD	TBD	Confirmatory test; one of the above four tests will be repeated.

Notes:

1. The parameters in Table 2 are those presented in Reference 2, which was active when Test #1 was conducted. Subsequent revision of Reference 2 reversed the order of Tests #3 and #4.
2. The duration of Test #1 will be 30 days.
3. During the first 30 min of Tests #1 and #3, NaOH will be injected in the spray fluid.

   The quantity of NaOH injected in the spray solution is subject to the following constraints:

   a. The pH of the spray fluid shall not exceed a value of 12 during this initial 30-min injection phase; and

   b. The target pH of the simulated sump fluid inventory at the termination of the containment spray simulation (e.g., after the 30-min NaOH injection phase), not considering pH effects due to CO_2 absorption and other chemical effects that may be occurring during NaOH injection, is a value of pH = 10.

3.4 Analytical Methods

Data collected during Test #1 include the on-line measurements of temperature, pH, and loop flow rate. During the water grab sample analysis, bench-top measurements are obtained for temperature, pH, turbidity, total suspended solids (TSSs), and kinematic viscosity. Water, fiberglass, and metal samples are taken to other laboratory locations for additional analyses. These analyses include strain-rate viscosity, scanning electron microscopy (SEM), energy dispersive spectrometry (EDS), transmission electron microscopy (TEM), inductively coupled plasma mass spectrometry (ICP), x-ray fluorescence (XRF), and x-ray diffraction (XRD). Shear-rate viscosity is discussed in Section 4.5.6. The other analytical methods are described below.

3.4.1 Scanning Electron Microscopy (SEM)

The primary use of SEM is to study the surface topography of solid samples. The resolution of this technique is approximately two orders of magnitude better than optical microscopes and one order of magnitude less than TEM.[3] Scanning electron microscopy (SEM) was used to examine the precipitate from the Day-15 and Day-30 high-volume water samples.

3.4.1.1 Principle of Operation

An electron beam passing through an evacuated column is focused by electromagnetic lenses onto the specimen surface. The beam is then scanned over the specimen in synchrony with the beam of the cathode-ray display screen. The incident beam electrons (from the electron gun) do not simply reflect off the sample surface. As the beam travels through the sample, it can do three things: First, it can pass through the sample without colliding with any of the sample atoms (matter is mostly space). Second, it can collide with electrons from the sample atoms, creating secondary electrons. Third, it can collide with the nucleus of the sample atom, creating a backscattered electron.[4]

The incident beam is composed of highly energized electrons. If one of these electrons collides with a sample atom electron, an electron will be knocked out of its shell.

Figure 13[5] illustrates this action. The released electron is called a secondary electron and is weak in energy. If these secondary electrons are close enough to the sample surface, they can be collected to form an SEM image.

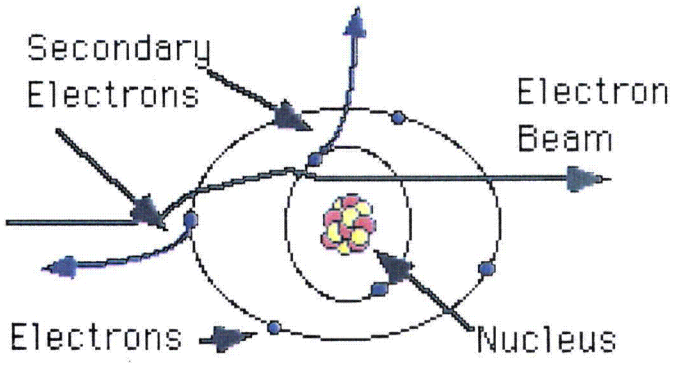

Figure 13. Production of secondary electrons from an electron beam.

The incident beam electron loses little energy in this collision. In fact, a single electron from the beam will produce a shower of thousands of secondary electrons until it does not have the energy to knock these electrons from their shells. Inelastically scattered secondary electron emission from the sample is used to modulate the brightness of the cathode ray display screen, thereby forming the image.

If the incident beam collides with a nucleus of a sample atom, it bounces back out of the sample as a backscattered electron (Figure 14).[6] These electrons have high energies, and because a sample with a higher density will create more of them, they are used to form backscattered electron images, which generally can discern the difference in sample densities. In this case, the image contrast is determined largely by compositional differences of the sample surface rather than by topographic features. Additional information on SEM may be found in Goldstein.[7]

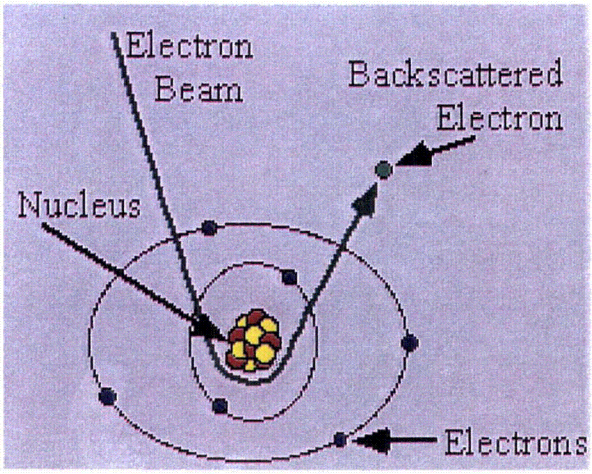

Figure 14. Production of backscattered electrons from an electron beam.

3.4.1.2 Limitations

The principle limitations of SEM are the resolution. Typical resolution is limited to between 1.5 and 3 nm, which is approximately an order of magnitude less than TEM.[8] In addition, only the surface of the specimen can be viewed. Finally, the SEM operates under high vacuum and therefore is unsuitable for examination of materials with a liquid component without suitable drying.

3.4.2 Energy Dispersive Spectroscopy (EDS)

EDS can provide information on the elemental composition of a specimen. Combining the EDS system with the SEM allows the microstructure-level identification of compositional gradients at grain boundaries, second phases, impurities, inclusions, and small amounts of material. EDS was used to examine the various structures formed on the fibers, which are similar for the Day-15 and Day-30 test samples. This examination allowed for a quantitative estimate of the elemental composition of the precipitate and the material deposited between the fibers.

3.4.2.1 Principle of Operation

As an incident electron beam interacts with the specimen, it loses energy. Characteristic x-rays are in turn emitted by the atomic species in the material. These characteristic x-rays are then converted into an electrical pulse with specific characteristics of amplitude and width. A multichannel analyzer measures the pulse and increments as a corresponding "energy slot" in a monitor display. The location of the slot is proportional to the energy of the x-ray photon entering the detector. The display is a histogram of the x-ray energy received by the detector, with individual "peaks," the heights of which are proportional to the amount of a particular element in the specimen being analyzed.[9] Additional information on EDS may be found in Goldstein.[10]

3.4.2.2 Limitations

The design of the equipment complicates the technique of detecting elements lighter than carbon. In general, a poorer sensitivity for light elements (low atomic weight) also exists in a heavy matrix. Resolution of the x-ray energy levels limits the positive identification of certain elements due to

overlapping energy slots. Quantitative analysis is usually limited to flat, polished specimens. Unusual geometries, such as fracture surfaces, individual particles, and films on substrates can be analyzed, but with considerably greater uncertainty.[11]

3.4.3 Transmission Electron Microscopy (TEM)

TEM is used to study the local structure, morphology, and chemistry of materials by examining the diffracted and transmitted electron intensities, as well as the characteristic x-rays and energies lost by the incident beam. TEMs are often coupled with EDS to give information about the local chemistry of the material. The high resolution of the transmission electron microscope (TEM), at least an order of magnitude greater than SEM, allows for qualitative size assessment of the underlying visible structures and aggregates. TEM was used on the precipitate from the 15-day and 30-day high volume samples.

3.4.3.1 Principle of Operation

In transmission electron microscopes, a beam of high-energy electrons, typically 100–400 KeV, is generated. The generated beam then is collimated by a magnetic lens and allowed to pass through the specimen under high vacuum. The resulting diffraction pattern, which consists of a transmitted beam and many diffracted beams, can be imaged on a fluorescent screen below the specimen. From the diffraction pattern, the lattice spacing information for the structure under consideration can be obtained. Alternatively, the transmitted beam or one of the diffracted beams can be used to form a magnified image of the sample. Finally, if the transmitted beam and one or more of the diffracted beams are allowed to recombine, a high-resolution image can be obtained that contains information about the atomic structure of the material.[12]

As the incident electron beam interacts with the specimen, it loses energy. Characteristic x-rays are in turn emitted by the atomic species in the material. These characteristic x-rays and the energy losses suffered by the incident electron then can be detected and analyzed to yield the EDS spectrum. Additional detail on TEM may be found in Williams.[13]

3.4.3.2 Limitations

A TEM can have extremely high resolution, and research-level instruments can see individual atoms. However, a TEM has some limitations because the electron beam must travel through the sample, and lengthy sample preparation is usually required to make the sample thin enough. Because the beam is traveling though the sample, the sample bulk, not the surface, is being imaged.[14]

3.4.4 Inductively Coupled Plasma by Atomic Emission Spectroscopy (ICP-AES)

ICP-AES is a rapid, sensitive way of measuring the elemental concentrations of solutions. More than 75 elements can be determined. ICP was used to determine the elemental composition of the daily water samples to assist in the overall understanding of the solution chemistry and corrosion behavior.

3.4.4.1 Principle of Operation

The first step in the procedure is conversion of the molecules in the sample to individual atoms and ions using a high-temperature, radio-frequency-induced argon plasma. The sample is introduced into the plasma as a solution. The sample is then pumped to a nebulizer, where it is converted to a fine spray and mixed with argon in a spray chamber. The purpose of the spray chamber is to ensure that only droplets in a narrow size range make it through into the plasma. Most of the sample drains away from the chamber; the rest is carried into the plasma and instantly excited by the high temperatures (5000–10,000 K). Atoms

become ionized with 99% efficiency. The excited elements emit photons that are detected by one or more photomultiplier tubes.[15] Additional information on ICP may be found in Montaser.[16]

3.4.4.2 Limitations

A notable limitation is the inability to measure hydrogen, carbon, nitrogen, and oxygen. In addition, silicon quantification is determined better by XRF because silicon will be lost to the vapor phase during ICP acid digestion procedures (as will certain trace elements, such as Hg, Se, As, and possibly Pb and Cd). The other notable disadvantage with the technique is that some minerals may not dissolve completely when employing the digestion procedure needed to use the ICP. Therefore, for samples containing substantial amounts of minerals (solids must be dissolved before analysis), XRF analysis is probably more appropriate for elemental determination. Interferences may also occur during ICP-AES due to overlap of the emission lines from the analyte and the interfering element and due to matrix effects. Finally, ICP is not suitable for determination of chemical speciation.[17]

3.4.5 X-Ray Fluorescence (XRF)

This x-ray technique is used to determine, both qualitatively and quantitatively, the elemental composition of a wide range of materials. XRF was used to examine the high volume water sample precipitate on days 15 and 30.

3.4.5.1 Principle of Operation

XRF is based on the photoelectric effect. When an atom is irradiated with highly energetic photons, an electron from one of the inner shells may be ejected (Figure 15). As the vacancy is filled by an electron from an outer shell, a photon is released, the energy of which is characteristic of the atom. This radiation is called fluorescent radiation, and each element has its own set of characteristic emission lines. The intensity and the energy of these lines are measured using a spectrometer that detects wavelength-dispersive XRF or energy-dispersive XRF.[18] Additional detail on XRF may be found in Jenkins.[19]

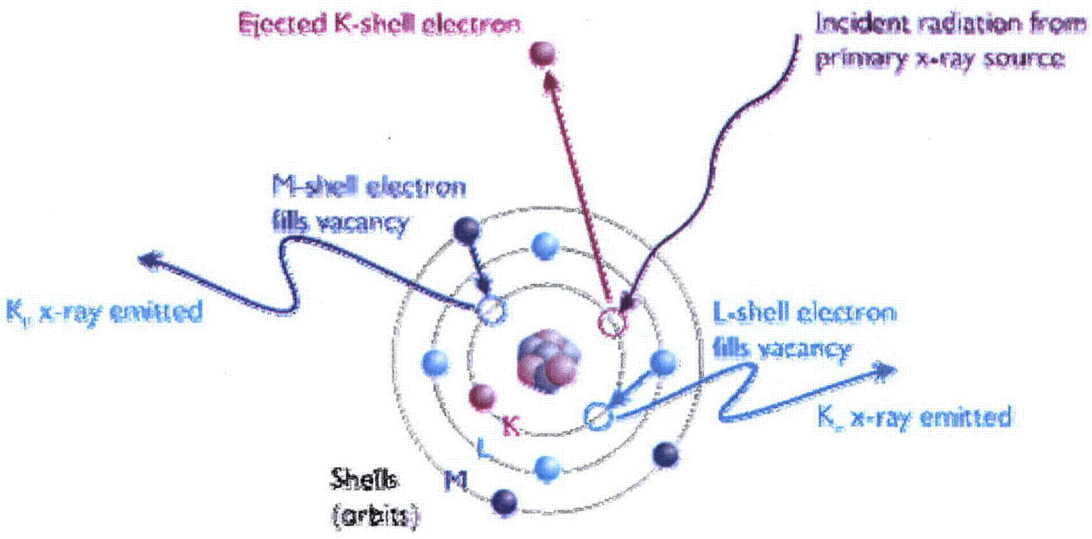

Figure 15. Illustration of the operation principle of XRF.

3.4.5.2 Limitations

The accuracy of the results depends on how closely the standards resemble the sample. In addition, the principle limitation with this technique is the decreased sensitivity that occurs with decreasing atomic weight. Most XRF instruments cannot reliably detect elements lighter than carbon. Another limitation is that for accurate quantitative analysis, standards that are similar in composition and morphology to the unknown are required.[20]

3.4.6 X-Ray Diffraction (XRD)

X-ray powder diffraction is used to obtain information about the structure, composition, and state of polycrystalline materials. The determination of the crystalline structure of the precipitate allows for the development of an understanding of the means by which the precipitate is formed. XRD analyses were performed on the post Test Sludge precipitate.

3.4.6.1 Principle of Operation

If a beam of monochromatic x-rays is directed at a crystalline material, reflection or diffraction of the x-rays is observed at various angles with respect to the primary beam. The relationship between the wavelength of the x-ray beam, λ, the angle of diffraction, 2θ, and the distance between each set of atomic planes of the crystal lattice, d, is given by the Bragg equation:

$$N\lambda = 2\,d\sin\theta$$

where N represents the order of diffraction.

From this equation can be calculated the interplanar distances of the crystalline being studied. The interplanar spacing depends solely on the dimension of the crystal's unit cell, whereas the intensities of the diffracted rays are a function of the placement of the atoms in the unit cell.[21] Additional detail on XRD may be found in Barrett.[22]

3.4.6.2 Limitations

Conventionally, the largest limitation of XRD is its restriction to crystalline materials because amorphous materials do not diffract. Milligram samples may be analyzed if the analysis time is not important. The requirement of sample quantity (typically several hundred milligrams) is to provide the enormous number of small crystallites oriented in every conceivable direction. Thus, when an x-ray beam traverses the material, a significant number of the particles can be expected to be oriented to fulfill the Bragg condition for reflection from every conceivable interplanar spacing.

3.4.7 Wet Chemistry Analyses

The standard methods used for wet chemistry analyses are shown in Table 3. Additionally, the following paragraphs provide supplemental data for nonstandard methods and quality control practices.

Table 3. Methods for Chemical Analysis

Parameter	Method[a]	Major Equipment
pH	SM 4500-H^+ (Electrometeric)	Orion Model 720 A
Turbidity	SM 2130 (Nephelometeric)	Hach Turbidimeter Model 18900
Total Suspended Solids	SM 2540D	–
Temperature	SM-2550	–
Kinematic Viscosity	–	Cannon-Fenske Capillary Viscometer

[a]SM = Standard Methods for the Examination of Water and Wastewater (20th Edition) (APHA et al. 1998).

The pH meter was calibrated before use with a three-point calibration curve using certified pH buffers at 4, 7, and 10. An automatic temperature compensation pH probe was used to provide a temperature-corrected pH. The pH was recorded to the nearest 0.01 pH unit.

The turbidimeter was calibrated with Gelex secondary standards before testing. Turbidity was recorded to the nearest 0.01 Nephelometric Turbidity Unit (NTU).

For TSS, the glass fiber filters were weighed in aluminum boats for the pre-sample and post-sample weights. A standard volume of approximately 500 ml was filtered for all samples. The TSS was recorded to the nearest 0.1 mg/L.

3.4.7.1 Constant-Shear Kinematic Viscosity

Kinematic viscosity was measured with a Cannon-Fenske capillary viscometer. Viscosity was measured on both filtered and unfiltered samples, each at a temperature of 60 (±1.0)°C [140 (±1.8)°F] and again at 23 (±2.0)°C [73.4 (±3.6)°F]. The viscosity of water is highly sensitive to temperature, and the allowed temperature range results in a variation of viscosity of 2% between 59°C (138.2°F) and 61°C (141.8°F) and a 9.3% variation between 21°C (69.8°F) and 25°C (77.0°F). For this reason, temperature was measured to 0.1°C accuracy with a National-Institute-of-Standards-and-Technology-traceable thermometer for all viscosity measurements, and the measured viscosity values were corrected to a common temperature to facilitate comparisons. The corrected temperatures chosen for comparison were 60.0°C (140°F) and 23.0°C (73.4°F). Equations were derived to correct viscosity by fitting an equation to viscosity data and minimizing the coefficient of determination (R^2). The formulas used to correct the viscosity were

$$\nu_{23} = \nu_M \left(1.0235\right)^{(T_M - 23)}$$

and

$$\nu_{60} = \nu_M \left(1.0146\right)^{(T_M - 60)}$$

where

T_M = temperature at which viscosity measurements are made (°C),
ν_M = measured kinematic viscosity at temperature T_M (mm^2/s),
ν_{60} = kinematic viscosity corrected to 60.0°C (mm^2/s), and
ν_{23} = kinematic viscosity corrected to 23.0°C (mm^2/s).

In addition, duplicate measurements were made at each condition until Day 25 of the test. In nearly all cases, the replicate viscosity measurements varied by considerably less than 1%. On December 16, 2004, Day 25 of the test, duplicate measurements of viscosity were no longer taken because of the consistency previously noted.

3.5 QA Program

A project QA manual was developed to satisfy the contractual requirements that apply to the ICET Project. Specifically, those requirements were to maintain an appropriate level of QA in the areas of test loop design, sampling, chemicals, operation, and analysis to provide for credible results. These requirements were summarized in the contract requirement that QA was to be consistent with the intent of the appropriate sections of 10CFR50, Appendix B.

The 18 criteria of 10CFR50, Appendix B, were addressed separately in the QA manual, and the extents to which they apply to the ICET Project were delineated. A resultant set of QA procedures was developed. In addition, project-specific instructions were written to address specific operational topics that required detailed step-by-step guidance. Test #1 project instructions were written for the following topics:

- Data Acquisition System (DAS)
- Coupon Receipt, Preparation, Inspection, and Storage
- Pre-Test Operations
- Test Operations, Test #1 (NaOH at pH = 10)
- Chemical Sampling and Analysis
- Post-Test Operations
- DAS Alarm Response

All aspects of the ICET Project QA Program were reviewed and approved by the Project sponsors. Project personnel were trained in the QA manual, QA procedures, and project instructions.

3.5.1 ICP Quality Control

To ensure the accuracy of the ICP results, several QA analyses are performed with every batch of samples run on the instrument. The QA samples are as follows:

Lab Control Spike (LCS): The LCS consists of a known concentration of each analyte (typically 1 to 5 mg/L, depending on analyte) in deionized water. The measured concentration is compared with the spike concentration, and a percent recovery is reported. An exception is noted if the percent recovery of any analyte is outside of the acceptable range. The acceptable range is based on previous QA procedures developed for the instrument.

Method Blank (MB): The MB is a sample of deionized water. All analytes are expected to be below the detection limit. An exception is noted if the measured concentration of any analyte is above the detection limit.

Matrix Duplicate (MD): The MD is a second analysis of one of the samples in the run. The measured concentration for each analyte is compared between the two samples, and an exception is noted if the two results do not agree to within 20 percent.

Matrix Spike (MS): The MS consists of a known concentration of each analyte (typically 1 to 5 mg/L, depending on analyte) added to one of the samples in the run. The difference in the measured

concentrations between the original sample and spiked sample is compared with the spike concentration, and a percent recovery of the spiked concentration is reported. An exception is noted if the percent recovery of any analyte spike is outside of the acceptable range.

Matrix Spike Duplicate Accuracy (MSDA): The MSDA is a repetition of the MS. An exception on the MSDA is identical to an exception on the MS.

Matrix Spike Duplicate Precision: The two runs of the matrix spikes (MS and MSDA) are compared with each other. An exception is noted if the two measured spike concentrations do not agree to within a relative percent difference of 20 percent.

Serial Dilution: One of the samples in the run is diluted with deionized water by a factor of 5. The measured concentration of the diluted sample is compared with predicted concentration, which is calculated from the dilution rate and the measured concentration of the original (undiluted) sample. An exception is noted if the differences between the measured and calculated concentrations are not within the acceptable range.

It was necessary for the analytical laboratory to perform a 10:1 dilution of the samples to lower the concentration of borate to reduce interferences between borate and the analytes. This process had the effect of raising the detection limit for these analyses to a value 10 times higher than the instrument detection limit, but the higher detection limit had no impact on the results. The instrument detection limit was significantly below 1 mg/L for all analytes, and the higher detection limit was still well below the levels of concern for this experiment.

4.0 EXPERIMENTAL RESULTS

This section begins with a description of the process control settings that were adjusted to match the target conditions specified for Test #1. Then representative results from every type of diagnostic are presented to illustrate the information that was monitored and collected on the ICET system for Test #1. This information is organized in categories relating more closely to operational activities than to diagnostic methods. For example, latent debris and chemical precipitates are presented in separate sections, even though SEM analysis was used for both types of sample. Data and photographs are provided here for the (1) coupon racks, (2) NUKON™ fiberglass samples, (3) concrete samples, (4) latent debris surrogate, (5) time-dependent solution chemistry, and (6) precipitated solids.

4.1 Test Operation and Sequence

4.1.1 Description

Preparation of ICET Test #1 (Run 1 in Table 2) began with the heating of 200 gal. of RO water to 60°C. Upon reaching the desired temperature, the premixed chemicals were added. Those chemicals consisted of boric acid, NaOH, LiOH, and HCl, which were added with the recirculation pump operating. After the chemicals were observed to be well mixed, an additional 50 gal. of RO water was added to reach the required test volume. The solution again was brought to the desired test temperature. Premeasured latent debris and concrete dust, metal coupons, and fiberglass samples then were put into the tank. After adding all required items into the tank, baseline grab samples and measurements of the test solution were taken.

Addition of the fiberglass and metal coupons took place on the evening of November 20, 2004. Because of the quantity of the metal mass added to the tank, the solution temperature dropped below the desired test range. The test apparatus was held in this state for approximately 12 hours until the next morning, when the temperature had again reached the desired value. Some settling of the added particulates was observed overnight, with the turbidity decreasing from 12 to 8 NTU over that time.

The experiment commenced at 10:00 A.M. on Sunday, November 21, 2004, and it ended on Tuesday, December 21, 2004, at 10:00 A.M. Time zero of the test commenced with initiation of the tank sprays, which lasted for 4 hours. During the first 30 minutes of the spray period, a chemical metering pump was used to inject, directly into the nozzle supply lines, additional NaOH into the solution. The total nozzle spray flow was 3.5 gpm, and the recirculation flow was set at 25 gpm. During the test, grab samples were taken on a daily basis for wet chemistry and ICP analyses. Water loss due to water sample removals and evaporation was made up with RO water. When the water inventory dropped to approximately 5% of the inventory (12.5 gal.), RO water was added to bring the inventory back to 250 gal. Over the course of the test, a total of 22 gal. of RO water was added, and the inventory at test termination was 239 gal. Post-test analyses of water samples, fiberglass, and metal coupons were performed. Sampling and analyses were conducted in accordance with approved project instructions.

4.1.2 Process Control

Process control consisted of monitoring online measurements of recirculation flow rate, test solution temperature, and pH. Flow rate and temperature were controlled to maintain the desired values.

Recirculation Flow Rate: The 30-day average recirculation flow rate was 95.2 L/min (25.1 gpm). The recorded recirculation flow rate had a standard deviation of 0.2 L/min, with a range of 94.3 to 98.2 L/min (24.9 to 25.9 gpm), excluding the spray cycle. Variations were slightly greater during the spray cycle

(range 88.8 to 99.1 L/min, or 23.5 to 26.1 gpm) because of the requirement to direct a portion of the flow manually to the spray nozzles.

Temperature: Temperature was recorded at three submerged locations in the ICET tank. The 30-day average recorded temperature at these locations was 60.1°C, 60.0°C, and 59.8°C (140.2°F, 140.0°F, and 139.6°F). The standard deviation in temperature recorded by all three thermocouples was within ±0.27°C (±0.48°F), with a maximum range of all thermocouples, of 58.5°C to 61.0°C (137.3°F to 141.8°F).

pH: The pH after initial chemical addition was complete was 9.1. During the 30 minutes of NaOH injection, the pH increased to 9.5. The pH value after NaOH injection was complete was within the range predicted by water chemistry calculations. The calculations predicted a pH between 9.4 and 10.0 at a standard temperature of 25°C. The low pH estimate was based on complete equilibration with atmospheric carbon dioxide (CO_2), and the high pH estimate was based on complete exclusion of atmospheric CO_2. Conditions during chemical addition favored the absorption of CO_2, resulting in a pH near the low end of the range. The conditions that favored CO_2 absorption were the result of actions designed to encourage boric acid dissolution. These conditions included (1) NaOH was added before boric acid, leaving the tank solution with a high initial pH; (2) the water level in the tank, as boric acid was being added, was below the level of the recirculation headers, thus creating a high degree of turbulence and also allowing intimate contact between air and water; and (3) the recirculation pump was operated at 390 L/min (103 gpm) as boric acid was being added, which increased turbulence and encouraged the entrainment of air.

4.1.3 Hydrogen Generation

As a safety precaution, the vapor space of the test apparatus was monitored daily for the presence of hydrogen gas. Measured concentrations never were observed to exceed the action level for flammability safety. Hydrogen concentrations were monitored for safety reasons only and cannot be interpreted quantitatively because (1) the tank lid was continuously but passively vented through two 3/4-in.-diam ball valves, (2) samples were taken through a plastic tube inserted through one of the valves so that the gas sample was extracted near the top of the tank, (3) no provisions were made for mixing gas in the well-insulated head space, and (4) the handheld hydrogen detector that was used provided sufficient sensitivity to avoid a safety concern but not sufficient accuracy to be used for quantitative assessment. Despite these limitations, it is instructive to note that nearly constant hydrogen levels were observed for the first 17 or 18 days of the test, and then the observed levels began to decline. For the last 5 days of the test, the hydrogen level was undetectable under the procedure described above.

4.2 Coupon Racks

The total of 373 metal coupons and 1 concrete coupon was contained in the tank during Test #1. Coupon types consisted of aluminum, copper, galvanized steel, carbon steel, and steel coated with inorganic zinc (IOZ) primer. Those coupons were loaded in seven coupon racks, with the numbering configuration shown in Figure 16. Racks #2 through #7 were exposed to the nozzle spray for the first 4 hours of the test. The nozzles were designed and oriented to provide a uniform, even spray over the racks. Following the spray phase of the test, those racks were left in the humid tank environment, and water drops were observed falling from the coupons and racks.

Coupon rack #1 was positioned so that it was submerged for the entire 30-day test. It remained located between the two recirculation flow headers in the tank to expose the coupons to a fairly uniform flow rate across their surfaces.

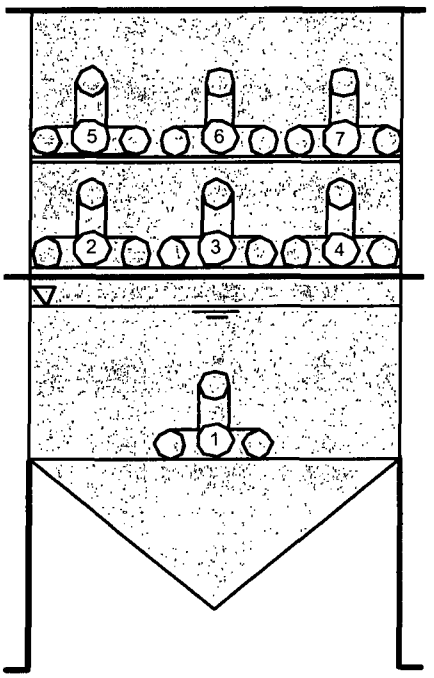

Figure 16. Coupon rack configuration in the ICET tank.

4.2.1 Physical Observations

All of the coupons were weighed before and after the test, photographed, inventoried, and stored. The surface appearance of the submerged coupons was changed considerably more than the non-submerged coupons.

Figure 17, looking down into the tank, shows portions of coupon racks #2 through #4 before test initiation. A SS mesh holder containing a fiberglass sample is shown on the end of rack #3. The angle iron shown above the racks is where racks #5 through #7 will rest. Figure 18 shows one of the coupon racks being hoisted into the tank before test initiation. Figure 19 shows the typical appearance of the unsubmerged racks after their removal from the tank.

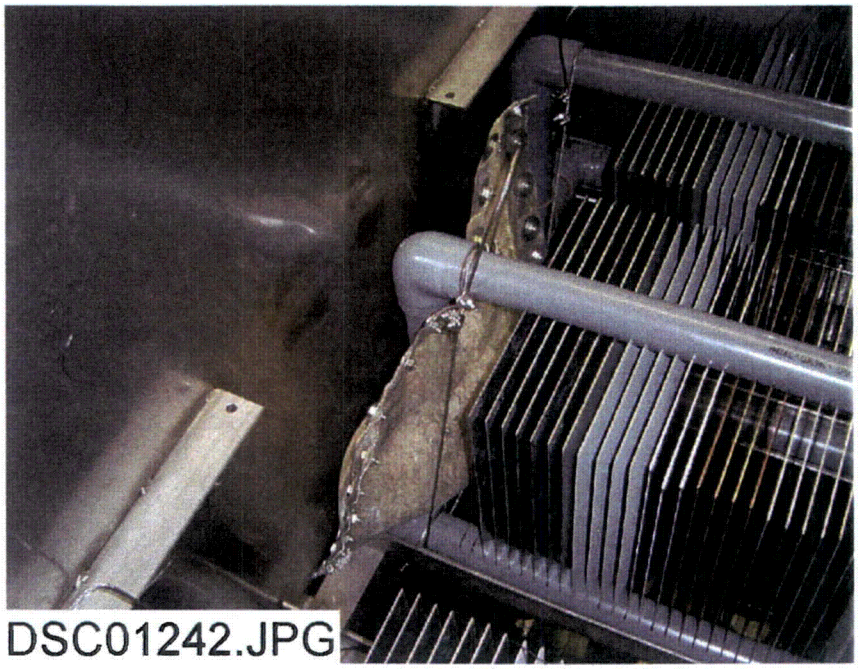

Figure 17. Coupon racks inside ICET tank before start of test.

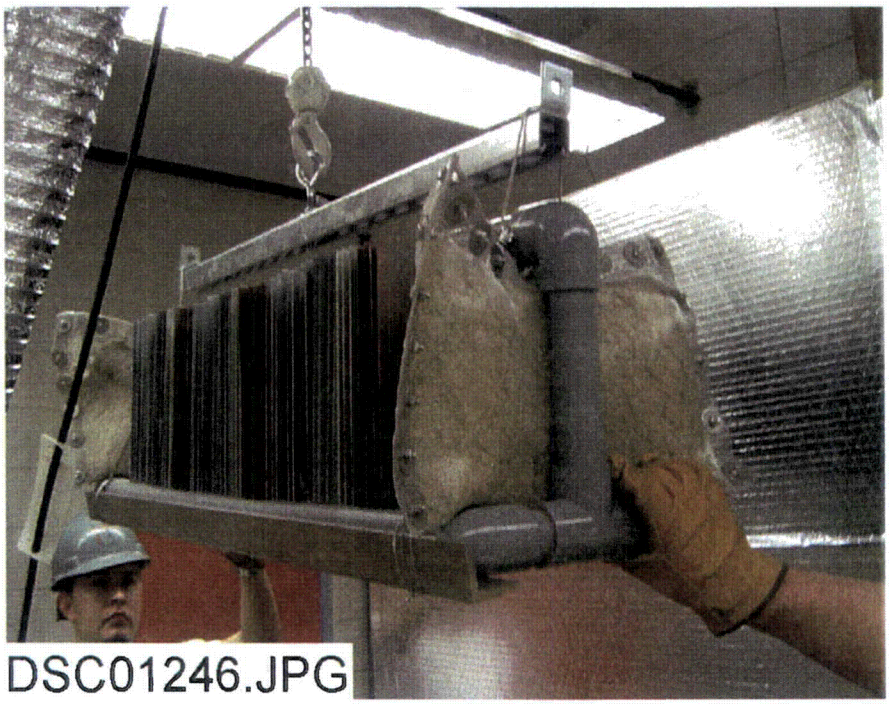

Figure 18. Coupon rack being loaded into the ICET tank.

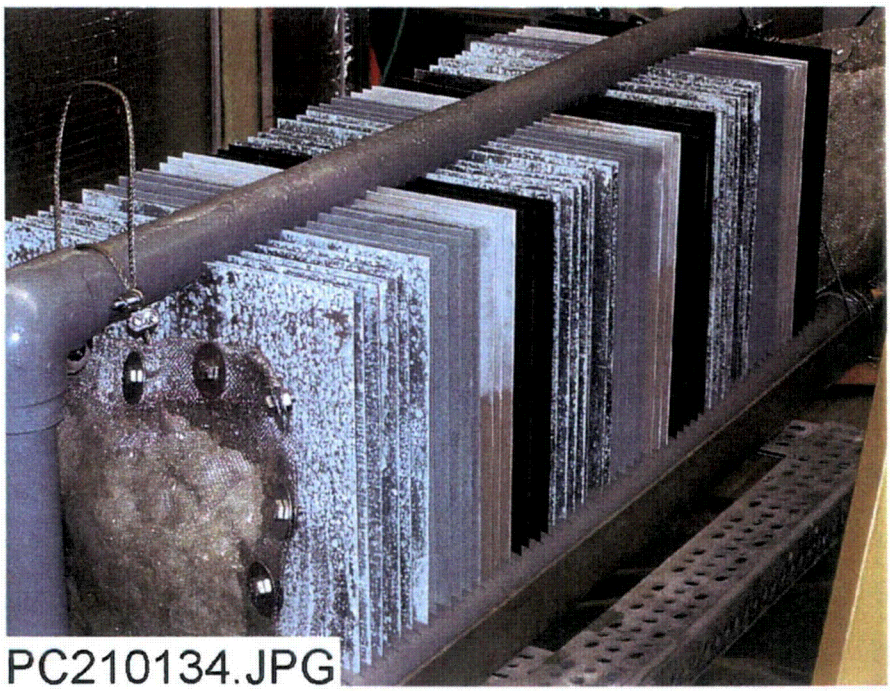

Figure 19. Coupon rack following removal from the ICET tank.

4.2.2 Weight Measurements

Measurements of coupon weights were taken on a calibrated scale. Weight differentials less than 0.1 g are within the measurement uncertainty, and measurements less than 1 g should be used as qualitative indicators of change.

4.2.2.1 Submerged Coupons

In one coupon rack, forty coupons were submerged in the chemical solution. Of these coupons, 25 were copper (average weight of 1317.7 g), and 24 of these experienced changes in weight that ranged between 0.0 g and 0.1 g. One copper coupon gained 2.0 g. That value appears to be an outlier, possibly caused by a faulty measurement. Weight changes for the seven galvanized steel coupons (average weight of 1054.83 g) ranged from 0.04 g to 0.06 g. The three IOZ-coated steel coupons (average weight of 1625.2 g) were less than 0.1 g. The three aluminum coupons (average weight of 392.0 g) experienced an average weight loss of 98.61 g. The single uncoated carbon steel coupon lost 23.3 g from an original weight of 1025.2 g. The concrete coupon gained 233 g from an original weight of 8586 g, possibly from retaining excess water that was not liberated after several days of air drying at room temperature.

4.2.2.2 Unsubmerged Coupons

Weight differentials (value of final weight minus initial weight) for the unsubmerged coupons were much smaller than those of the submerged coupons, and they varied between small positive and negative values. A total of 334 coupons were unsubmerged and were contained in 6 coupon racks. The distribution of coupon materials was 127 galvanized steel, 75 copper, 74 coated steel, 56 aluminum, and 2 uncoated carbon steel. The mean weight differential of the two carbon-steel coupons was 0.2 g. The maximum weight gains experienced by the remaining unsubmerged coupon materials are summarized in Table 4.

Table 4. Range of Weight Gains for Each Unsubmerged Coupon Material Type

Material	No. of Coupons	Maximum Gain (g)
Coated Steel	74	2.3
Aluminum	56	1.9
Galvanized Steel	127	0.7
Copper	75	0.4

It should be noted that the greatest single weight differential of 2.3 g on a coated steel coupon is ~0.14% of the original weight.

4.3 NUKON™ Fiberglass Samples

One of the common types of insulation used in nuclear power plants is NUKON™ fiberglass insulation, which is composed of a glass compound with various oxides and a binder. The glass composition of Owens Corning's NUKON™ insulation is given in Table 5 (data provided by the manufacturer). The NUKON™ fiberglass provided for the ICET tests was heat treated and shredded. Note that the information in the following two paragraphs was provided by the NUKON™ manufacturer.

Table 5. NUKON™ Glass Composition

Oxide	Maximum, %	Minimum, %
SiO_2	64.4	60.6
Al_2O_3	4.4	2.8
CaO	8.7	7.7
MgO	3.7	3.2
Na_2O	16.7	14.9
B_2O_3	5.8	4.2

According to the manufacturer, the binder on the NUKON™ Base Wool is a phenolic resin binder that starts decomposing at about 400°F and is probably totally decomposed at 600°F. After heating this insulation material on a 600°F hot plate for several hours, typically one-third of the binder decomposes into thermal decomposition gases, which represents the weight loss. Because the unheated NUKON™ Base Wool has 3% binder content by weight, the insulation material loses approximately 1% of its weight through heating on a hot plate.

Also according to the manufacturer, the binder left on the insulation has some discoloration, particularly in the transition zone between that on the yellow, cold insulation side and that on the white, hot insulation side (white indicating total binder loss and yellow indicating zero binder loss). In this transition zone, the binder is partially decomposed and the discoloration includes the color brown. The exact chemical identity of this brown, partially decomposed binder is not known, nor is its solubility in a water-based solution, such as boric acid. However, it is likely that this partially decomposed binder would discolor the boric acid solution into which it has been placed. It is not likely that the discoloration of the boric acid solution is caused by the glass fibers themselves because of the fact that this leaching process would have resulted in an apparent build-up of the discoloration that was not observed. Likewise, it is not likely that

the binder on the cold insulation side would dissolve in the boric acid solution and contribute to its discoloration.

For Test #1, 4.58 ft^3 of NUKON™ fiberglass enclosed in a fine SS mesh was placed in the tank. Of this amount, 75% was submerged below the water level and 25% was placed above the water level and exposed to sprays. The fiberglass had been heated before the test, as described above, to remove in part the organic binder in a manner consistent with the service life of similar products found in containment.

4.3.1 SEM/EDS

Fiberglass debris is encased in SS mesh bags to minimize migration throughout the tank. Small SS mesh envelopes approximately 4 in. square containing approximately 5 g of fiber are pulled out of the tank periodically for SEM examination. These sample envelopes are placed in a range of water flow conditions, but none have direct water flow through the fiber, and all are thoroughly immersed in the test solution until they are recovered from the tank. After exposure for some period of time, deposits are formed throughout the fiber matrix that appear to be of chemical origin. SEM images show that various structures formed on the fibers are similar for the Day-15 and Day-30 test samples. However, coverage and thickness of deposits are more advanced in the Day-30 samples. Fiberglass material extracted from the surfaces of larger clumps shows the greatest buildup, whereas fibers on the interior of larger clumps appear to be almost unaffected.

Several different deposition structures are observed on the fibers, progressing in coverage from individual particles deposited on each fiber to sheets of film and very thin crusts that stretch between multiple fibers. When viewing the following photographs, note that all samples are thoroughly desiccated before examination. Figure 20 shows an SEM image for a pretest sample of fiberglass. The fibers are clean, with no particles deposited on them. Figure 21 shows a Day-15 test sample, where particles are beginning to deposit on the fibers. Figure 22 shows an SEM image for a Day-30 test sample. Sheets of thin film are forming over and between the fibers. Figure 23 shows an SEM image for a Day-15 test sample that illustrates similar deposits between fibers. The deposits observed in these samples appear to be capable of changing the head-loss characteristics of a fiber bed, but it has not been conclusively demonstrated that similar deposits would form under directed water flow similar to that present at the face of a sump screen.

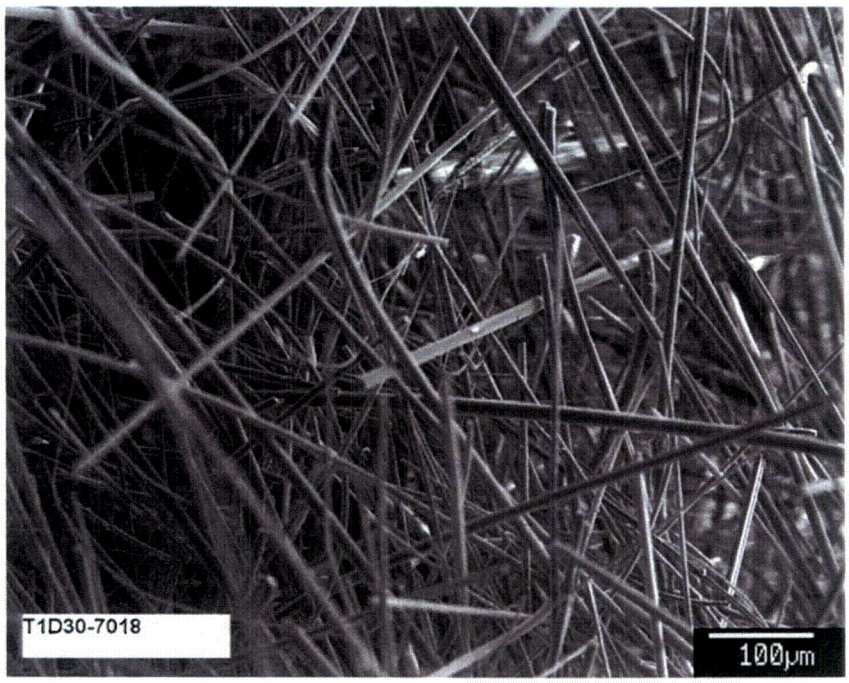

Figure 20. SEM image for a pretest sample of clean fiberglass.

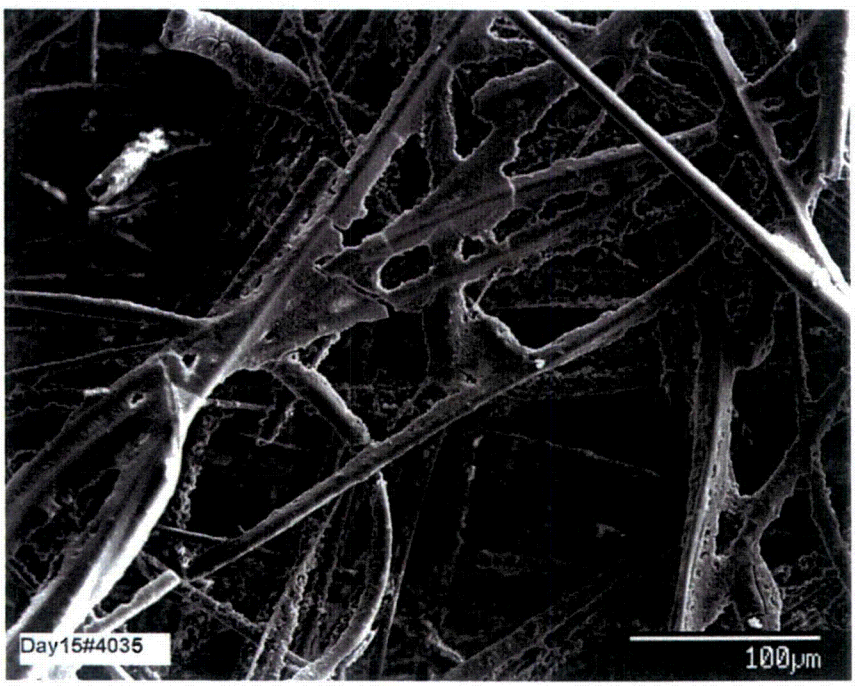

Figure 21. SEM image for a Day-15 test sample illustrating crusty deposits or growth on fiberglass.

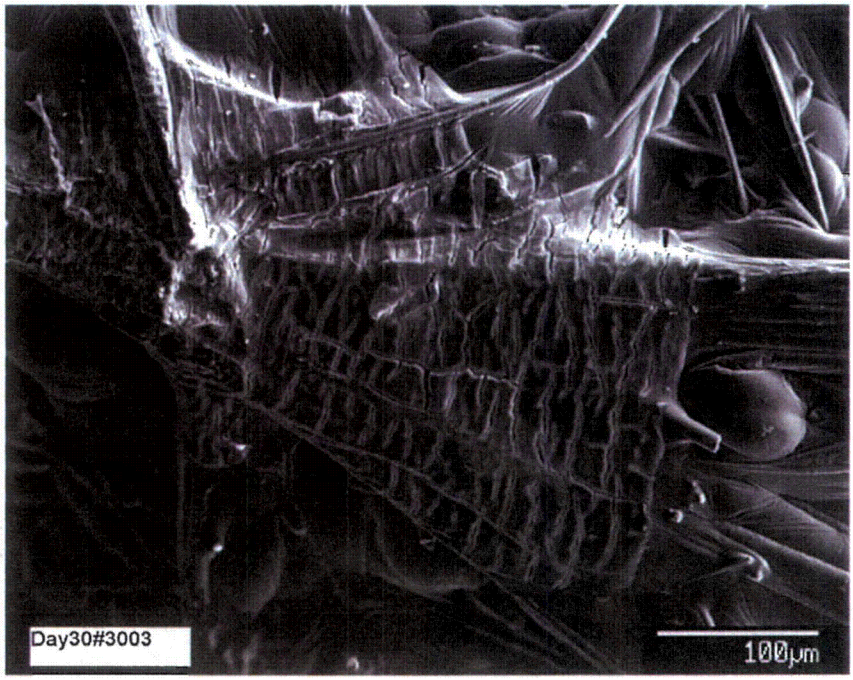

Figure 22. SEM image for a Day-30 test sample illustrating membrane films deposited between fibers.

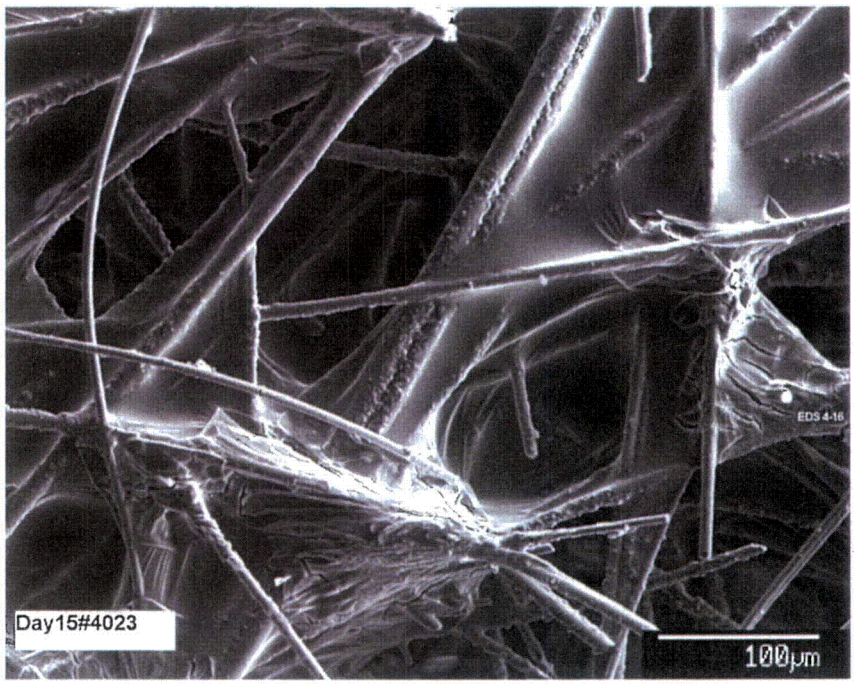

Figure 23. SEM image for a Day-15 test sample (sample #4023) magnified 230 times, illustrating deposits between fibers.

Figure 24 shows a typical EDS spectrum for a Day-15 test sample. This particular sample is dominated by oxygen and sodium. These test samples typically contain various elements, such as carbon, oxygen,

sodium, magnesium, bromine, silicon, calcium, manganese, iron, and zinc. It should be noted that gold (Au) and palladium (Pd) are present in almost all EDS spectra because of the sputtering technique used to prepare the SEM samples. The highly conductive sample surface provided by metallic sputtering prevents charge buildup under the electron beam that would destroy image quality. Peak counting intensities are proportional to elemental concentration but must be compensated by the energy-dependent detector response function and normalized to an assumed set of elemental constituents before proportional compositions can be inferred. Further explanation of EDS spectra and many additional examples are provided in the appendices, including many with accompanying composition analyses.

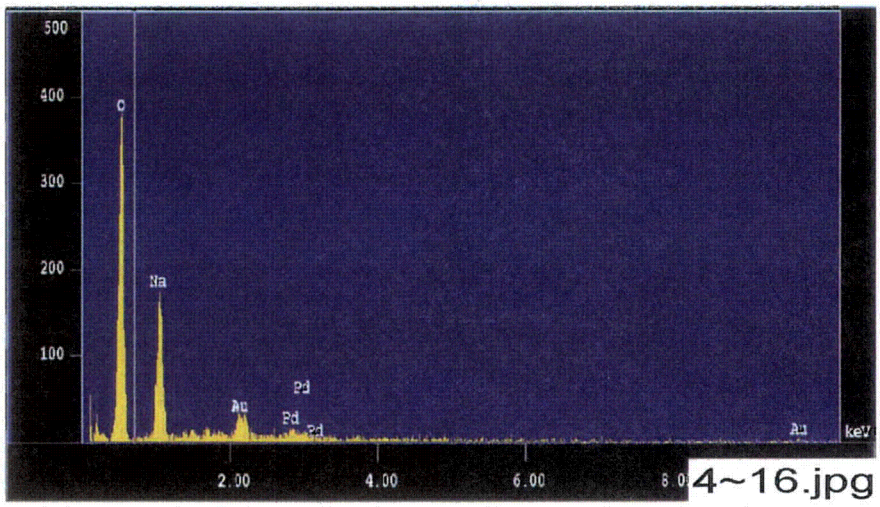

Figure 24. Day-15, sample #4 counting spectrum (EDS 4-16) taken for the cracked deposits at the right-hand side of Figure 23.

4.4 Concrete Samples

A scaled amount of concrete and its aggregate were ground up into dust. The amount used for the 250-gal. test volume was 21.2 g. In addition to the concrete, 63.7 g of a latent debris surrogate was prepared. The surrogate consisted of three size distributions and two different materials. Sand was used for the two larger sizes, which were 0.075–0.59 mm and 0.59–2 mm, respectively. These two sizes accounted for 35% and 28% of the total added. Clay was used for the smallest size, which was <0.075 mm. The concrete dust and latent debris were added to the test solution just before the start of the test.

4.5 Solution Chemistry

Daily water samples were extracted from the ICET tank in accordance with written instructions. Portions of these samples were archived in airtight plastic bottles for longer duration observation and analyses. Each sample was identified by a four-field tag containing the ICET acronym and test number, the date of extraction, the time of extraction, and the filtration status (U for unfiltered, F for filtered). For example, an unfiltered sample collected on November 20 at 5:03 P.M. would be labeled as ICET-1120-1703-U.[1] Figure 25 illustrates the water sample collection process.

[1] Slight variations on this nomenclature have been used to label filter papers and other solid samples. For example, tags such as T1D30 have sometimes been used to designate Test #1, Day 30.

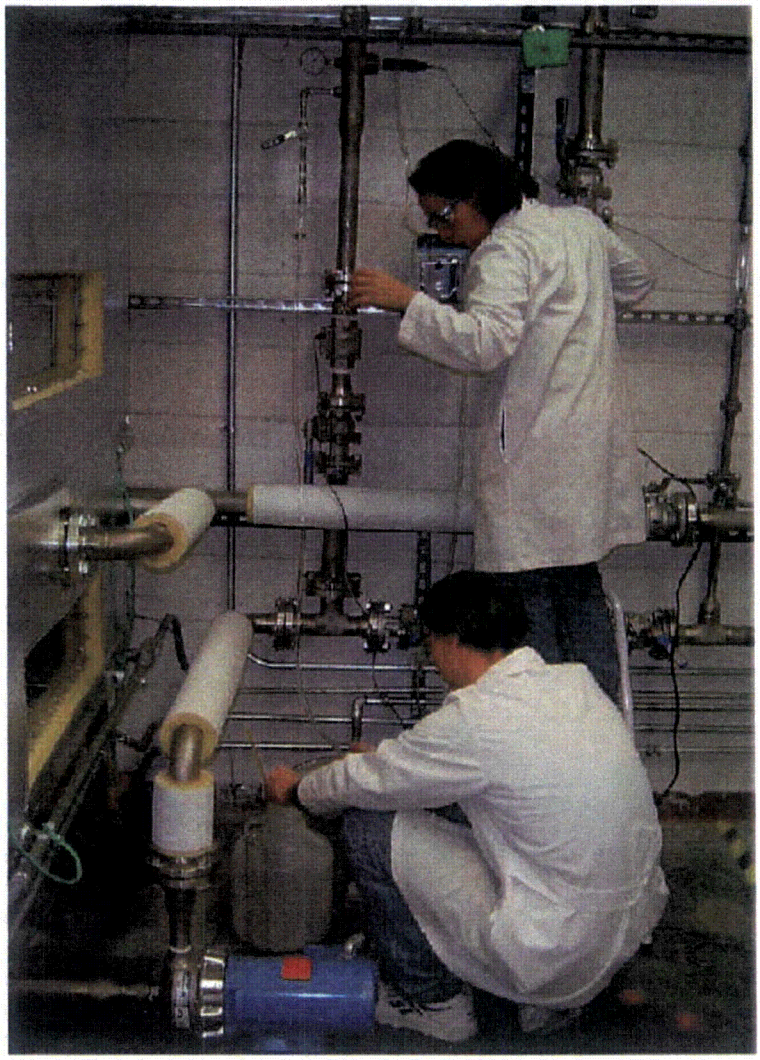

Figure 25. Daily water grab sample extraction.

4.5.1 Water Color

After chemical addition but before placement of coupons, fiberglass, and debris, the water was clear. After placement of the coupons, fiberglass, and debris, the water had a distinct yellow color. Even after particulate debris settled in the tank and the turbidity and TSS dropped to low levels, the yellow color remained. Examination of the stored sample bottles reveals that the color qualitatively remained nearly constant over the duration of the test, although the final day or two may have been slightly less yellow than the previous days. The precipitation and settling of solids in the stored bottles did not appear to have had a significant impact on the color. Although several sources for this color are possible, the most likely source is the fiberglass insulation, based on an evaluation of the materials in the tank. The NUKON™ fiberglass placed in the tank was yellow, and the vendor of the fiberglass indicated that the yellow color was due to the presence of a phenolic resin binder. No other materials placed in the tank had a yellow color. Corrosion products from metal coupons can be colored, but of the materials placed in the tank, only iron oxides will produce color similar to the color observed in the tank, and the iron concentration was below the detection limit in the solution.

Figure 26 and Figure 27 illustrate the bench-top measurement area used for tests on water samples.

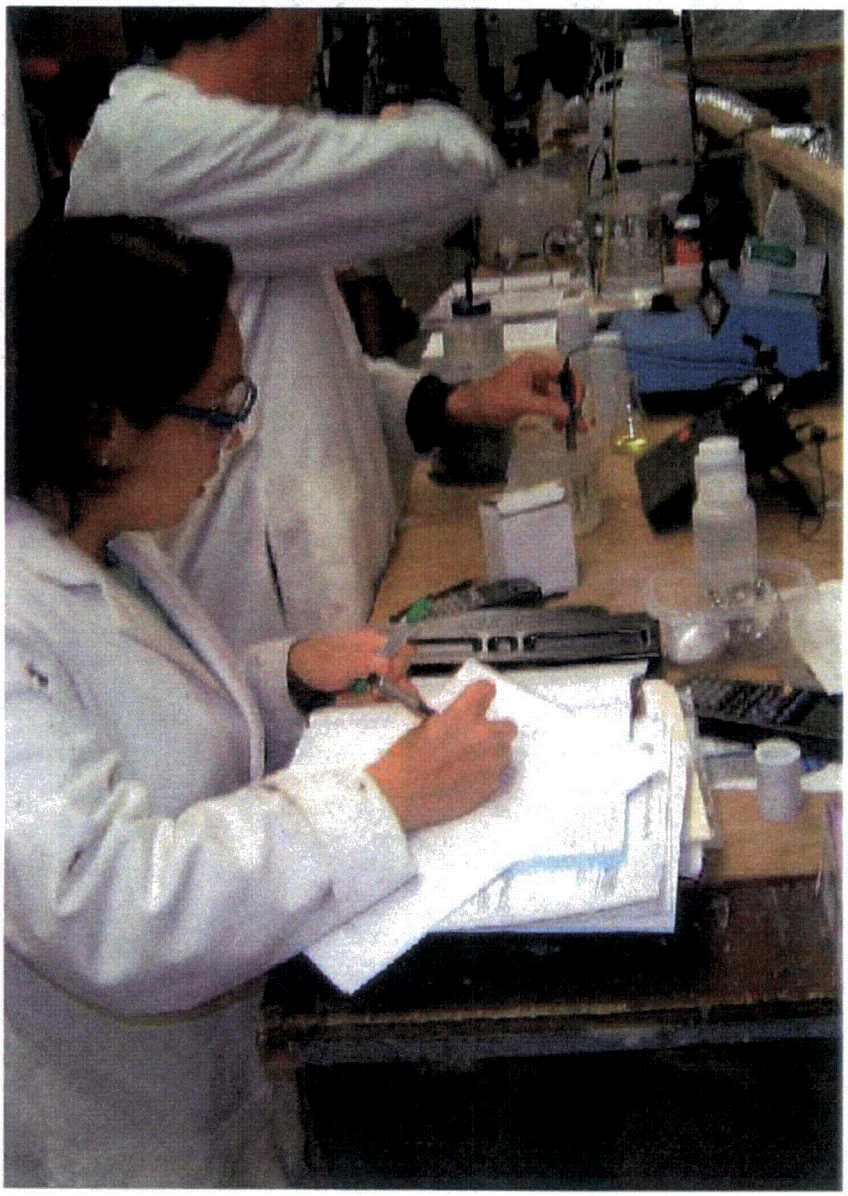

Figure 26. Wet chemistry analyses.

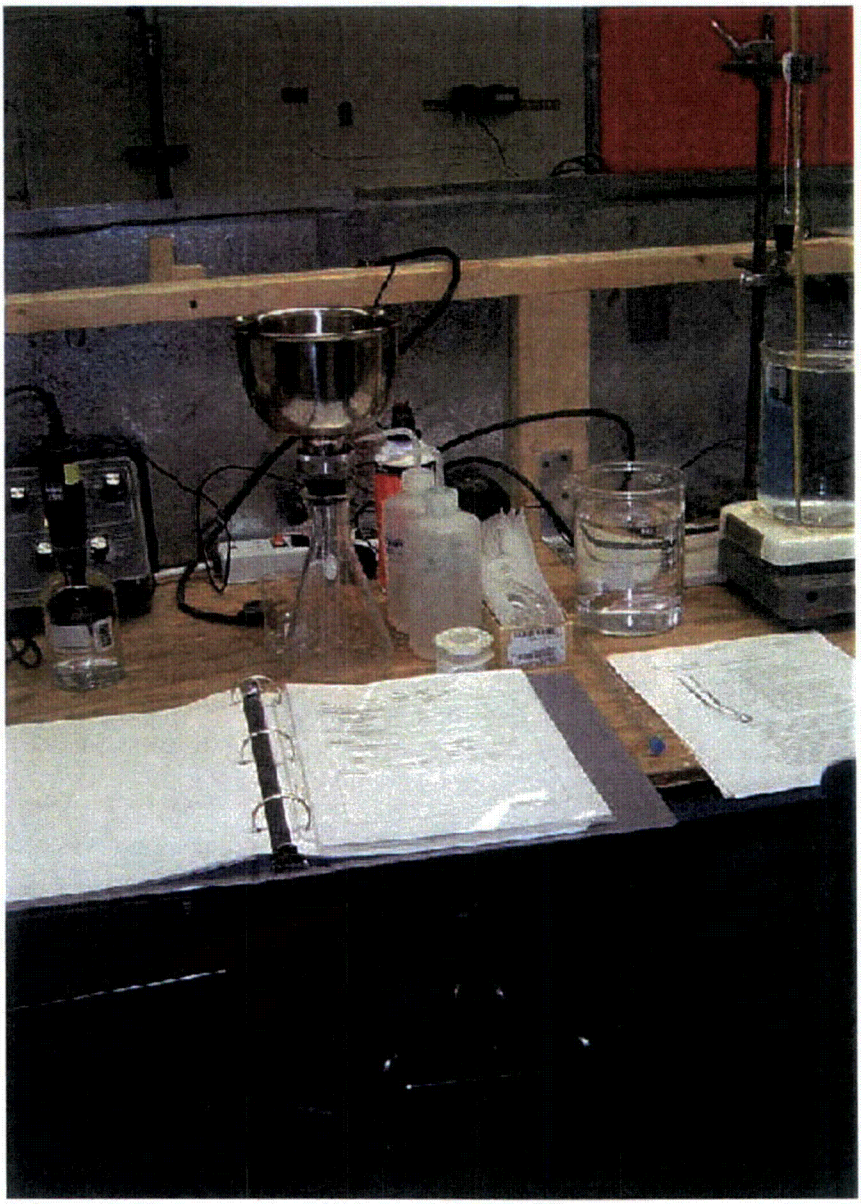

Figure 27. Bench-top water sample characterization.

4.5.2 Turbidity

Figure 28 displays the turbidity trend observed during Test #1. There are 3 different values shown on the plot for time zero. The first point was taken after adding chemicals, concrete dust, and latent debris but before adding coupons or fiberglass. The turbidity was then measured to be 0.61 NTU. After adding the sample coupons and fiberglass samples, the solution was murky and it was impossible to see more than a couple of inches into the tank. The measured turbidity at that point was 12 NTU. The next morning, the turbidity had decreased to 8 NTU. Following the start of the test, turbidity was measured to be 14.4, 13.3, 11.4, and 8.3. Those values were at 0.5, 2, 4, and 8 hours, respectively, after the test start. At 24 hours, the turbidity had dropped to 1.3 NTU, and it continued to drop over the next two days, reaching a value of about 0.3 NTU by Day 3. The turbidity remained relatively steady throughout the remainder of the test.

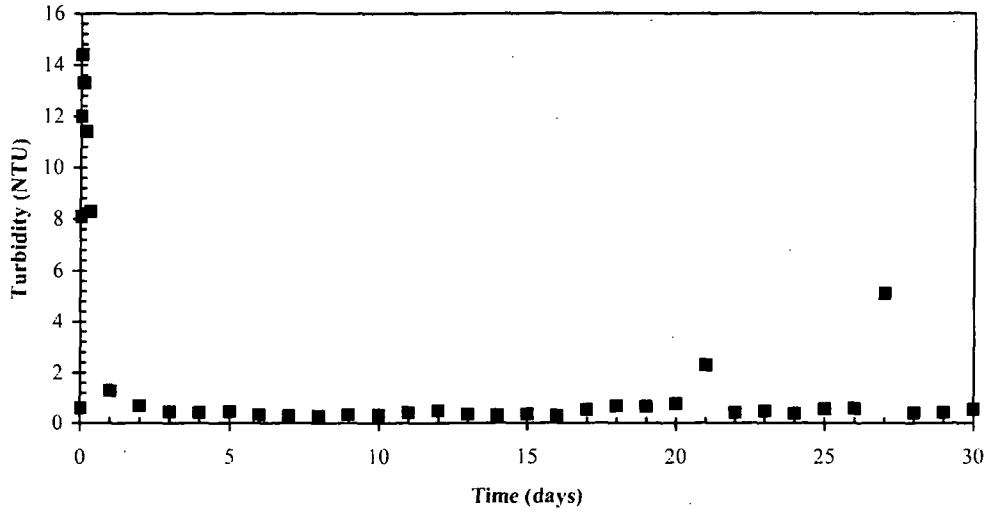

Figure 28. Turbidity trend at the test temperature observed during ICET Test #1.

Turbidity values were measured while the solution was still near the process temperature of 140°F. It was observed that the precipitation that occurred in the sample solution was very time- and temperature-sensitive. Therefore, lapses of just a couple of minutes would cause a higher turbidity reading, which appears to be the case for the values at 21 and 27 days shown in Figure 28. A longer period of time may have elapsed between the sample taking and the measurement.

The turbidity values shown in Figure 28 were measured while the solution was still near the process temperature of 140°F. The test plan also included a requirement to measure turbidity at ambient temperature [23 (±2.0) °C], which is presented in Figure 29. During the first day, turbidity at ambient temperature was identical to turbidity at process temperature. However, on Day 2, it was noted that turbidity at ambient temperature was higher than at process temperature. It was also noted on Days 2 and 3 that the turbidity at room temperature was time dependent and increased as the holding time increased. Therefore, a procedure was implemented on Day 4 that required the ambient-temperature turbidity to be recorded after a cooling time of 10 minutes. The 10-minute ambient-temperature turbidity asymptotically increased over the duration of the test, reaching a value of 133 NTU by Day 30. The cause of the rapid rise in turbidity while cooling was attributed to a white, finely divided precipitate that gradually settled to the bottom of the sample storage bottles.

The presence of precipitate in the 10-minute daily samples indicates that the tank solution reached room-temperature saturation of at least one species very rapidly. Post-test examination of the stored water from the daily samples indicates that the quantity of precipitate continued to increase as testing time progressed. The amount of precipitation appears to be temperature and time dependent. Water held at 60°C was never observed to form precipitates, but when the water is cooled to 23°C, precipitates form gradually over time.

Turbidity appears to be a sensitive indicator of the rate of the precipitation reaction. As the water cooled from 60°C to 23°C, the turbidity was observed to increase from 0.3 NTU to more than 133 NTU in a 10-minute period. In addition, the viscosity results at 23°C are more variable (see Section 4.5.5). As with turbidity after Day 2, viscosity was time and temperature dependent. It was not possible to hold each viscosity sample for the exact same amount of time before taking the measurement at 23°C.

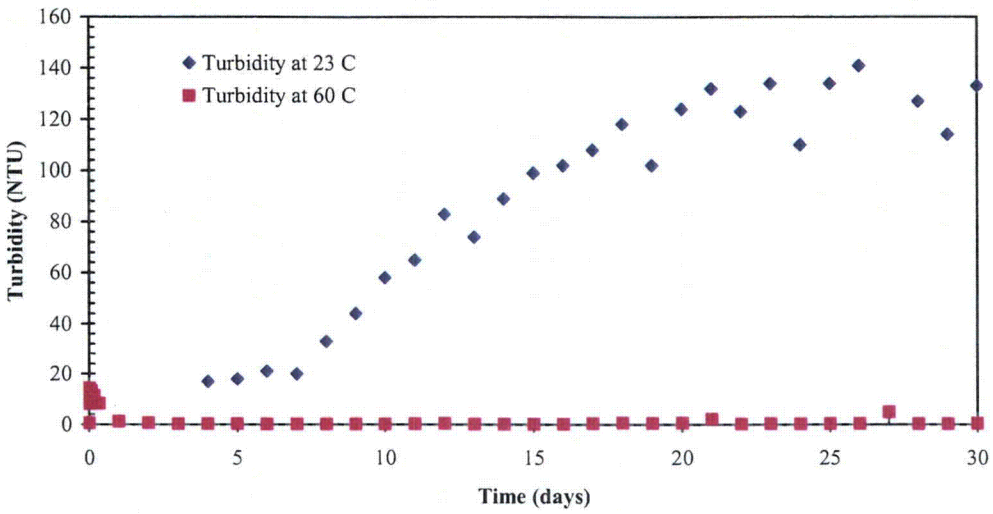

Figure 29. Turbidity measured at 23°C and 60°C during ICET Test #1.

4.5.3 Total Suspended Solids

Total suspended solids (TSSs) are measured by filtering a volume of approximately 500 mL through an in-line, 0.7-µm, glass microfiber filter directly at the sample tap and drying and weighing the filter paper to determine what was collected. The selected equipment and procedure ensure that TSS measurements are not affected by temperature-dependent or time-dependent precipitation reactions that may occur once the process solution is removed from the tank. The TSS concentration was 27 mg/L after the coupons, fiberglass, concrete dust, and latent debris were introduced to the tank. The next morning, the concentration was 29 mg/L. Values were 43, 32, 27, and 23 mg/L at 0.5, 2, 4, and 8 hours, respectively, after the test start. The TSS started dropping after the NaOH spray cycle was complete, reaching 27 mg/L at the end of the 4-hour spray cycle. TSS continued to drop during the test, which is consistent with the turbidity measurements. During Days 2 through 12, the TSS stayed low and within the range of 10 to 25 mg/L. From Day 13 to the end of the test, the TSS concentration rose but stayed consistently between 19 and 29 mg/L. The standard deviation in the measurement was experimentally obtained to be approximately 3 mg/L. An evaluation of variability outside of that number was not performed. The TSS concentrations are shown in Figure 30

On the last day of the test, 1 L of the end-of-test solution was taken for TSS analysis. The solution was shaken and then divided into seven samples that were held at different temperatures, ranging from room temperature (22.8°C) to 55°C. The solution was left at the desired temperatures for 72 hours before being filtered for TSS analysis. Various laboratory ovens and one water bath were used to control the temperature of the various containers so that analysis could be performed in a timely fashion. The desired temperatures ranged from room temperature to 60°C, decreasing in 5°C increments.

Figure 31 presents the results from this test. The TSS concentration increased relatively linearly, from approximately 100 to nearly 1800 mg/L as the constant sample temperature decreased from 55°C to 22.8°C.

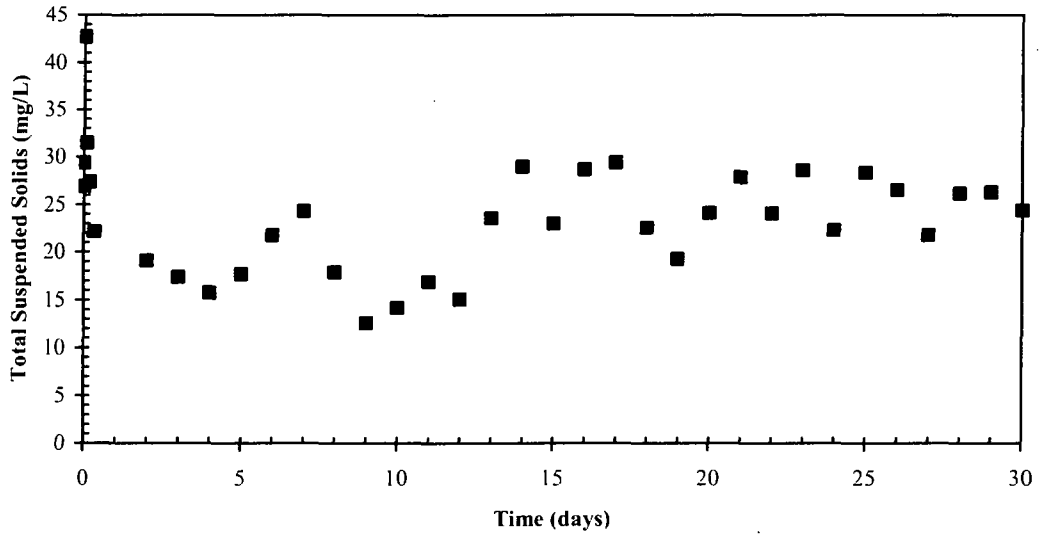

Figure 30. Total suspended solids during ICET Test #1.

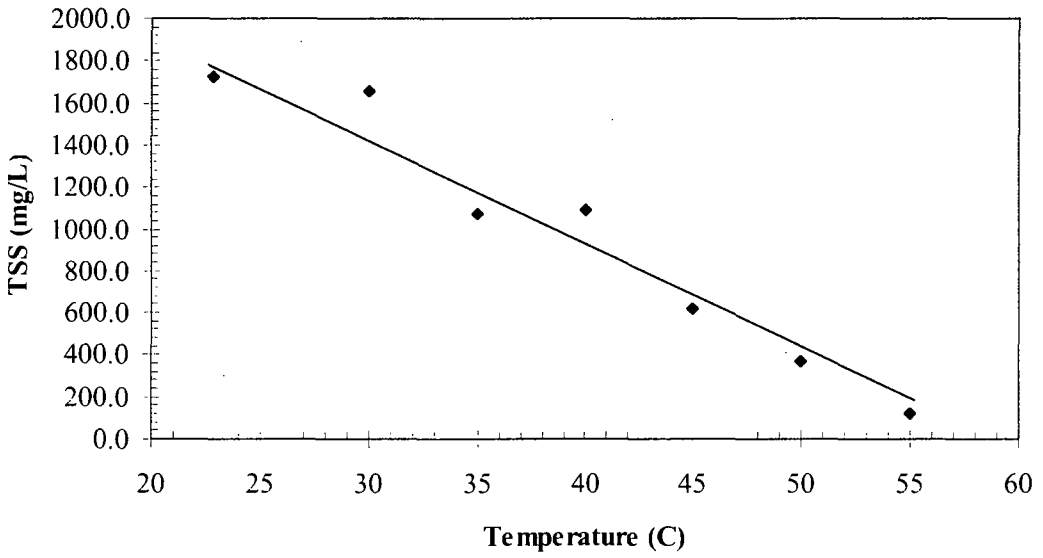

Figure 31. TSS results for the end-of-test precipitation experiment.

A similar study was conducted to determine if the precipitate that formed in the end-of-test solution upon cooling would redissolve into solution upon reheating to the test temperature. Several assumptions apply to this study:

1. The end-of-test solution is homogenous.
2. No change has occurred within the solution while being stored for 30 days at room temperature.
3. Temperature variation between heating baths and ovens used is negligible.

One-L bottles of end-of-test solution were subjected to constant desired temperatures for 72 hours. After 72 hours, the solutions were vigorously shaken to provide a homogenous sample that was then filtered for TSS analysis.

For reheating of the end-of-test solution, only one water bath was used to control the temperature because of the unavailability of the laboratory ovens. The only exceptions to this practice were the 60°C and room temperature samples. The same 1-L sample bottle was placed in the water bath at the desired temperature for 72 hours. After 72 hours, a 100-ml sample was taken from the well-shaken 1-L sample bottle. The 1-L sample bottle, minus the volume taken for sampling purposes, was returned to the water bath. The water bath was adjusted to the required temperature for the next step in the experiment. The desired temperatures ranged from room temperature to 60°C, increasing in 10°C increments. See Figure 32 for the resulting TSS as a function of temperature.

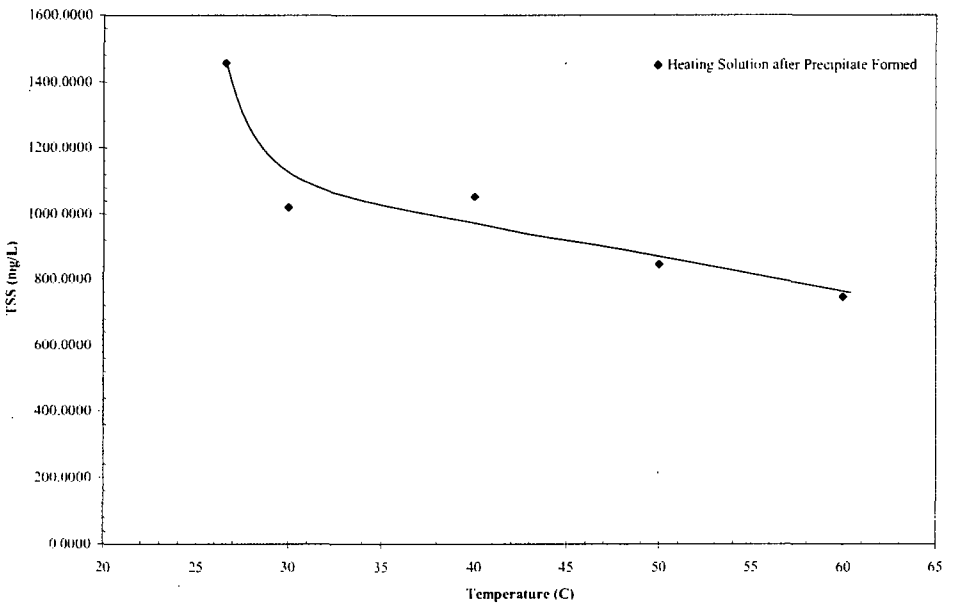

Figure 32. Temperature-precipitate relationship upon heating the end-of-test solution after precipitate has formed.

While the end-of-test solution was cooling, precipitates formed in a linear fashion with varying temperature, as seen in Figure 31. After the precipitate formed, heating of the solution caused some of the precipitate to redissolve into solution, as seen in Figure 32. Figure 33 displays the distinct difference in precipitation concentration due to heating and cooling of the solution. Also, from Figure 33, it can be seen that not all of the precipitate returned to solution when the test temperature is reached. The standard deviations of the results are unknown because of time constraints, so further testing must be done to correctly quantify precipitate concentrations under these time and temperature profiles.

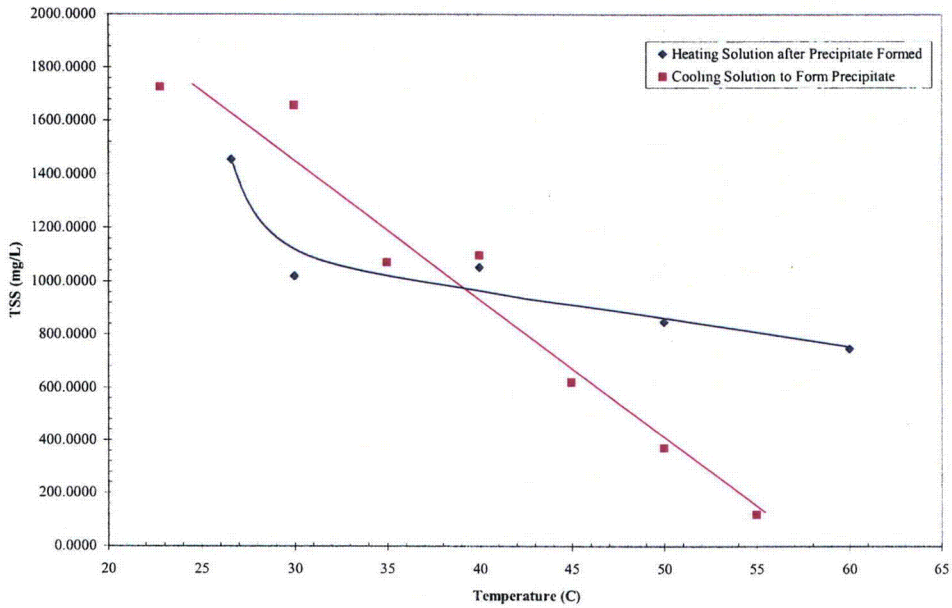

Figure 33. Temperature-precipitate relationship upon cooling and heating of end-of-test solution.

4.5.4 pH

As shown in Figure 34, the pH slowly decreased over the duration of the test. By the end of the test, the grab sample pH and the DAS pH differed from each other by approximately 0.10 pH units. The grab sample pH decreased from pH = 9.5 to pH = 9.35, whereas the DAS pH decreased from pH = 9.5 to pH = 9.28. This slight decrease in pH may have been caused by adsorption of additional atmospheric CO_2 or by corrosion reactions that resulted in the production of acid.

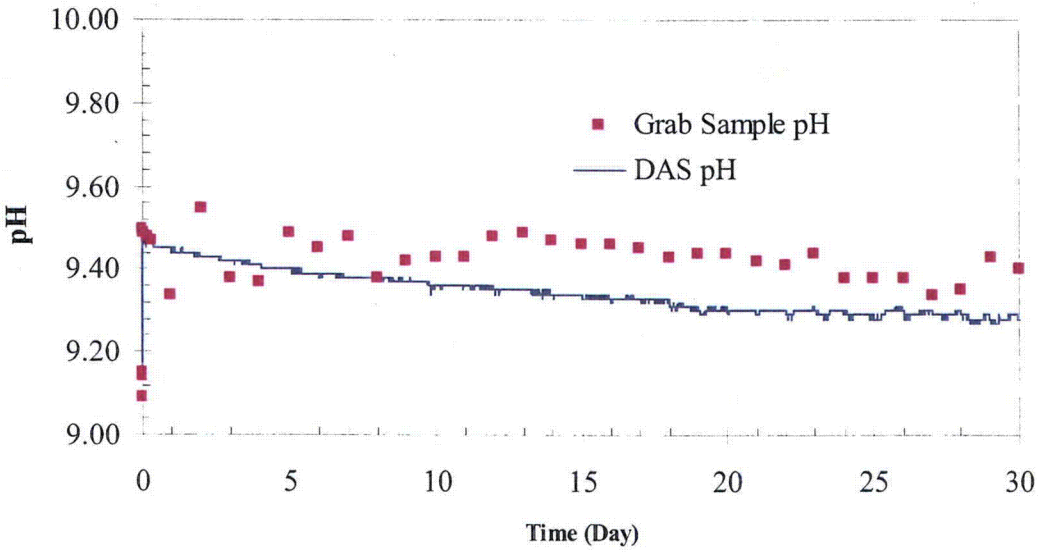

Figure 34. pH trend observed during ICET Test #1.

4.5.5 Constant-Shear Kinematic Viscosity

The viscosity of filtered and unfiltered solutions at 60.0°C is shown in Figure 35. Filtered and unfiltered viscosity at 60.0°C remained virtually unchanged. The filtered viscosity had a standard deviation of 0.014 mm^2/s (average = 0.514 mm^2/s, range = 0.469 to 0.552 mm^2/s) over the first 24 days of the test. Thus, on Day 25 of the test, filtered viscosity measurements were discontinued. The unfiltered viscosity had a standard deviation of 0.01 mm^2/s (average = 0.514 mm^2/s, range = 0.482 to 0.560 mm^2/s) through the duration of the test.

A slight increase in the viscosity measurements was observed from Day 11 through Day 14, and it was noticed that the viscometer contained visible residue after the standard cleaning procedure was completed. On Day 15, the viscometer was cleaned in an acid bath before use and the viscosity returned to the previous expected value. Thereafter, the viscometer was cleaned with acid after each measurement for the duration of the test.

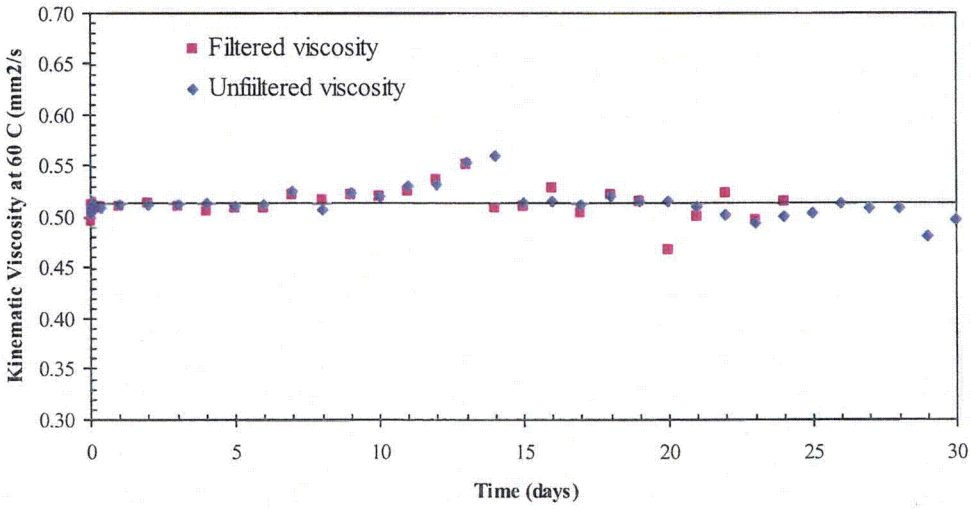

Figure 35. Kinematic viscosity of solution in ICET Test #1 at 60.0°C.

The viscosity of filtered and unfiltered solutions at 23.0°C is shown in Figure 36. Viscosity at 23.0°C has been more variable than viscosity at 60.0°C. This variability can probably be attributed to the time-dependent precipitation of solids at ambient temperature that was observed in the turbidity measurements. Over the duration of the test, the viscosity at 23.0°C gradually increased. The onset of precipitation of solids as a function of cooling also advanced over the test duration, which could account for the increase in viscosity observed under the established test procedure. The filtered viscosity had a standard deviation of 0.235 mm^2/s (average = 1.208 mm^2/s, range = 0.962 to 1.713 mm^2/s) over the first 24 days of the test. Again, on Day 25 of the test, filtered viscosity measurements were discontinued. The unfiltered viscosity had a standard deviation of 0.249 mm^2/s (average = 1.240 mm^2/s, range = 0.959 to 1.745 mm^2/s) through the duration of the test.

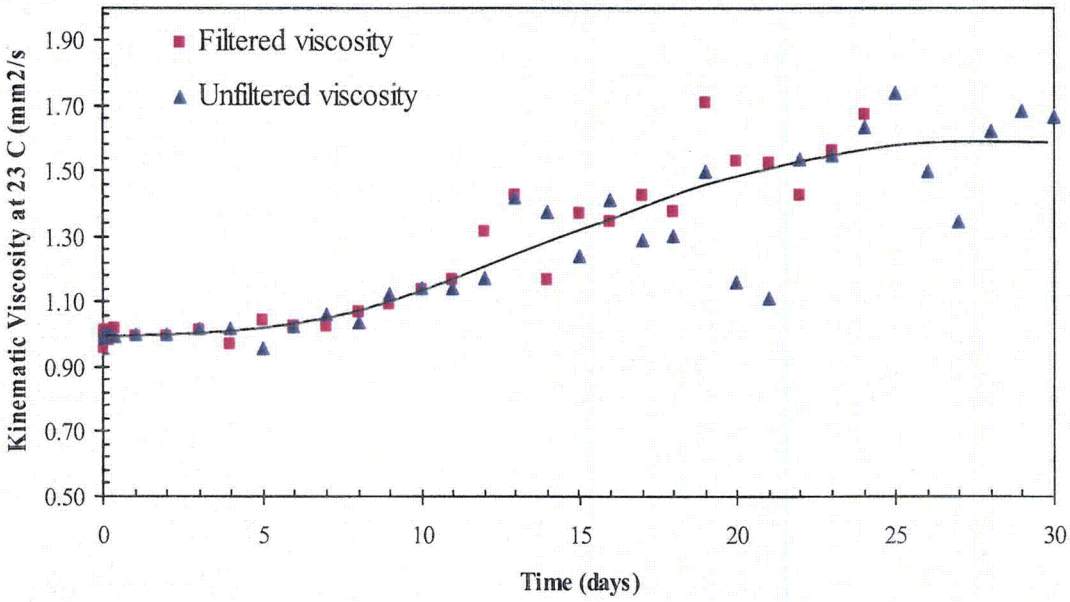

Figure 36. Kinematic viscosity of solution in ICET Test #1 at 23.0°C.

4.5.6 Shear-Dependent Viscosity

Newtonian fluids such as pure water are characterized by the constant proportionality between shear stress and deformation rate. This constant of proportionality is defined as the dynamic viscosity, μ. Most SolGels and gelatinous hydrated reaction products exhibit non-Newtonian behavior such that the deformation rate depends on shear stress in a nonlinear manner. For example, a non-Newtonian fluid may flow readily under low strain rates but respond more rigidly to resist high strain rates and vice versa. Thus, the measurement of shear-dependent viscosity can provide a sensitive indication of the presence of gelation or gel precursors. Shear-dependent viscosity of the tank solution (both filtered and unfiltered) was measured at several time points during Test #1. Results are presented and compared in this section for all time points in a comparison plot; however, basic trends are illustrated using the Day-30 sample results.

A Bohlin CS10 Controlled Stress Rheometer (also called a viscosimeter) was used to measure the shear-dependent viscosity. The instrument was calibrated, and a trained operator followed the manufacturer's instructions to obtain the actual measurements.

All measurements were conducted with a shear-stress range of 0.0095 to 0.12 Pa. Samples were measured at 60°C first and then cooled to 25°C. The samples were transported to the Bohlin CS10 Rheometer via a cooler containing a hot-water bottle to maintain a warm temperature. Any samples that were not immediately analyzed were placed into an oven set at 60°C until they could be measured according to procedure. When samples were placed in the rheometer, their temperatures were controlled to the desired value. Through this procedure, the test sample was maintained continuously at the desired temperature.

Samples analyzed for shear stress viscosity are referenced using the following nomenclature. Results labeled "10am" were obtained on November 21, 2004, at 10:00 A.M. Results labeled "1800" were

obtained on November 21, 2004, at 6:00 P.M. "10am" corresponds to the start of Test #1, and "1800" corresponds to t = 8 hours into the test. Results labeled "1206-F" and "1206-U" are used for the water samples collected from the tank on December 6, 2004, that were filtered and unfiltered, respectively. Similarly, results labeled "1214" and "1220" are used for water samples collected from the tank on December 14, 2004, and December 20, 2004, respectively.

General Observations:

1. When the 25°C measurements were taken, it was necessary to allow the samples to reach an equilibrium condition at the new temperature. If the measurement was taken too quickly, then a curve similar to the high temperature result was obtained.
2. The 1214 series samples exhibit Bingham-plastic flow.
3. The 1800 and 10 A.M. samples were measured at higher shear stresses than the 1206 series, while the viscometer was being set to capture the characteristics of the sample and the instrument settings adjusted to their appropriate ranges. Consequently, the 10 A.M. sample was discarded because it was nearly the same as the 1800 series.

The following plots illustrate basic trends observed in the shear-stress viscosity data and compare key results obtained from all the time points that were analyzed. Note that Figure 37 through Figure 40 represent samples taken on Day 30 of the test.

Figure 37 and Figure 38: In these plots, blue data lines (boxes) indicate viscosities read on the right-hand scale, and red data lines (circles) indicate shear stresses read from the left-hand scale. The behavior shown in these figures is typical of shear-thinning flow, where a yield stress needs to be overcome for flow to occur. Essentially, this means that at very low shear rates, the material exhibits high viscosities. Once enough stress is applied to the system to overcome the yield stress, the material begins to flow as a Newtonian fluid. According to the viscosimeter operator, this behavior could be evidence that a gel is forming or that, upon cooling, a sufficient amount of precipitation is available to cause an increase in viscosity. A water sample collected late in the test was examined after the precipitate settled in the water. This sample was taken of just the water above the settled precipitate (the so-called supernate), and that indicated that the supernate exhibited Newtonian behavior.

Figure 39: This plot compares the 25°C viscosities of the 1220 series samples labeled 1220-F and 1220-U, which correspond to the filtered and unfiltered samples, respectively. Note that the filtered sample has lower shear stresses and viscosities than the unfiltered sample. When these results are compared with Figure 40, this behavior appears consistent with an increase in temperature, as well.

Figure 40: These results are representative of Newtonian flow, with secondary flow. The instrument parameters in the 1220 series of measurements were set at the lowest end of shear stress measurable by the Bohlin CS10 viscosimeter.

Figure 41 and Figure 42: These concurrent plots show viscosities for the 1800, 1206, 1214, and 1220 series at two different temperatures. The flow changes with the 1206, 1214, and 1220 series, and the viscosities increase as a function of time into the test. In addition, from the 1206 sample measured at 25°C, the fluid exhibits non-Newtonian behavior that could be evidence that the system is gelling or that a significant amount of precipitation is occurring, thus causing an increase in the solids loading.

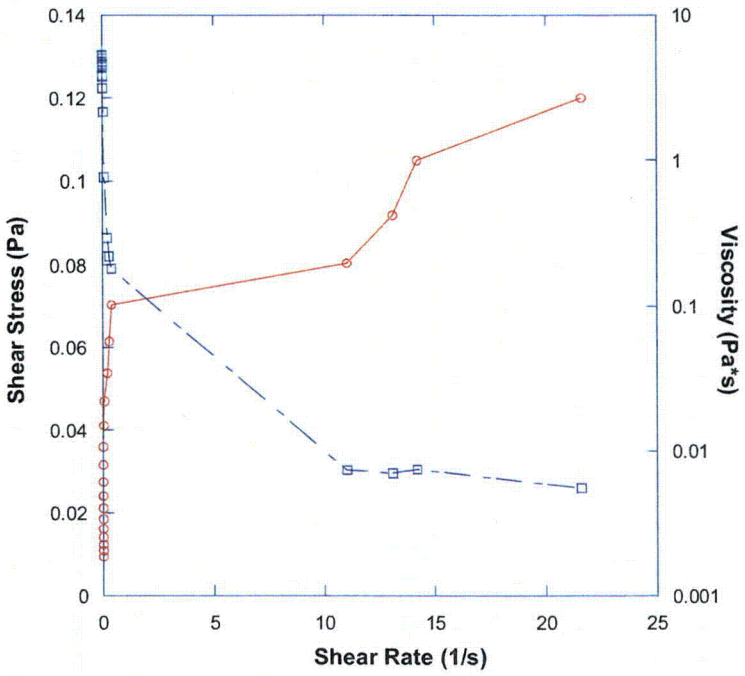

Figure 37. Sample 1220-U at 25°C rheology. Blue data lines (boxes) indicate viscosity. Red data lines (circles) indicate shear stress.

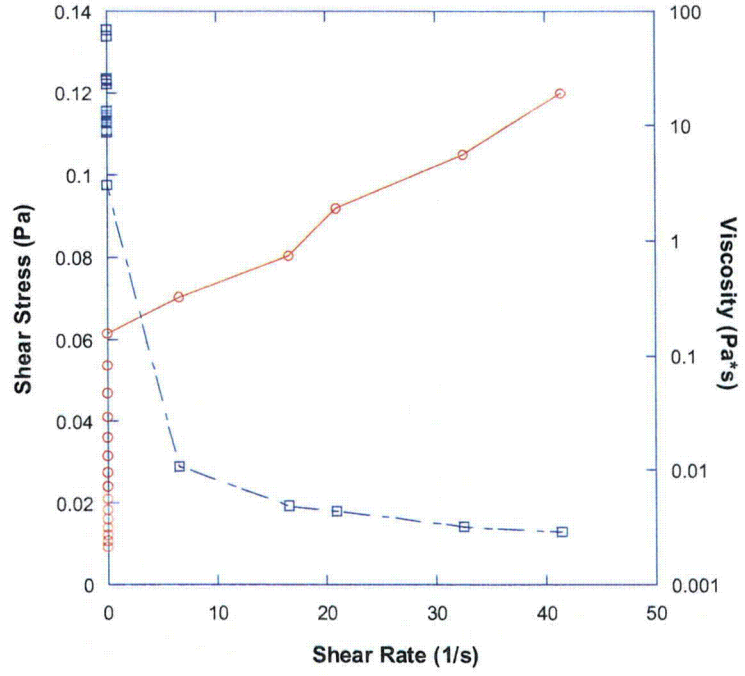

Figure 38. 1220-F at 25°C rheology. Blue data lines (boxes) indicate viscosity. Red data lines (circles) indicate shear stress.

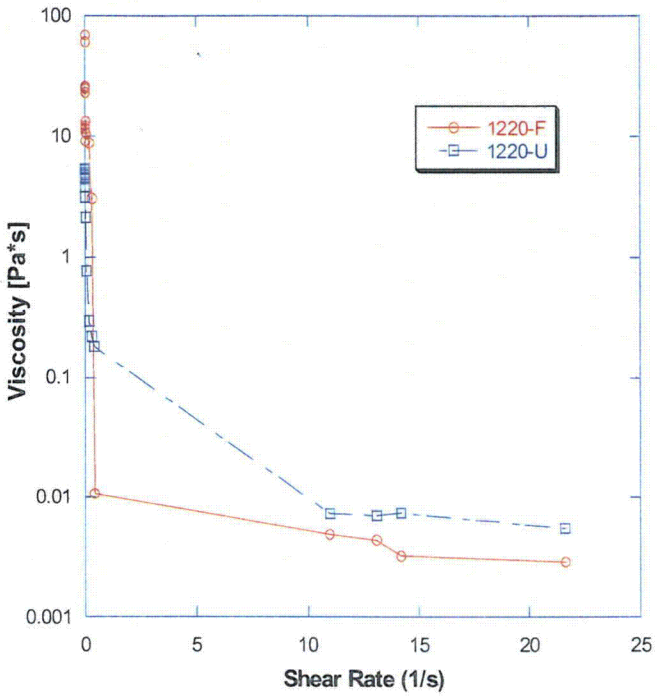

Figure 39. 1220 U and 1220 F viscosity series comparison at 25°C.

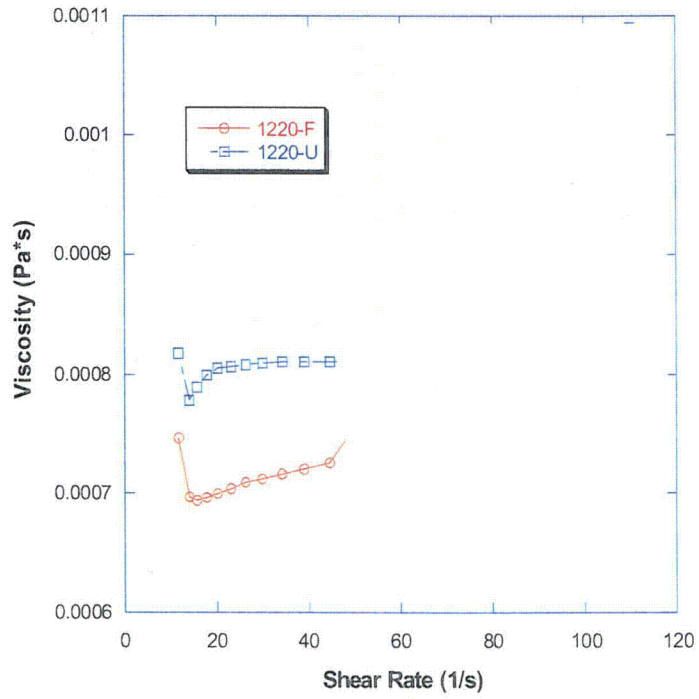

Figure 40. 1220 U and F series viscosity comparison at 60°C.

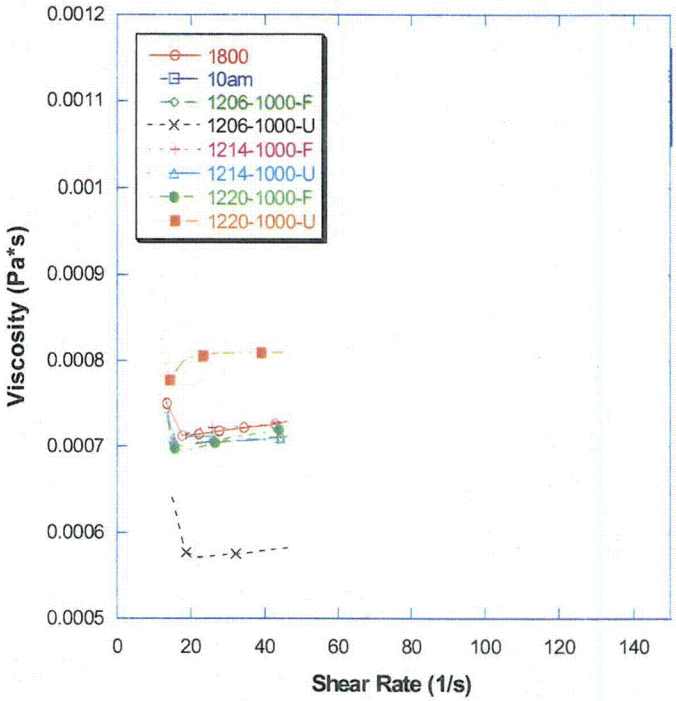

Figure 41. 60°C viscosity aging study plot.

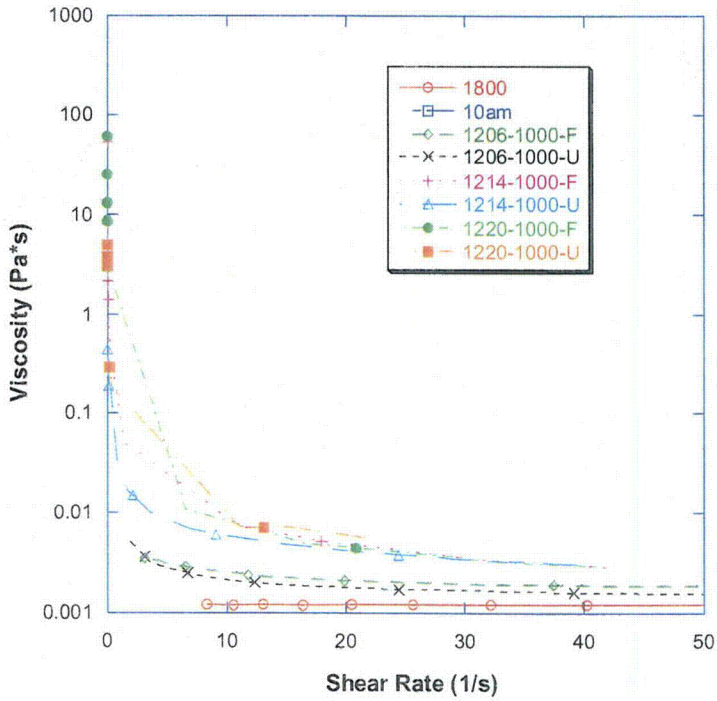

Figure 42. 25°C viscosity aging study plot.

4.5.7 Metal Ion Concentrations

Metal ion concentrations in the daily water samples were analyzed by Assaigai Analytical Laboratories, Inc. (AALI), using inductively coupled plasma (ICP) spectroscopy. During the first 25 days of the test, both filtered and unfiltered samples were taken for analysis. Because of nondistinct differences between the filtered and unfiltered samples, only unfiltered samples were taken to be analyzed after Day 25 for the duration of the test. Filters used were Whatman GF/F glass microfiber filters with a 47-mm diameter and a nominal pore size of 0.7 micron. Individual metal concentration results are presented in Figure 43 through Figure 48.

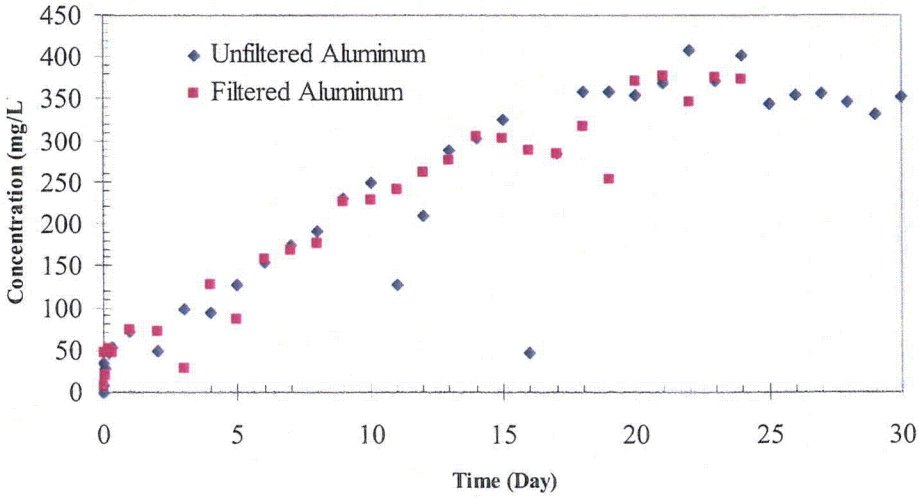

Figure 43. Aluminum concentration trend in ICET Test #1 daily water samples.

As seen in Figure 43, the aluminum concentration increased in a linear fashion over the test period until Day 16. After Day 18, the concentration appeared to level off at approximately 350 mg/L.

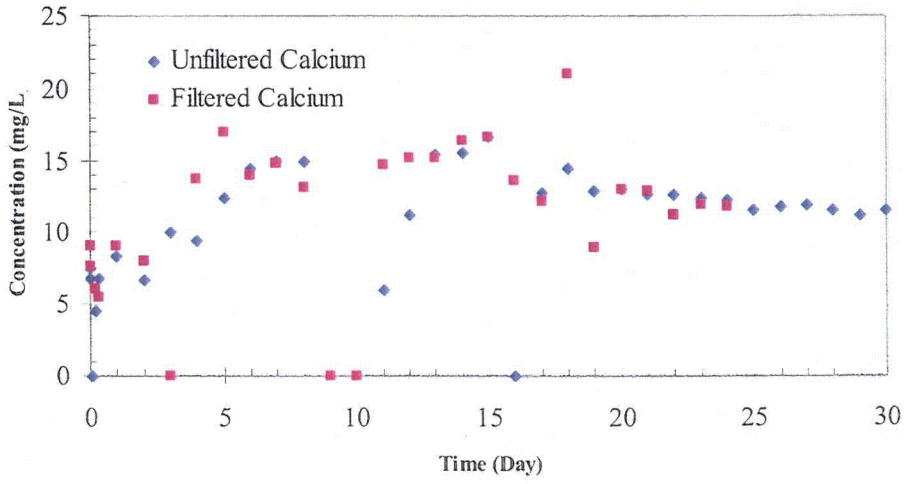

Figure 44. Calcium concentration trend in ICET Test #1 daily water samples.

Referring to Figure 44, the calcium concentration increased until Day 7, after which the concentration held somewhat constant until Day 13. From Day 13 to the end of the test, the calcium concentration decreased slightly to a value of 11.6 mg/L. As shown in Figure 45, the copper concentration remained moderately constant throughout the test.

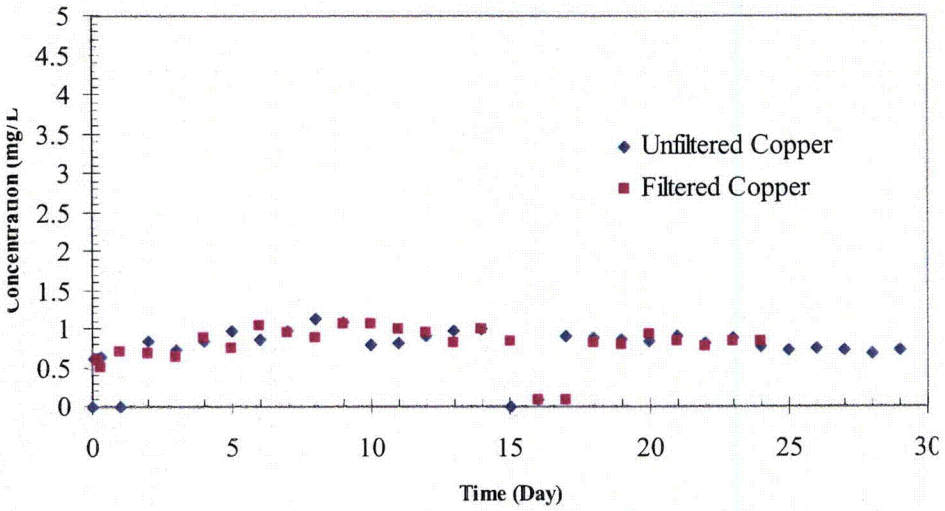

Figure 45. Copper concentration trend in ICET Test #1 daily water samples.

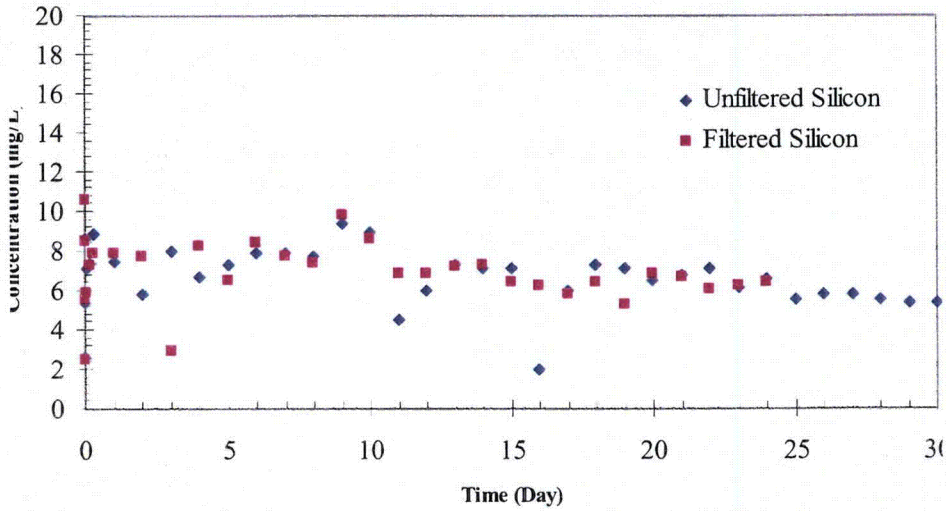

Figure 46. Silicon concentration trend in ICET Test #1 daily water samples.

Figure 46 shows that the silicon concentration was increased to approximately 10 mg/L at the beginning of the test. This concentration can be attributed to the addition of latent debris and fiberglass. The concentration stabilized at approximately 8 mg/L and gradually decreased over the duration of the test. It is apparent that silica concentrations in solution, as indicated by the presence of silicon, did not increase over time.

Figure 47 illustrates that the zinc concentration increased from 0.5 to 2 mg/L during the first day of the test. By the end of the first day, the concentration had decreased in an exponential fashion until it became undetectable on Day 13. It remained undetectable for the duration of the test. Sodium concentrations in solution remained relatively constant throughout the test, as shown in Figure 48.

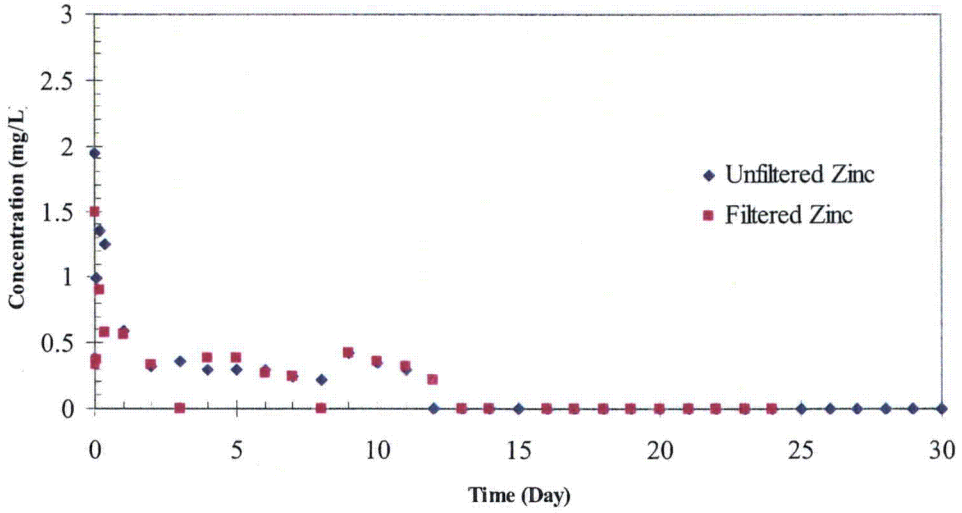

Figure 47. Zinc concentration trend in ICET Test #1 daily water samples.

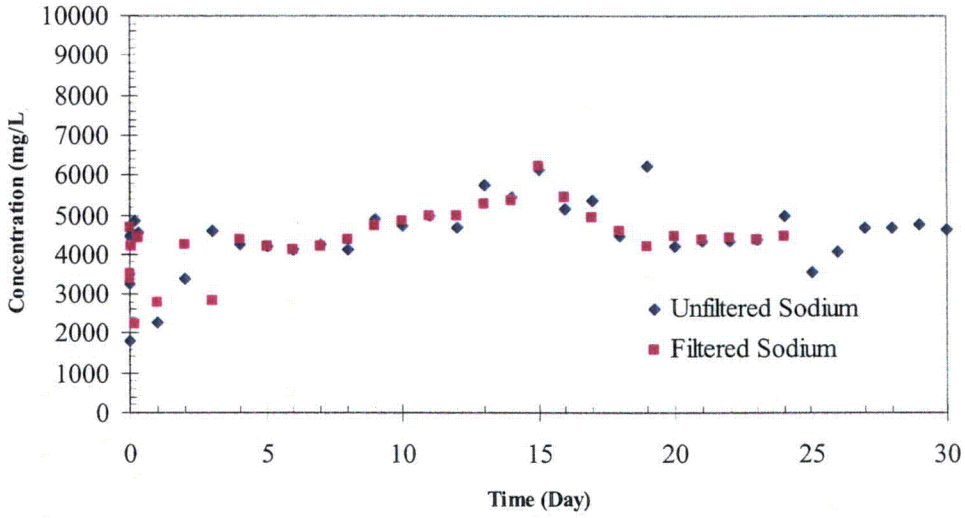

Figure 48. Sodium concentration trend in ICET Test #1 daily water samples.

Concentrations of various elements in the Metals I group, including chloride, boron, lithium, and potassium, were also monitored during the test. The first measurement was taken before the addition of NaOH spray, and the second measurement was taken after the NaOH spray. A third measurement was taken on Day 15, the middle of the test, and a fourth measurement was taken at the end of the test. As seen in Table 6, the experimental measurements were relatively constant throughout the test and within measurement uncertainties.

Table 6. Metal Concentrations for ICET Test #1

Time (Day)	Sample ID	Chloride	Boron	Lithium	Potassium
		mg/L			
0 (Before Spray)	ICET-1120-1703-U	80.3	3050	0.161	ND[a]
0 (Before Spray)	ICET-1120-1710-F	79.8	3120	0.19	ND
0 (After Spray)	ICET-1121-1035-U	81.4	2860	0.176	3.2
0 (After Spray)	ICET-1121-1035-F	82	2840	0.218	2.8
15	ICET-1206-1000-U	80.6	3090	0.34	9.1
15	ICET-1206-1000-F	82.1	2840	0.32	9.1
30	ICET-1221-800-U	78.6	2400	0.23	5.3
Min		78.6	2400	0.161	2.8
Max		82.1	3120	0.34	9.1
Standard Deviation		1.26	246.43	0.07	3.07

[a]ND = nondetect

4.6 Precipitated Solids

The most physically homogeneous samples extracted from the ICET experiment are those of the white chemical products formed in T1 solution upon cooling. This material is generically referred to as a "precipitate," but the exact physical formation mechanism has not been confirmed. Although consistent in appearance with a chemical flocculent formed via precipitation, the white material may also be formed by aggregation of smaller particles that are not visible at the test temperature or by nucleation upon small particles of other compounds that reside in solution at the test temperature.

Samples of filtered and unfiltered solution were collected in 250-mL plastic containers during each sampling episode and have been stored in the laboratory at ambient temperature. These samples were examined after being stored for several days. The initial samples (before initiation of the test) do not contain precipitate. The sample collected at 30 minutes into the test (after the NaOH addition was terminated) contains trace amounts of white precipitate, which can be seen if the bottle is gently tilted from side to side. However, the amount is so small that the precipitate is not visible on the bottom of the container. The 8-hour sample contains sufficient precipitate that the entire bottom of the bottle is coated with white precipitate. The quantity of precipitate appears to increase with each subsequent daily sample. The precipitate is a white, nearly neutrally buoyant material that qualitatively looks like aluminum hydroxide with boron. This precipitate does not appear to aggregate or coagulate into a cohesive mass, even after days of undisturbed settling. Only slight agitation is needed to remix the entire quantity into a uniform suspension with the supernate. A representative composition of this material is discussed in Section 4.6.2.

Sediment was observed on the bottom of the tank after the water column became less turbid. The material on the bottom of the tank is mostly white but with more color variation than the precipitate in the bottles. It also has a more granular appearance and is likely an agglomeration of the latent debris and concrete dust added to the tank, combined with a small quantity of the white precipitate observed in the bottles. No visible suspended precipitate was ever observed in the fluid inside the tank at the test temperature. Appendix H contains a more detailed evaluation of the tank sediment, including SEM images illustrating that a significant amount of fragmented fiberglass is also present in the settled debris.

4.6.1 TEM

The high resolution of the TEM, at least an order of magnitude greater than SEM, allows for qualitative size assessment of the underlying visible structures and aggregates. Small sample bottles of test solution were provided to the TEM laboratory, from which single drops of solution were extracted for examination. Settled precipitate was visible in most of the bottles that were transferred for TEM, and although the vials were not intentionally mixed before extracting droplets from the supernate, the semisolid particles visible in the following images represent suspended precipitate. The primary objective of TEM analysis is to determine whether the solids have a physical structure that is more consistent with microcrystalline flocculent or with amorphous hydrated gels. The TEM sample holder consists of a lacy carbon-coated grid that serves to suspend a liquid sample so that the diagnostic beam can be transmitted through the sample without interference from the sample mount. The sample grid is evident in many of the following images as a network of large sharply defined structures of uniform shading. In contrast, the appearance of suspended solids is very irregular, with much more color variation and evidence of structure on a much smaller scale than the sample grid.

Figure 49 presents a TEM image of a Day-15 filtered water sample that was allowed to cool to ambient temperature before examination. In fact, the TEM laboratory has no provisions for maintaining an in-situ sample temperature during analysis. From this figure, it appears that the larger aggregate structure comprises units of approximately 10 nm in diameter. After only 15 days of agglomeration and "aging," smaller unit structures are still readily apparent.

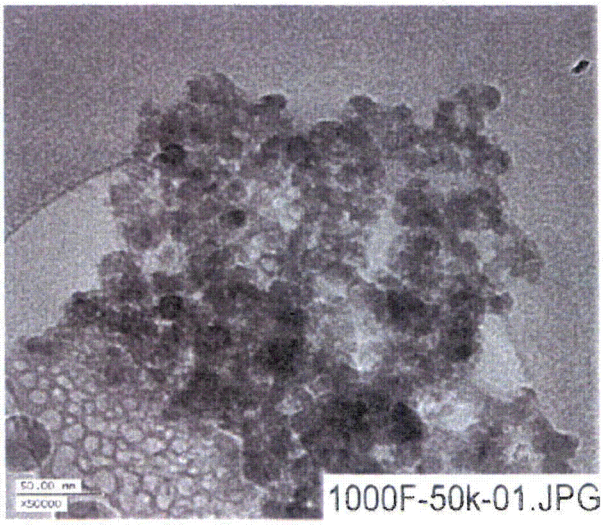

Figure 49. Electron micrograph magnified 50,000 times for the Day-15 filtered test sample.

Figure 50 through Figure 52 present comparisons of electron micrographs magnified by 4000, 10,000, and 50,000 times for the Day-30 unfiltered test samples. Increasing resolution reinforces the visual impression that suspended particulates with characteristic dimensions ranging from a few to tens of micrometers are actually agglomerations of globular nanoscale structures that may represent the characteristic minimal unit size of the aggregate. Similar comparisons for the Day-15 and Day-30 filtered test samples are presented in the appendices. Visual comparisons show that the Day-30 micrographs appear more granular than the Day-15 photographs. A comparison of Figure 49 and Figure 52 indicates a greater degree of aggregation in the Day-30 sample in that the basic structures are more uniformly packed.

It is unlikely that the precipitate material examined here will behave in the same manner as more familiar particulates such as iron oxide and silica-based soil with respect to its inherent head-loss properties. Furthermore, it would be difficult to estimate these properties based on geometric approximations that are based on particle size alone, given the difficulty of defining from these images a discrete physical element that would dominate flow resistance.

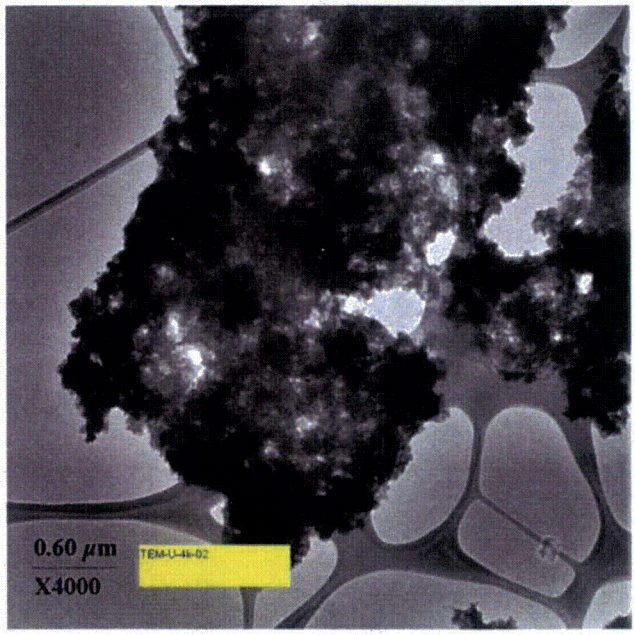

Figure 50. Electron micrograph magnified 4000 times for the Day-30 unfiltered test sample.

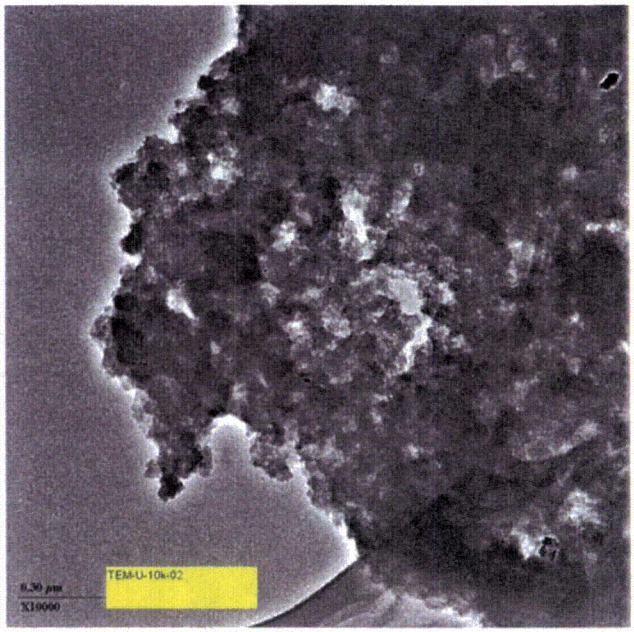

Figure 51. Electron micrograph magnified 10,000 times for the Day-30 unfiltered test sample.

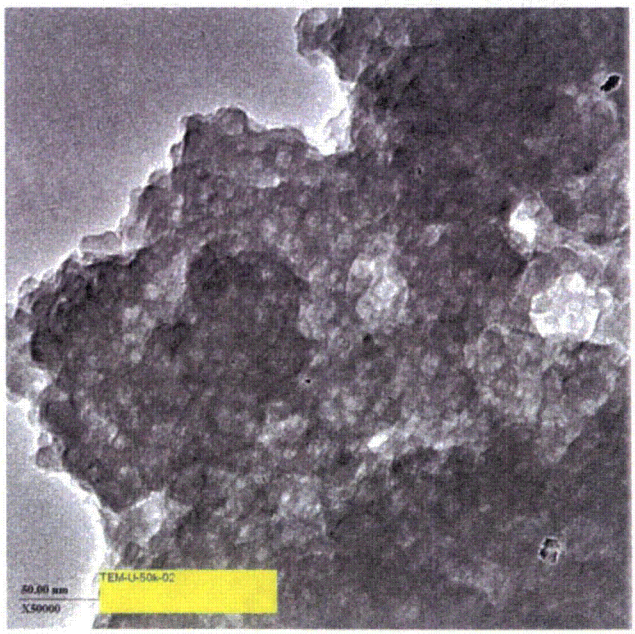

Figure 52. Electron micrograph magnified 50,000 times for the Day-30 unfiltered test sample.

Figure 53 and Figure 54 show TEM diffraction images magnified by 20 times for the Day-15 filtered and Day-30 unfiltered samples. The diffraction patterns represent structures present at one spatial location within an image such as those presented above. Some evidence of coherent diffraction patterns (bright spots) are observed at some sample locations, but no evidence of microcrystalline diffraction is observed at other locations (smooth uniform rings). In general, the TEM diffraction patterns are more similar to Figure 54. Filtered and unfiltered test samples show similar variations in transmission diffraction patterns,

suggesting that hot filtration either did not remove or did not prevent the formation of the suspend particulates identified in these examinations. TEM images for the Day-30 samples, which are included in the appendices of this report, show much less evidence of structure for the locations that were analyzed.

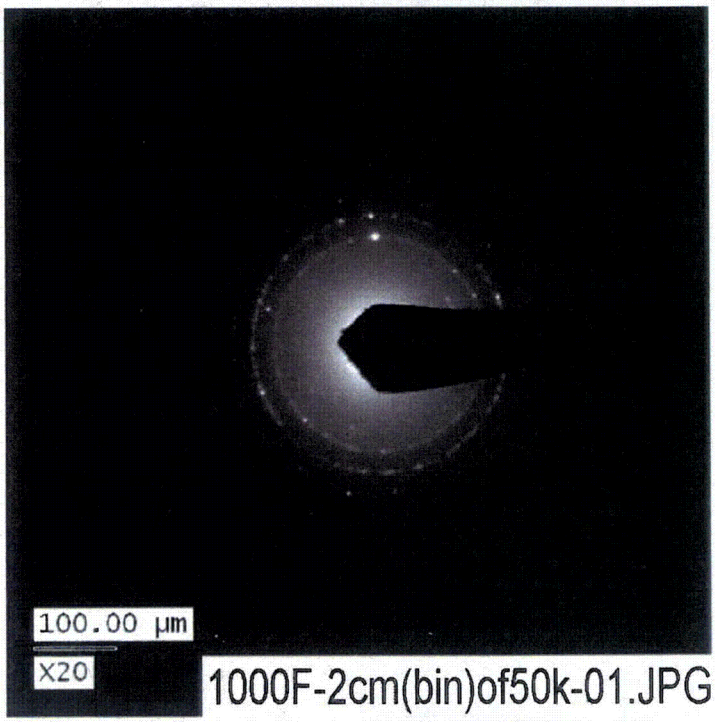

Figure 53. TEM image magnified 20 times for Day-15 filtered water sample.

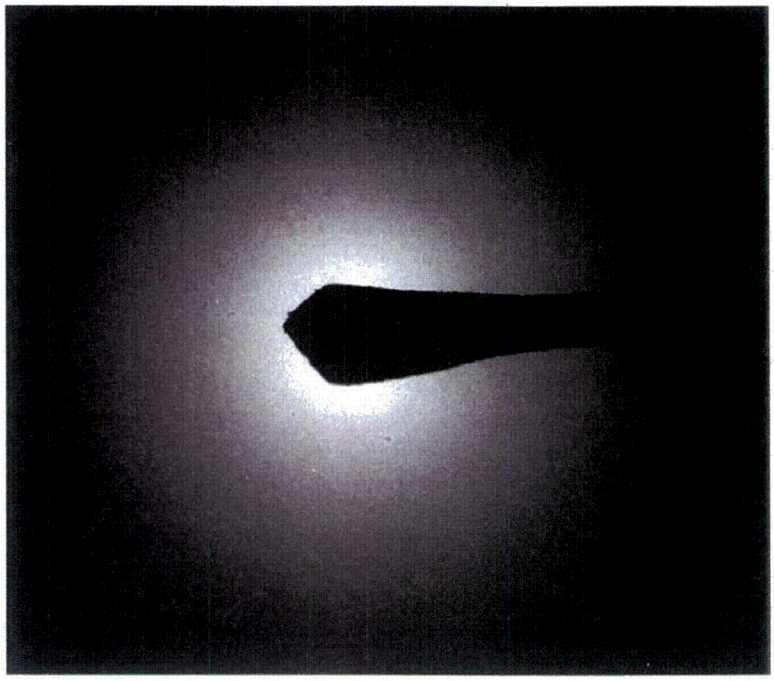

Figure 54. TEM micrograph magnified 20 times from the Day-30 unfiltered sample. (TEM-U-20cm-bin-03)

4.6.2 Additional Analytical Results

As described in Section 3.4, XRD, XRF, and ICP are potentially useful methods to determine compositions of materials. XRD is used to determine the composition and the structure of solid polycrystalline substances. This technique was used in an attempt to characterize two separate samples from Test #1. Figure 55 and Figure 56 present, for samples 1 and 2, respectively, data from XRD examinations of the post T1 sludge that was obtained upon draining and storage of the effluent. The sludge examined in Figure 55 was dried in stages within a small liquid sample bottle containing suspended material using a 50°C hotplate. One sample of semidry paste was extracted for examination, and then the remainder was dried more completely and powdered for the x-ray mount. The bottom pattern shown in Figure 55 corresponds to the moist paste, whereas the top pattern corresponds to the dried then powdered sludge.

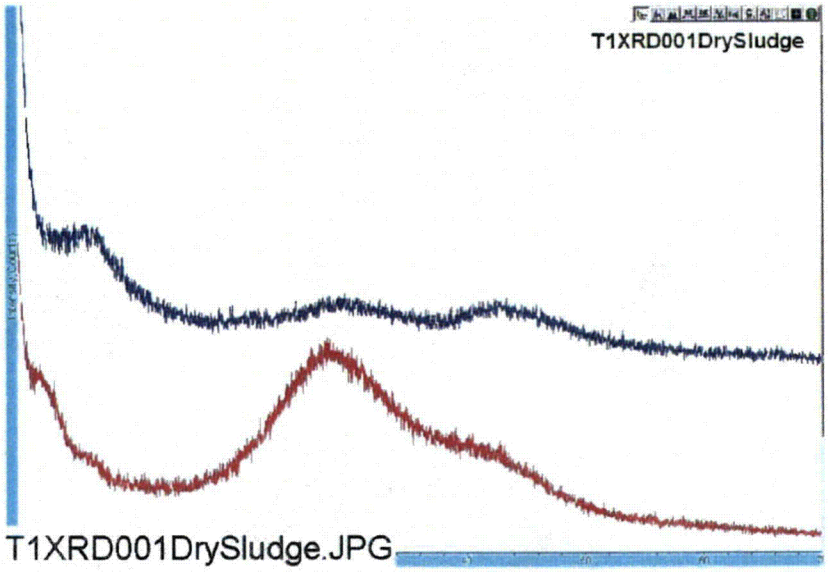

Figure 55. Intensity vs scattering angle for post-T1 dry sludge (sample 1), bottom–moist paste, top–dry powder.

A second sample of the precipitate was air dried overnight in a convection oven at approximately 38°C. Figure 56 presents the XRD analysis results for this sample, which exhibits a significant amorphous component along with tincalconite and borax at a ratio of ~90:10 weight percent of tincalconite to borax.

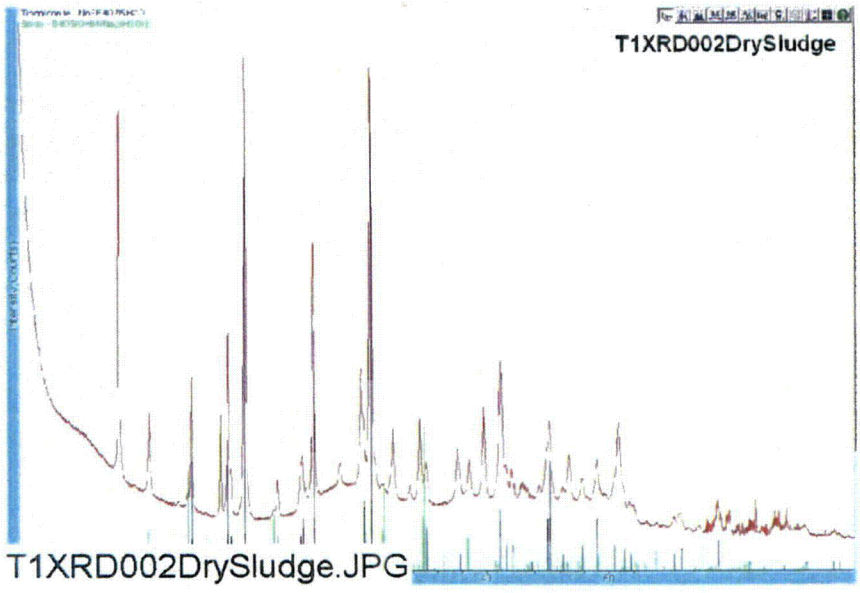

Figure 56. Intensity vs scattering angle for post-T1 dried sludge (sample 2).

As may be seen from a comparison of Figure 55 and Figure 56, one of the samples exhibited a crystalline structure with the characteristic scattering properties of tincalconite superimposed on an underlying amorphous trend, whereas the other sample was wholly amorphous in nature. Additional investigations are necessary to determine the exact origin of the difference, but thermal history clearly plays a role in determining the structural configuration at the time of examination.

XRF was also used to determine, both qualitatively and quantitatively, the elemental composition of the precipitates from Test #1. The elemental composition of solid samples is obtained from XRF instead of specific substances (i.e., compounds). The results of this testing indicate that the precipitates of Test #1 were mainly composed of Na, Al, Ca, and Si. The accuracy of the results depends on how closely the comparative standards resemble the sample. Also, the sensitivity of XRF decreases with decreasing atomic weight, so it is normally difficult to identify an element with an atomic number that is less than that of carbon.

Table 7 presents an elemental summary of the ICP analysis for the precipitate. This analysis is reflective of the typical test analysis performed during Test #1, with the exception of carbonates. All elements, except for carbonates, were analyzed by ICP-AES. The carbonate value was obtained by titration using EPA method 310.1.[23] The elements detected accounted for 55%, 84%, and 78% of the total sample composition. The precipitate is largely composed of carbonate, aluminum, boron, and sodium, which can be seen in Table 8. The remainder consists of elements not detected by ICP, which notably includes oxygen.

Table 7. Composition of Precipitates

Element	mg/kg		
	11/27 Precipitate (Day 6)	**12/08 Precipitate (Day 17)**	**12/17 Precipitate (Day 26)**
CO_3^{2-}	208,000	169,000	217,000
Al	38,600	99,600	89,200
B	125,000	202,000	139,000
Ca	3980	3800	3660
Cu	145	126	118
Fe	ND[a]	5	ND
Pb	ND	ND	ND
Li	9	9	ND
Mg	63	34	28
Ni	1	1	2
K	310	354	359
Si	733	754	422
Zn	76	6	ND
Na	170,000	363,000	334,000
Wt % of Total Sample	55	84	78

[a]ND = nondetect.

Table 8. *Main Elemental Components of Precipitate*

Element	Mass % of Detected Sample			
	11/27 Precipitate (Day 6)	12/08 Precipitate (Day 17)	12/17 Precipitate (Day 26)	Average Precipitate
CO_3^{2-}	38	20	28	29
Al	7	12	11	10
B	23	24	18	22
Na	31	43	43	39
Other	1	1	1	1

Table 9 presents an elemental summary of the ICP analysis for the filtered precipitate. The glass fiber filter was digested with the filtered precipitate; thus, the weight percent includes the filter. However, the ICP results of the filtered precipitate have been corrected to help eliminate any elemental contribution from the digested glass fiber filter. This correction was done by performing ICP-AES elemental analyses on a blank filter from the same batch of filters as that used for the filtered precipitate. The results of that analysis were subtracted from the overall results of the filtered precipitate. It appears that the filtered precipitate is largely composed of sodium, boron, and aluminum.

Table 9. Filtered Precipitate ICP Results

Element	mg/kg		
	11/27 Filtered Precipitate (Day 6)	12/08 Filtered Precipitate (Day 17)	12/17 Filtered Precipitate (Day 26)
Al	351	3,989	641
B	6864	5935	5863
Ca	ND[a]	ND	ND
Cu	ND	ND	ND
Fe	ND	ND	ND
Pb	ND	ND	ND
Li	ND	ND	ND
Mg	ND	ND	ND
Ni	ND	ND	ND
K	ND	ND	ND
Si	551	285	321
Zn	ND	ND	ND
Na	12,275	4511	13,055
Wt % of Total Sample	2	1	2

[a]ND = nondetect.

Table 10 presents the ICP results for the test sediment, concrete, dirt, and fiberglass insulation. The concrete, dirt, and fiberglass-insulation ICP results were performed in attempts to normalize the sediment results to produce a qualitative composition. Because very small amounts of the dirt and concrete were added to the tank, their contribution may be negligible, although their compositions were of interest. The sodium concentration of the sediment was not provided; thus, the results were not normalized because it was assumed, based on the composition of the previous precipitates, that sodium may be a major part of

the sediment composition. Further analysis of the sediment must be performed before any definite conclusions can be reached.

Table 10. Solid Sample and Reference ICP Results

Element	mg/kg			
	Fiberglass Insulation	Dirt	Concrete	Sediment
Al	114	7230	2770	6460
B	1440	NA[b]	8	3750
Ca	3920	9820	47,300	3090
Cu	ND[a]	34	112	744
Fe	201	12,200	3120	6100
Pb	4	9	4	32
Li	3	6	3	12
Mg	1100	2290	905	883
Ni	ND	7	5	327
K	526	926	434	153
Si	110	965	1850	670
Zn	11	42	30	5600
Na	10,100	868	474	NA
Wt % of Total Sample	1.75	3.44	5.70	3

[a]ND = nondetect.
[b]NA = not applicable.

The elemental composition of the precipitate has been investigated by EDS, XRF, and ICP spectroscopy. Substantial variability in measured elemental concentrations was observed between samples analyzed with the same method and between diagnostic methods applied to the same sample. A survey of these measurements was performed to recommend suitably averaged mass proportions for the dominant constituents that were observed (see Table 11).

Table 11. Elemental Composition (wt %) of 30-Day High-Volume Filtrate

Element	Method		
	EDS	ICP	XRF
O	48	–	45
Al	11	11	7
Ca	2	0.4	0.8
Na	16	43	24
B	21	18	–
CO_3^{2-}	–	28	–
$H_2O + CO_2$	–	–	34

5.0 RECOMMENDATIONS

Many practical lessons were learned during ICET Test #1 that may serve to improve the quality of information obtained in subsequent tests and the efficiency with which daily operations can be managed. The following items have been discussed with the NRC/industry sponsors, with input from LANL and UNM investigators for consideration as minor modifications to the ICET Test #2 plan and procedures.

- Continue the practice of daily water sampling, but reduce the frequency of comparison between filtered and unfiltered samples if the differences again become negligible. In Test #1, there was no measurable difference in TSS, viscosity, or ICP elemental composition after the bulk turbidity dropped.

- Given the continued increase in the rate of observed precipitation in extracted samples and the continued increase in aluminum concentrations beyond 15 days, plan all subsequent tests for a duration of 30 days.

- Acquire duplicate water baths to improve control of water temperature for extracted samples waiting for viscosity and turbidity measurement. The post-Test #1 interest in controlled-temperature precipitation studies further justifies the need for this equipment.

- Continue the practice of daily water sample viscosity measurements, but eliminate the requirement for replicate measurements if the same level of precision is achieved. Variations between repeated measurements under the Test #1 protocol were less than 1%.

- The presence of deposits on exposed surfaces of the fiberglass blankets and the decline of silicon concentrations in solution raise questions about realistic exposure of fiberglass debris to the test solution. SS mesh sample bags were prepared for Test #1 to confine the fibers, but deposits were noted only on fiber layers next to the mesh, even for mesh envelopes embedded in larger blankets.

  - For Test #2, construct a small mesh sample box (in addition to the original bags) to hold a loose collection of fiber that is not compressed on all sides.

  - Wrap a 1/2-in.- to 1-in.-thick mesh bag around the lower 4 in. of the drain screen to expose a small amount of fiber to higher water velocities.

6.0 REFERENCES

1. MOU on Cooperative Nuclear Safety Between NRC and EPRI, Addendum on Integral Chemical Effects Testing for PWR ECCS Recirculation, NRC ADAMS Record No. ML042880402.

2. "Test Plan: Characterization of Chemical and Corrosion Effects Potentially Occurring Inside a PWR Containment Following a LOCA, Rev. 12a," October 6, 2004.

3. Macur, J., Chapter 8 "Materials Characterization and Chemical Analysis," 2nd ed., John Sibilia, Ed., VCH Publishers, Inc., New York (1996).

4. Ibid 3.

5. Iowa State Materials Science Homepage.

6. Ibid 5.

7. Goldstein, J., Scanning Electron Microscopy and X-ray Microanalysis, 2nd ed., Plenum Press: New York (1992).

8. Ibid 3.

9. Ibid 3.

10. Ibid 7.

11. Ibid 3.

12. Ibid 3.

13. Williams, D. B., "X-ray Spectrometry in Electron Beam Instruments; Plenum Press: New York (1995).

14. Ibid 3.

15. Williams, R., Chapter 6 "Materials Characterization and Chemical Analysis," 2nd ed., John Sibilia, Ed., VCH Publishers, Inc., New York (1996).

16. Montaser, A., "Inductively Coupled Plasmas in Analytical Atomic Spectrometry"; VCH Publishers, Inc., New York (1987).

17. Ibid 15.

18. Murthy, N. Chapter 7, "Materials Characterization and Chemical Analysis," 2nd ed., John Sibilia, Ed., VCH Publishers, Inc., New York (1996).

19. Jenkins, R., "Quantitative X-Ray Spectrometry, Marcel Dekker Inc., New York (1981).

20. Ibid 18.

21. Ibid 18.

22. Barrett, C. S., "Advances in X-ray Analysis." Vol. 29, Plenum Press, New York (1986).

23 U.S. Environmental Protection Agency, "EPA Method 310.1, Alkalinity - Titrimetric, pH 4.5 Alkalinity," EPA Report No. 600/4-79-020.

Preface to Appendices

This preface provides a brief guide to assist in the access and interpretation of the data appendices that follow. Standardized nomenclature is defined first to clarify the origin of samples that are described in the data sets. Then an outline of the appendices is provided with a description of how they were compiled. A list of figures with captions and page numbers is provided for each individual appendix to facilitate access of the desired information.

Nomenclature

Many spatially unique but physically similar sample types were collected in ICET Test 1. To ensure that consistent interpretations and comparisons of data sets are made, it is imperative that a standardized nomenclature be adopted when referring to each sample type. Many different qualitative descriptions of these samples might be equally suitable, but different adjectives convey different connotations to each observer. Therefore, the following definitions establish the convention used in this report when making generic references to sample type. Every effort should be made to adhere to this standard when interpreting the data so that all future audiences will have a common understanding of sample origins from the ICET series.

White Precipitate — Upon cooling below the test temperature, T1 daily water samples extracted from the tank formed a visible white material that is referred to as a precipitate. Although the exact formation mechanism has not been confirmed, the material exists as a distinct physical phase separate from the aqueous solution from which it evolved.

Latent Debris — Commercial power plants gradually accumulate dust, dirt, and fibrous lint that are generically referred to as latent debris. This classification distinguishes resident material from debris generated during the accident scenario. At the beginning of T1, measured quantities of crushed concrete and soil were added to simulate the latent debris present in containment. These materials were examined via SEM/EDS to establish a baseline composition for comparison to sediment samples (see "Sediment" below).

Sediment — Surrogate latent debris particulates and fugitive fiberglass fragments that were initially suspended in water at the beginning of T1 gradually settled to the bottom of the tank to form a layer of sediment. During the course of the test, additional material may have been deposited in this layer. At the conclusion of the test, the sediment layer was recovered as completely as possible.

Sludge — At the conclusion of T1, all water was drained slowly from the tank and stored in a large plastic reservoir. Upon cooling, this

liquid effluent also precipitated white material that collected in large quantities at the bottom of the reservoir. Although the material produced at the end of the test is certainly related to the precipitate observed in the daily water samples, it will be referred to as "sludge" to connote the quantities that were produced and to identify the exact source of the samples that were examined.

White Residue

At the conclusion of T1, all water was drained slowly from the tank. Exposed metal surfaces that cooled rapidly collected a thin deposit of white residue or scale. Some of this material was scraped from internal piping surfaces and tank walls for comparison with other sample types, such as white precipitate from the daily water samples.

Fiberglass

One of the principal debris types introduced to T1 was shredded fiberglass insulation. This debris was bundled in 3-in.-thick bags (or blankets) made of SS mesh to prevent ingestion through the pump and to better control the placement of debris in various flow regimes. Fiberglass samples are designated by their placement in high-flow and low-flow areas of the tank. Additional, small, 4-in.-square envelopes of fiberglass were also prepared for extraction during the course of the test. These samples are referred to as "sacrificial" samples. Some amount of fiber, especially short fiber fragments, escaped the mesh bags and was deposited in other locations within the tank. This material is referred to as "fugitive" fiberglass.

Drain Screen

A 10-in.-tall screen made of coarse SS mesh wrapped into a 2-in.-diameter cylinder was inserted into the outlet drain at the bottom of the tank to protect the pump from ingestion of large debris items. Because the drain screen was exposed to higher velocity-directed water flow, it gradually accumulated a layer of debris around the lower few inches of mesh. This material was examined as a separate debris location to identify any apparent differences with other sample locations, such as fiberglass blankets and tank sediment.

Gelatinous Material

This term generically refers to any observed sample constituent with amorphous, hydrated, or noncrystalline physical characteristics.

Colloidal Suspension

Several different diagnostic techniques have shown evidence of microscopic particles suspended in T1 test liquid that are invisible to the unaided eye. The extremely small sizes of these particles (5 to 20 nm) suggest that they may be colloidal in nature and that

they remain in suspension or are formed in suspension after larger particulates have settled to the bottom.

Water Sample — Daily water samples are extracted from the ICET tank for elemental concentration analyses. After properly flushing the sample line, some of this water is extracted directly from the tap. An equal amount of water is also generally collected through a micropore filter. Thus, daily water samples are designated as filtered (F) and unfiltered (U), and a corresponding filter paper exists in the sample archive for each daily sample that is collected.

High-Volume Filter — In addition to the relatively small volumes collected during daily water sampling, larger quantities were periodically extracted for filtration to determine whether suspended chemical products were present in the test liquid under in situ conditions. The intent of this exercise was to maintain the liquid temperature while forcing the liquid through a micropore filter under vacuum. Temperature control for the T1 high-volume filter samples was not ideal, so the collected filtrate may show evidence of temperature-dependent precipitation similar to that described for white precipitate.

Filter Paper — Many different samples of tank solution were fractionated by micropore filtration into a liquid supernate and a solid filtrate that existed at the time and temperature condition of the filtering process. These samples include (1) daily water samples filtered during extraction, (2) daily water samples filtered after cooling to room temperature, and (3) high-volume water samples.

Chemical Deposits — Sacrificial fiberglass samples that were extracted at Day 15 and Day 30 showed evidence of chemical products forming on and between fiber strands. These products are referred to as "deposits," although the exact physical mechanism of formation is not well understood. The physical appearance suggests growth, agglomeration, or crystallization on and around the fiber strands over time rather than capture or impaction of particles from the bulk solution. This observation is supported by the fact that the small fiberglass samples were located in a region of very low directed water flow (i.e., in the interior of larger blankets).

Concrete Sample — Several chips of concrete (1/4 in. to 3/4 in. in diameter) were broken from the primary slab of submerged concrete and introduced to the tank in a small SS envelope at the start of the test. Examinations of these chips were conducted to determine if concrete surfaces provide a preferential site for gel formation.

Having defined these terms, the reader may note, nonetheless, minor inconsistencies in the caption labels of these appendices. The caption labels use the same descriptions that were applied in laboratory notebooks to improve traceability of the data.

Usage

Eight appendices are provided that present data collected for the following sample types and analysis methods:

(A)	SEM data for 24-hour high-volume filtrate;	p. A-1
(B)	SEM/EDS of the Test-1 Day-15 fiberglass and filtrate;	p. B-1
(C)	SEM/EDS data for Test-1 Day-30 fiberglass and filtrate;	p. C-1
(D)	SEM/EDS data for white precipitate, Day-30 fiberglass, drain screen debris, pipe residue, tank sediment, concrete samples, latent debris baselines, and Test-1 Day-30 high-volume filtrate;	p. D-1
(E)	TEM analyses of Test-1 Day-15 water samples;	p. E-1
(F)	TEM analyses of Test-1 Day-30 water samples;	p. F-1
(G)	TEM analyses of pre-test 1 laboratory solution;	p. G-1
(H)	Sediment Analysis for Test #1.	p. H-1

These data are largely qualitative in nature, consisting primarily of SEM and TEM micrographs and EDS spectra. Each appendix represents a separate session of laboratory work that can be traced to a batch of samples that were processed in chronological order. This organization scheme preserves the connection with laboratory notebooks and timelines that naturally developed during operation; however, in a few cases, results for a given sample type may be mixed across two or more appendices because of the order in which the individual samples were analyzed.

Transcriptions of the logbooks are provided for each appendix to document better commonalities that existed among the samples at the time of analysis. Interpretation and understanding of the images and their accompanying EDS spectra will be greatly improved by referring frequently to the logbook sample descriptions and sequences. Typically, a relative large quantity of a test sample was delivered for SEM or TEM analysis, and then several small subsamples of each item were examined. Note that each subsample was assigned a sequential reference number during the laboratory session. These reference numbers have been cited in the figure captions wherever possible to preserve the connection between the micrographs and the notebook descriptions. Electronic filenames have also been stamped on the images to permit retrieval of the original data files that are archived elsewhere. Individual data sets for a given sample item have been collated into a typical sequence of (1) visual image, (2) EDS spectra, and (3) semiquantitative mass composition.

For most of the EDS spectra, semiquantitative mass compositions are also presented. These results are obtained from a commercial algorithm that decomposes the spectra into the separate contributions of each element. Several caveats should be considered when interpreting the numeric compositions thus obtained; however, despite these caveats, semiquantitative EDS analysis offers a natural complement to micrographic examination as a survey technique for identifying trends in composition.

1. The spectral deconvolution algorithm is based on a library of unique signatures of each element that were obtained for pure samples using a standard beam setting that may not match identically the conditions applied for the test item.

2. The operator must select a limited number of elements to be used in the proportional mass balance. These candidates are chosen from among the peaks that are observed in the spectrum; however, the composition percentages can vary, depending on which elements are included in the list. In a few cases, two or more alternative compositions have been generated by selecting a different set of elements from the same spectrum to illustrate the sensitivity of this technique to operator input.

3. The spectral unfolding algorithm is a statistical technique having a precision that depends on the relative quality of the data in each peak. Compositions with high R^2 correlation coefficients and total-mass normalization factors closer to unity represent the more reliable estimates. The precision obtained in the fit depends on the duration of the scan and the number of counts received in each energy bin.

4. All subsamples examined in the SEM microprobe facility are coated with a thin layer of either carbon or gold/palladium alloy to prevent charge accumulation from the impinging electron beam. Spectral peaks visible for gold (Au) and palladium (Pd) are not indigenous to the samples.

5. The EDS spectral analysis software contains a peak-recognition algorithm and an automated cursor that snaps across the spectrum to locate each peak. An accompanying library of elemental energy signatures is also provided to suggest what constituents might be contributing to a given energy bin, but the operator must judge what label to assign to the spectral image. It is possible that some peaks near closely neighboring elements have been mislabeled in these appendices. However, every effort was made to choose from candidate elements that were most likely to be present in the test material. In a few cases, the spectral peaks were not labeled by the SEM operator. These spectra should be viewed as corroborating evidence for similar samples that are labeled in a definitive manner. Careful comparisons of the energy scales in combination with a library of electron scattering energies can also be used to infer the origin of the more prominent peaks that are present in unlabeled spectra.

6. In general, the scan area of an EDS is comparable to 10 × 10 μm unless noted otherwise for a special purpose, such as examination of a 7-μm-diameter fiber strand or obtaining a bulk-average composition over a heterogeneous sample.

7. Unless an obvious spatial heterogeneity is being examined, the exact location of an EDS spectrum is not always relevant because the operator chooses arbitrary sites that are visually judged to be representative. It is not possible to sample a surface comprehensively on a microscopic basis and compute average compositions. In many cases, two or three replicate spectra are provided for this purpose, but SEM/EDS is most effective as a survey diagnostic.

8. For several reasons, EDS analysis is not particularly sensitive to the presence of boron: (a) boron has a low atomic mass that does not interact well with electrons in the beam, (b) the emission lines are very close to those of carbon, and (c) the beam port material has a high absorption cross section for these emission energies. Therefore, the correction factors used in the semiquantitative composition analysis are quite large, as are the uncertainties in the estimated percentage of total composition for this element. There may spectra presented in these appendices where the lowest energy peak is labeled as either B or C when in fact either both are present or the opposite element is present.

EDS locations were chosen manually at regions of specific interest. In many cases, multiple spectra were collected from a single sample and an annotated image is provided to identify the specific location. These annotated images are not generally noted in the laboratory log book entries, but they are provided in proper sequence within the appendices.

Appendices E and F present transmission electron microscopy data for water samples extracted from the ICET solution at Day 15 and Day 30, respectively. The purpose of this examination was to determine whether the physical structure of any suspended products exhibits crystalline or amorphous characteristics. These data are also qualitative in nature, consisting generally of a set of high-resolution micrographs followed by companion electron diffraction images. The TEM sample holder consists of a carbon grid that is "lacey" or filamentary in nature. This grid is visible as a relatively large-scale structure in the background of most images. Surface tension in a droplet of liquid suspends the particulates of interest across the grid so that the electron beam can illuminate the sample through the holes without interference from a substrate. Crystalline material will exhibit diffraction patterns unique to the molecular arrangement. Amorphous material that is diffuse or disorganized in structure will not exhibit regular diffraction patterns that can be identified.

Water samples submitted for TEM analysis are not temperature controlled because the temperature cannot be maintained during the examination. Therefore, the particulates that are observed in these samples are closely related to, if not identical to, the visible white precipitate that is observed in the daily sample bottles at room temperature.

In a few cases, data file names that were noted by the operator in the laboratory log were not successfully saved in electronic form. These cases are noted in the transcribed log sheets, but the corresponding images are unavailable and therefore cannot be presented in the data sequence.

Appendix A

SEM Data for 24-Hour High-Volume Filtrate

Figures

Figure A-1. Twenty-four-hour, high-volume-sample SEM image (HighVol_24hr002). A-2
Figure A-2. Twenty-four-hour, high-volume-sample SEM image (HighVol_24hr003). A-2
Figure A-3. Twenty-four-hour, high-volume-sample SEM image (HighVol_24hr004). A-3
Figure A-4. Twenty-four-hour, high-volume-sample SEM image (HighVol_24hr005). A-3
Figure A-5. Twenty-four-hour, high-volume-sample SEM image (HighVol_24hr006). A-4
Figure A-6. Twenty-four-hour, high-volume-sample SEM image (HighVol_24hr007). A-4
Figure A-7. Twenty-four-hour, high-volume-sample SEM image (HighVol_24hr008). A-5
Figure A-8. Twenty-four-hour, high-volume-sample SEM image (HighVol_24hr009). A-5
Figure A-9. Twenty-four-hour, high-volume-sample SEM image (HighVol_24hr010). A-6
Figure A-10. Twenty-four-hour, high-volume-sample SEM image (HighVol_24hr011). A-6
Figure A-11. Twenty-four-hour, high-volume-sample SEM image (HighVol_24hr012). A-7
Figure A-12. Twenty-four-hour, high-volume-sample SEM image (HighVol_24hr013). A-7
Figure A-13. Twenty-four-hour, high-volume-sample SEM image (HighVol_24hr014). A-8
Figure A-14. Twenty-four-hour, high-volume-sample SEM image (HighVol_24hr015). A-8
Figure A-15. Twenty-four-hour, high-volume-sample SEM image (HighVol_24hr016). A-9
Figure A-16. Twenty-four-hour, high-volume-sample SEM image (HighVol_24hr017). A-9
Figure A-17. Twenty-four-hour, high-volume-sample SEM image (HighVol_24hr018). ... A-10
Figure A-18. Twenty-four-hour, high-volume-sample SEM image (HighVol_24hr019). ... A-10
Figure A-19. Twenty-four-hour, high-volume-sample SEM image (HighVol_24hr020). ... A-11
Figure A-20. Twenty-four-hour, high-volume-sample SEM image (HighVol_24hr021). ... A-11
Figure A-21. Twenty-four-hour, high-volume-sample SEM image (HighVol_24hr022). ... A-12
Figure A-22. Twenty-four-hour, high-volume-sample SEM image (HighVol_24hr023). ... A-12
Figure A-23. Twenty-four-hour, high-volume-sample SEM image (HighVol_24hr024). ... A-13
Figure A-24. Twenty-four-hour, high-volume-sample SEM image (HighVol_24hr025). ... A-13
Figure A-25. Twenty-four-hour, high-volume-sample SEM image (HighVol_24hr026). ... A-14

A high-volume water sample was extracted and filtered at 24 hours after the initiation of ICET Test #1. This appendix presents SEM images of the filtrate that was collected from the high-volume sample. As indicated by turbidity measurements, significant quantities of surrogate latent debris were still suspended at the time of extraction. In general, filtrates of small suspended matter exhibit the most homogeneous physical features of the various samples that have been examined because they represent aggregated masses of very fine particulates. This attribute is illustrated in the relatively smooth background fields of the following images that are broken only by occasional flakes, granules, and biological remains that were present in the surrogate debris. (Recall that common soil is a major constituent of the surrogate debris). Elemental compositions of latent debris are examined in Appendix D. These analyses were performed on December 7, 2004. No EDS spectra or compositions were taken at that time.

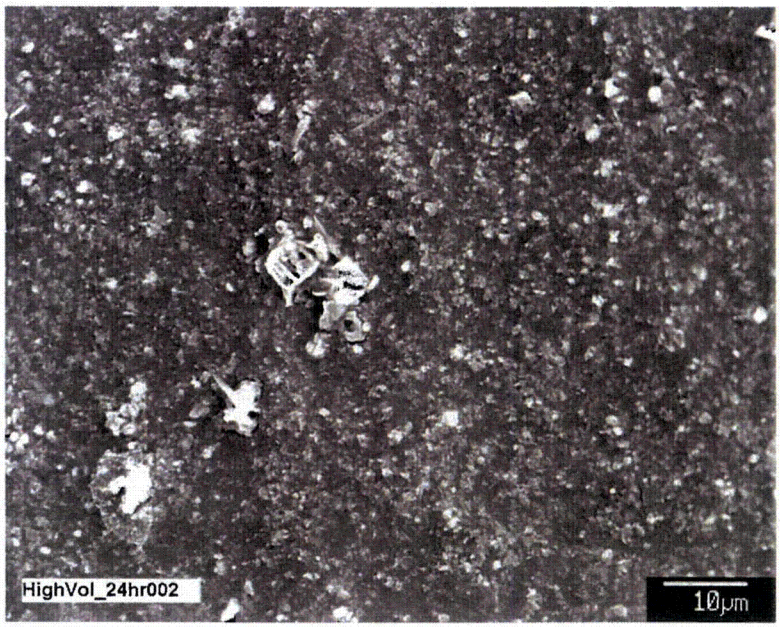

Figure A-1. Twenty-four-hour, high-volume-sample SEM image (HighVol_24hr002).

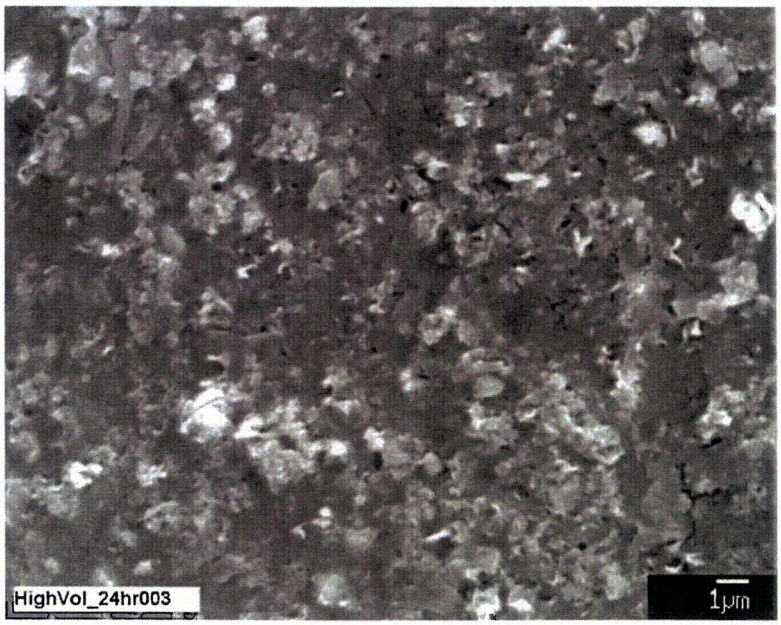

Figure A-2. Twenty-four-hour, high-volume-sample SEM image (HighVol_24hr003).

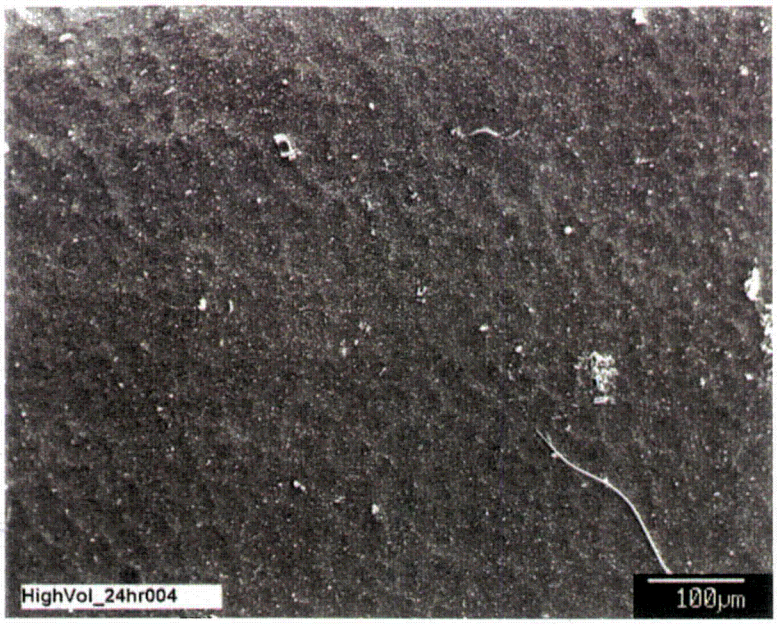

Figure A-3. Twenty-four-hour, high-volume-sample SEM image (HighVol_24hr004).

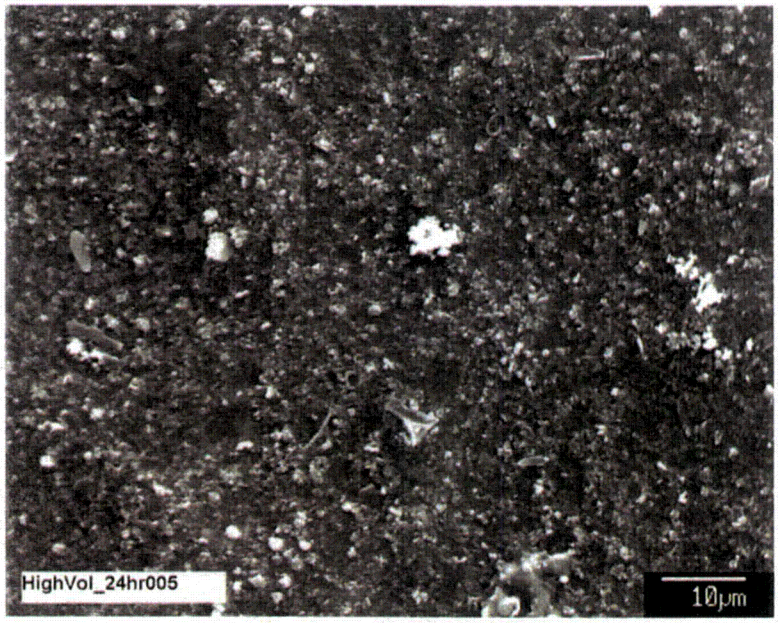

Figure A-4. Twenty-four-hour, high-volume-sample SEM image (HighVol_24hr005).

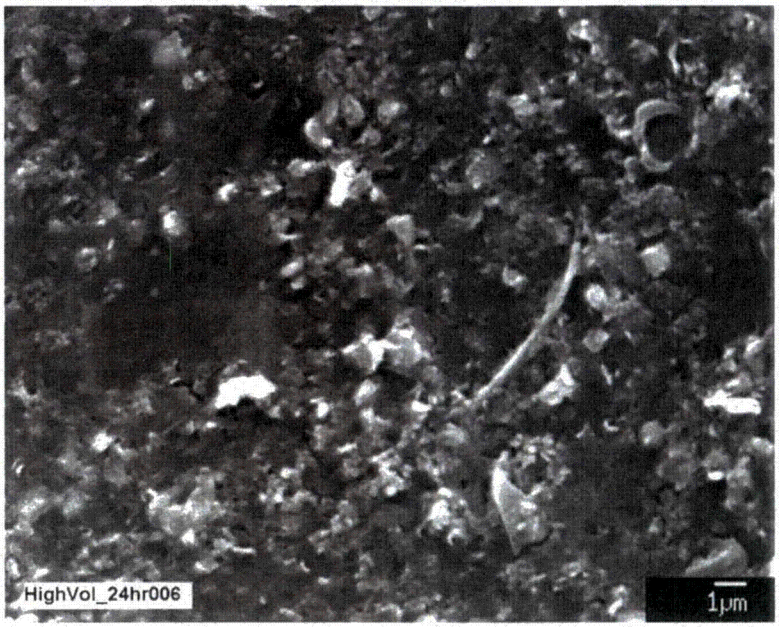

Figure A-5. Twenty-four-hour, high-volume-sample SEM image (HighVol_24hr006).

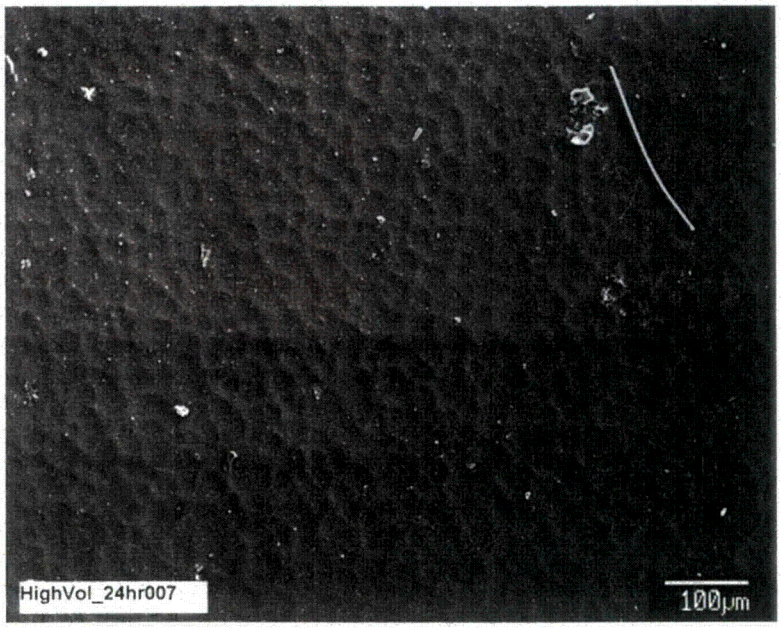

Figure A-6. Twenty-four-hour, high-volume-sample SEM image (HighVol_24hr007).

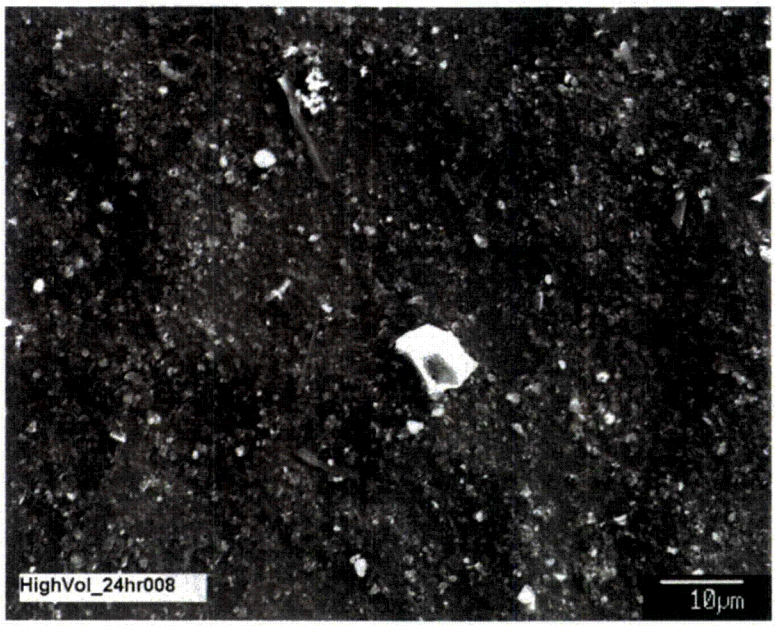

Figure A-7. Twenty-four-hour, high-volume-sample SEM image (HighVol_24hr008).

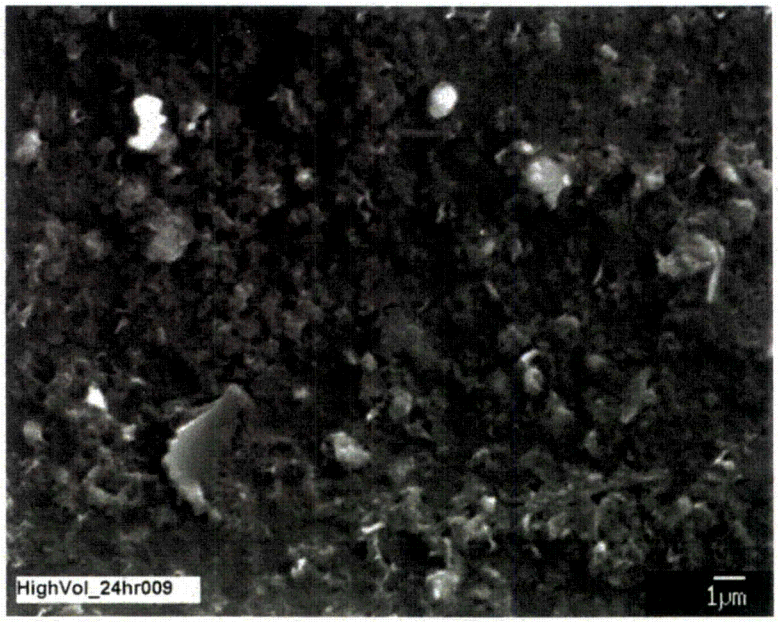

Figure A-8. Twenty-four-hour, high-volume-sample SEM image (HighVol_24hr009).

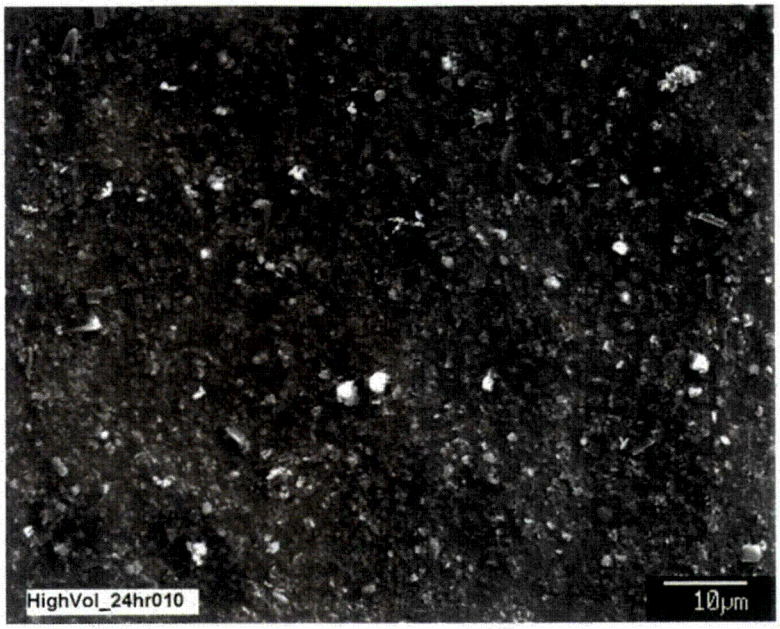

Figure A-9. Twenty-four-hour, high-volume-sample SEM image (HighVol_24hr010).

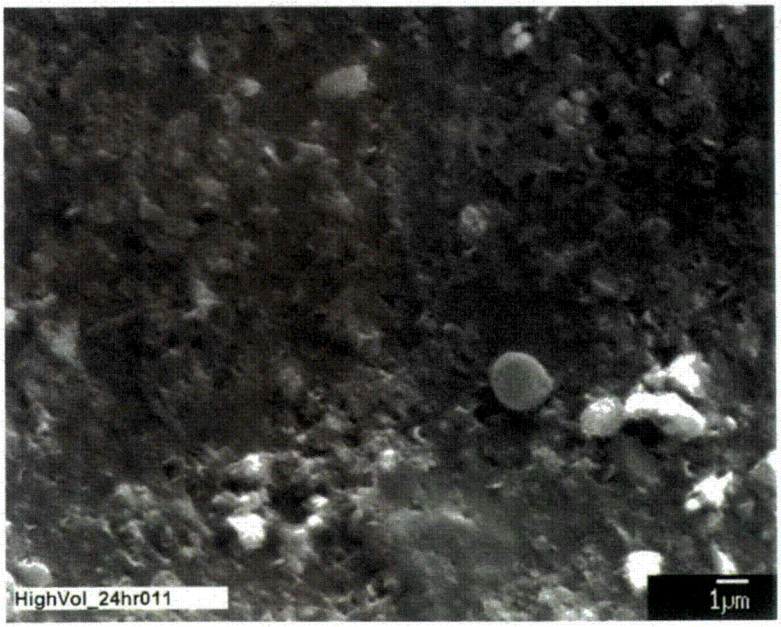

Figure A-10. Twenty-four-hour, high-volume-sample SEM image (HighVol_24hr011).

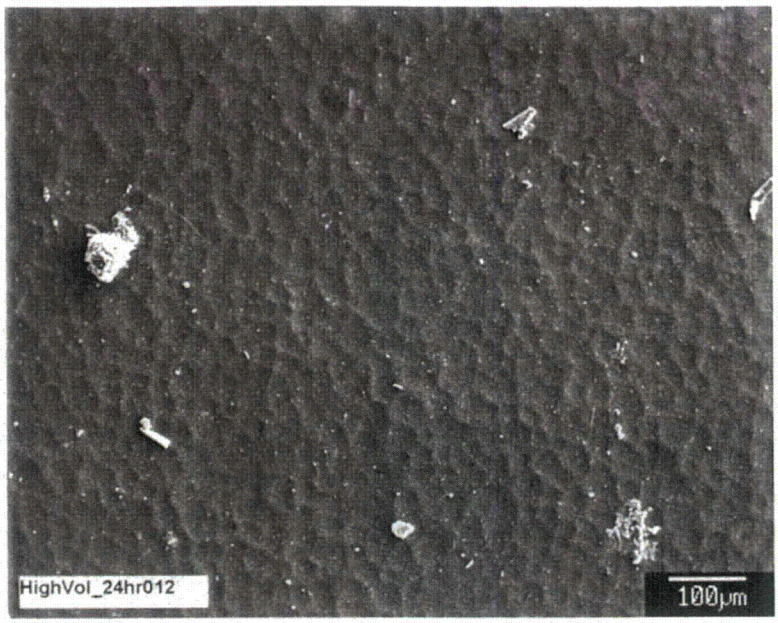

Figure A-11. Twenty-four-hour, high-volume-sample SEM image (HighVol_24hr012).

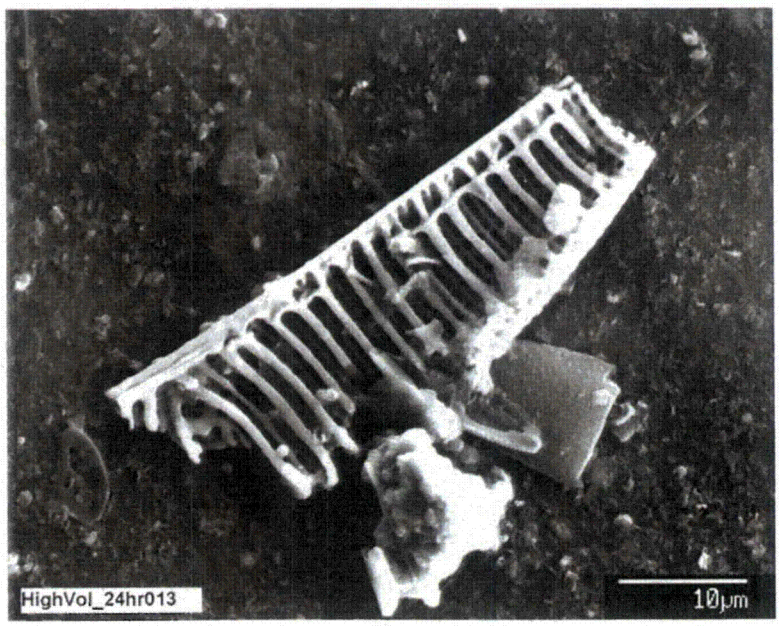

Figure A-12. Twenty-four-hour, high-volume-sample SEM image (HighVol_24hr013).

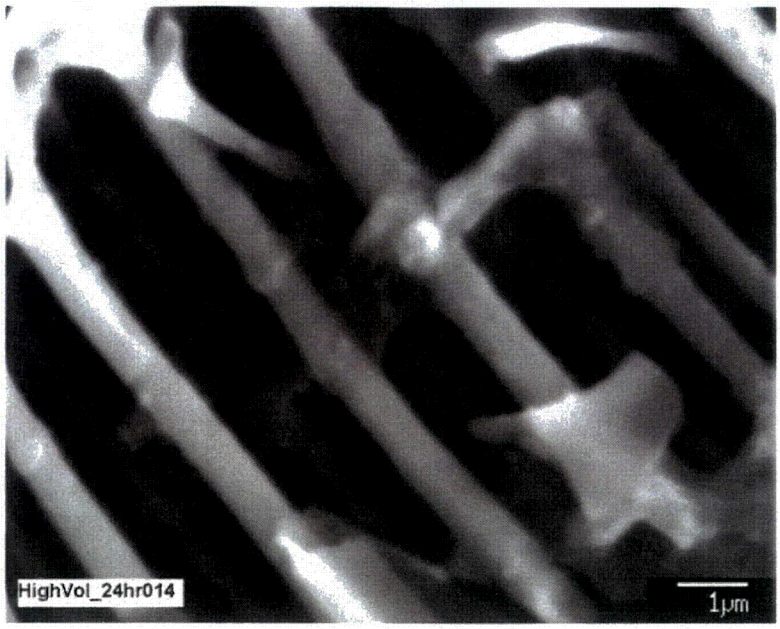

Figure A-13. Twenty-four-hour, high-volume-sample SEM image (HighVol_24hr014).

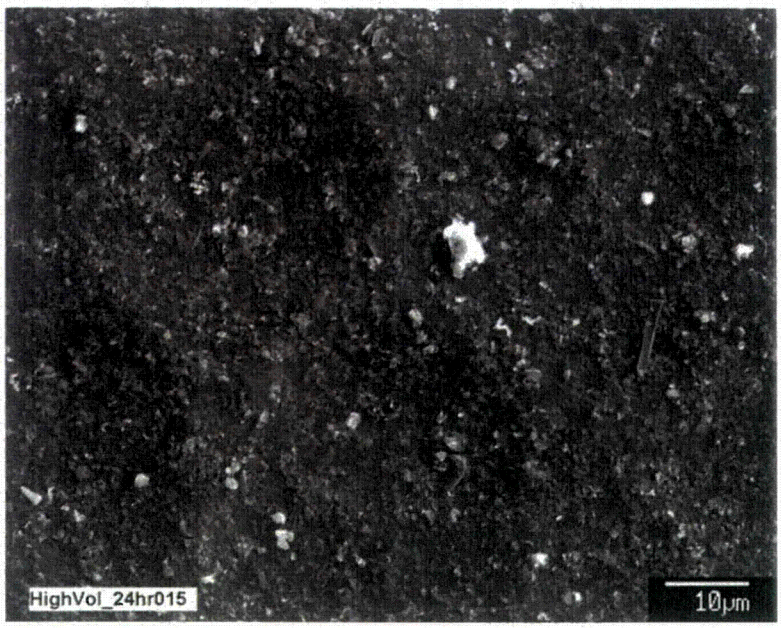

Figure A-14. Twenty-four-hour, high-volume-sample SEM image (HighVol_24hr015).

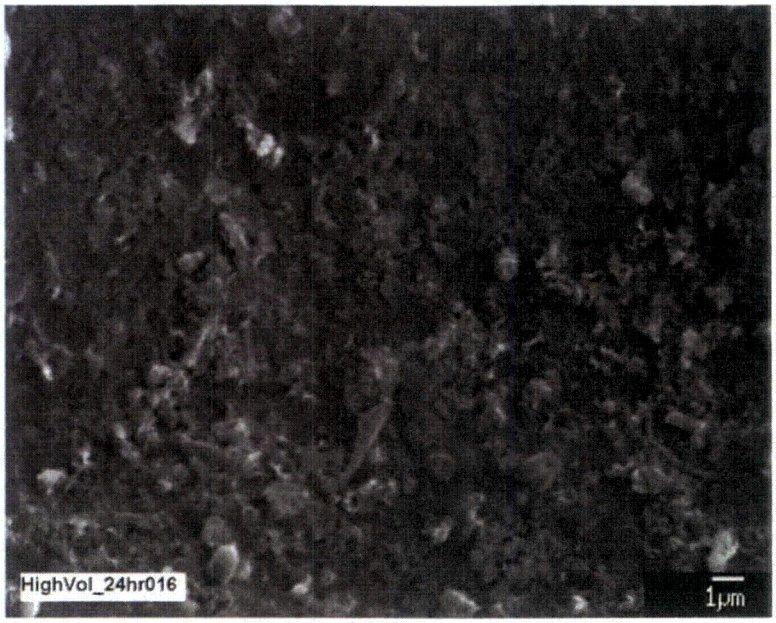

Figure A-15. Twenty-four-hour, high-volume-sample SEM image (HighVol_24hr016).

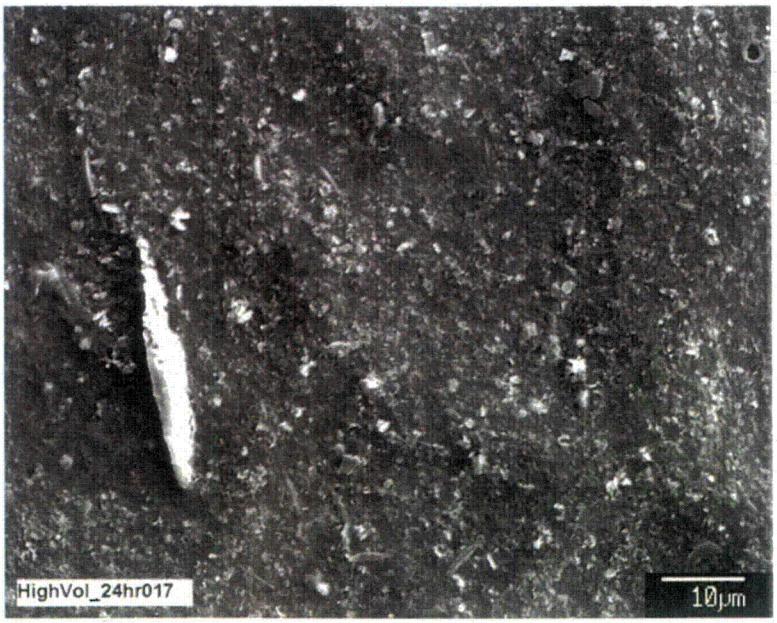

Figure A-16. Twenty-four-hour, high-volume-sample SEM image (HighVol_24hr017).

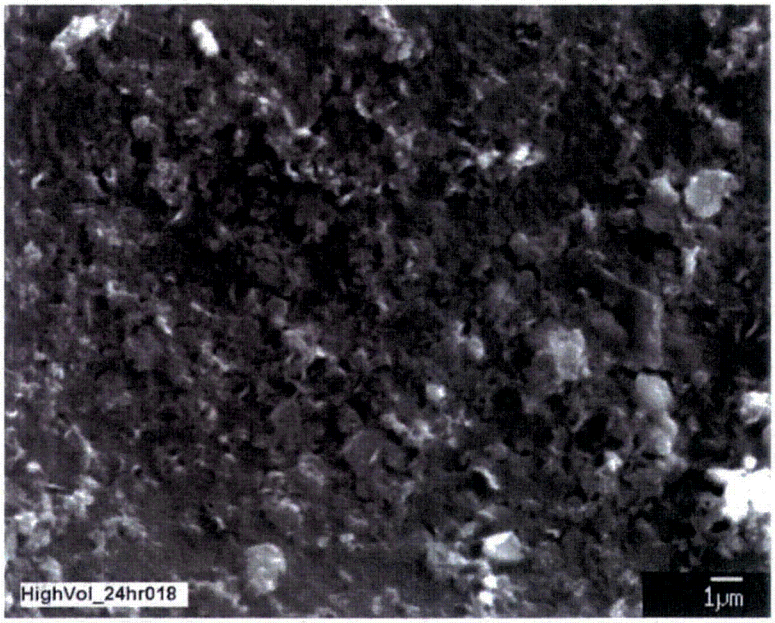

Figure A-17. Twenty-four-hour, high-volume-sample SEM image (HighVol_24hr018).

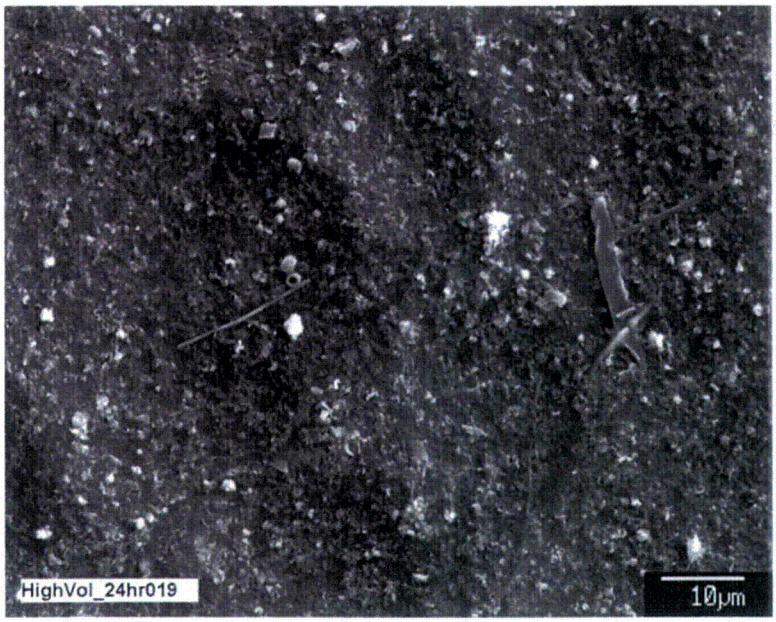

Figure A-18. Twenty-four-hour, high-volume-sample SEM image (HighVol_24hr019).

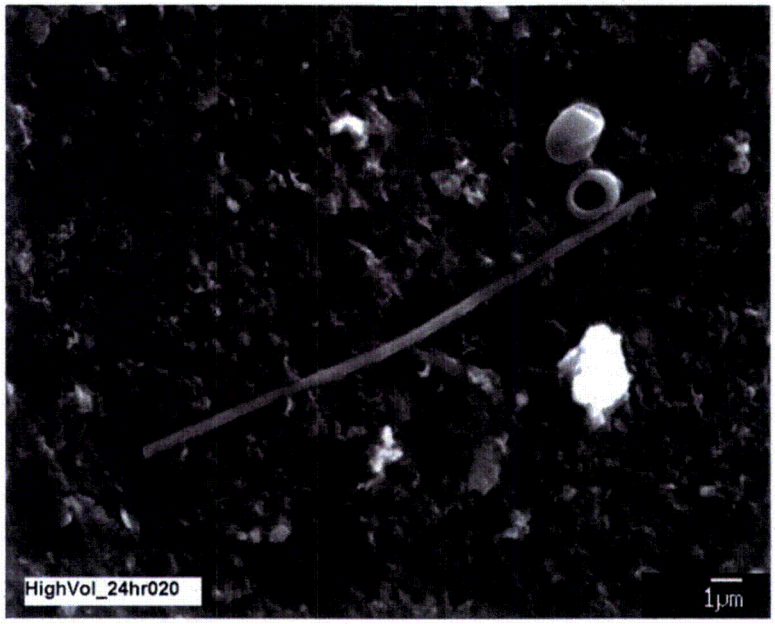

Figure A-19. Twenty-four-hour, high-volume-sample SEM image (HighVol_24hr020).

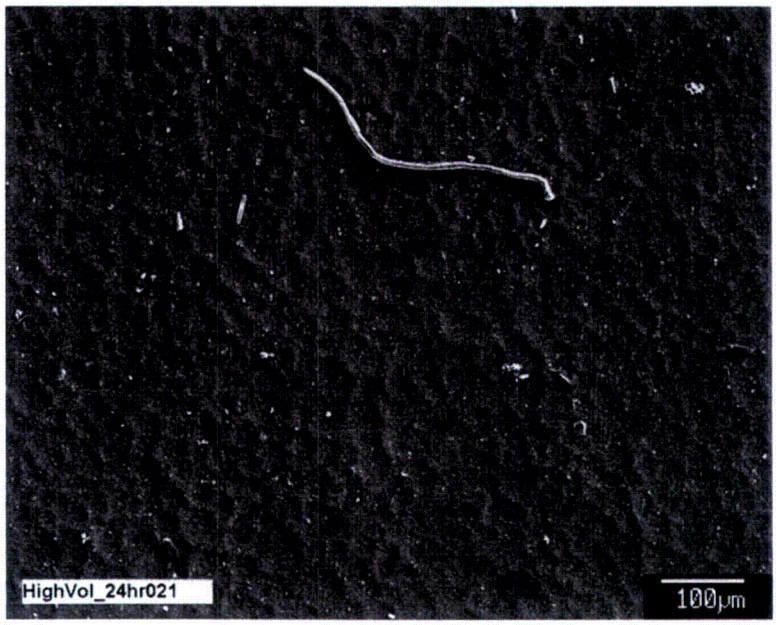

Figure A-20. Twenty-four-hour, high-volume-sample SEM image (HighVol_24hr021).

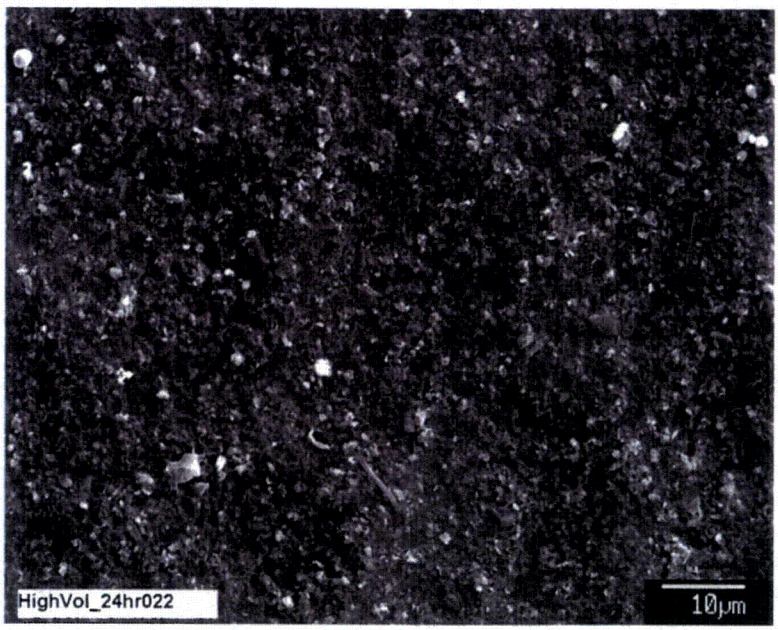

Figure A-21. Twenty-four-hour, high-volume-sample SEM image (HighVol_24hr022).

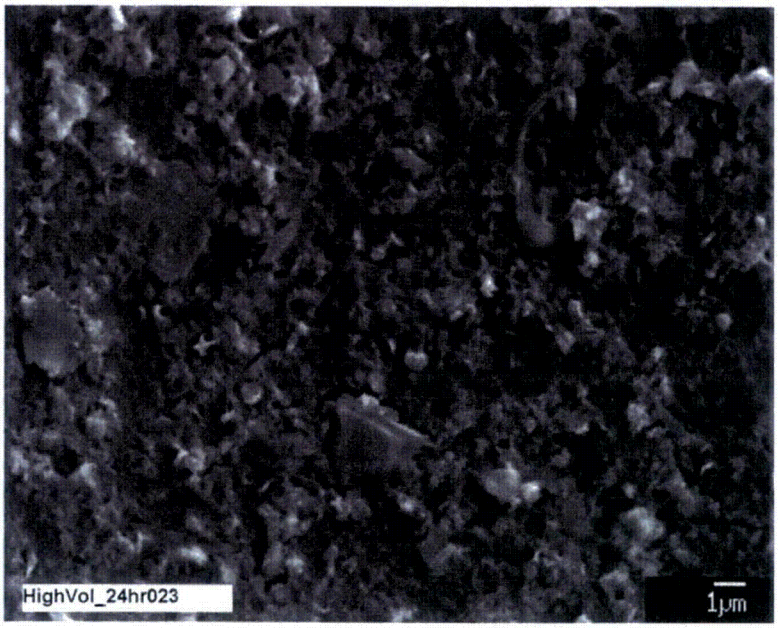

Figure A-22. Twenty-four-hour, high-volume-sample SEM image (HighVol_24hr023).

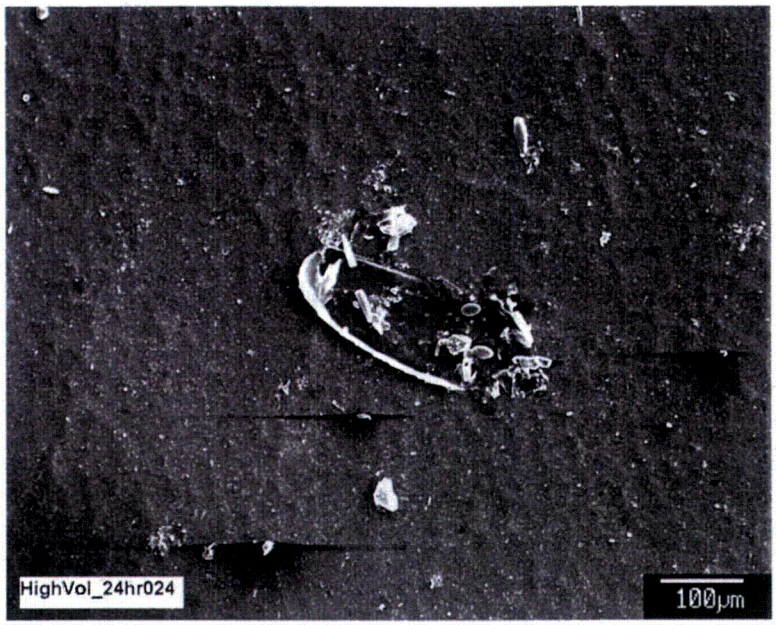

Figure A-23. Twenty-four-hour, high-volume-sample SEM image (HighVol_24hr024).

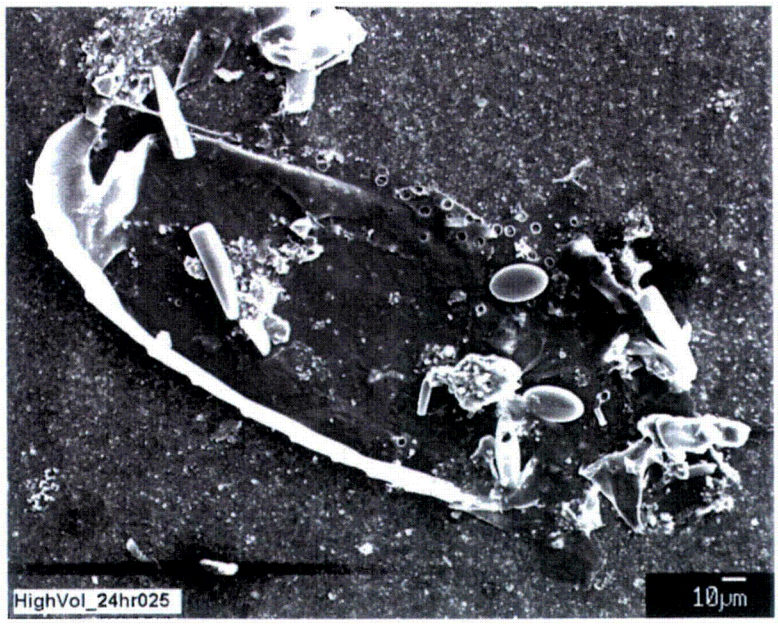

Figure A-24. Twenty-four-hour, high-volume-sample SEM image (HighVol_24hr025).

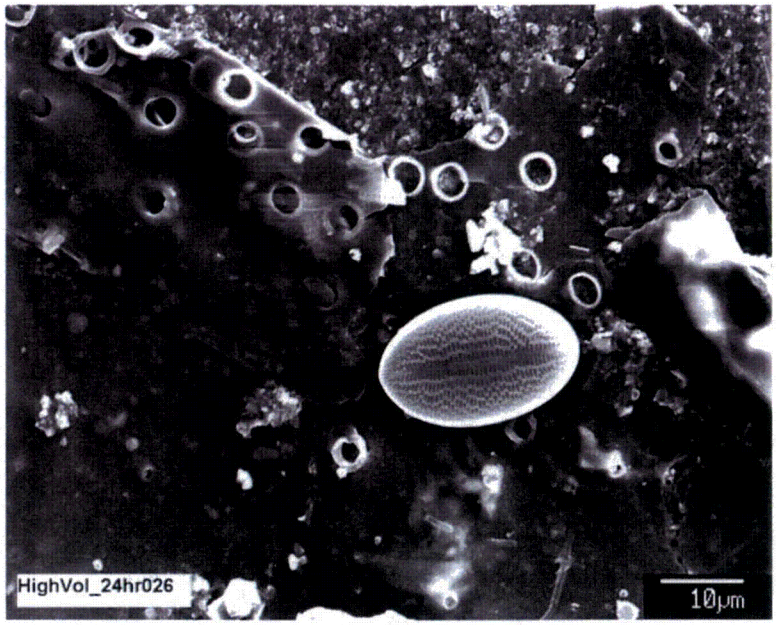

Figure A-25. Twenty-four-hour, high-volume-sample SEM image (HighVol_24hr026).